PERFORMANCE OF LARGE SCALE STEEL FIBER REINFORCED CONCRETE DEEP BEAM WITH SINGLE OPENING UNDER MONOTONIC LOADING

by

CARLOS A. FLORES

Presented to the Faculty of the Graduate School of

The University of Texas at Arlington in Partial Fulfillment

of the Requirements

for the Degree of

MASTER OF SCIENCE IN CIVIL ENGINEERING

The University of Texas at Arlington

August 2009

ACKNOWLEDGEMENTS

I would like to express my sincere appreciation to my research advisor, Dr. Shih-Ho Chao. Dr. Chao was persistent from the projects' inception, giving priceless advice on ideas and critiquing. I would also like to thank Dr. Guillermo Ramirez and Dr. John Matthys for their patience with me and in providing ideas and advice on the research project. I would also like to thank Hanson Pipe and Precast, Grand Prairie, TX, who donated materials for the test specimen. I would like to thank Jae-sung Cho, Netra Karki, Reza Mohammed, who where invaluable aid in the lab in this project. Finally, I would like to thank all the support staff at from the Department of Civil and Environmental Engineering at The University of Texas at Arlington. Without their continued support this project would never had been possible.

July 27, 2009

ABSTRACT

PERFORMANCE OF LARGE SCALE STEEL FIBER REINFORCED
CONCRETE DEEP BEAM WITH SINGLE OPENING
UNDER MONOTONIC LOADING

Carlos Flores, M.S.

The University of Texas at Arlington, 2009

Supervising Professor: Shih-Ho Chao

The design of complex, discontinuous stress trajectory regions (D-regions) is complex in nature and cumbersome to design. The performance of a large scale steel fiber reinforced concrete (SFRC) deep beam with single opening under monotonic loading was tested under controlled conditions. The main objective of this study was to see if Steel Fiber Reinforced Concrete (SFRC), used as a better material than reinforced concrete (RC) offered an alternate to the cumbersome and iterative steps involved in strut-and-tie (STM) methodology. Additionally, a similar reinforced concrete (RC) specimen was tested under the same controlled condition designed with classical strut-and-tie model design methodology reinforced using conventional steel bars.

Material testing was conducted on the materials tested on the large scale specimens to ensure that the actual material mechanical properties were known for the analysis. Computer Aided Strut and Tie (CAST) software was used to quantify the experimental data obtained from the controlled conditions testing.

The two beams were compared and contrasted throughout the study to indicate the performance of one beam compared to the other. This study provides information on the viability of using steel fiber reinforced concrete in complex D-regions in structural elements.

TABLE OF CONTENTS

LIST OF ILLUSTRATIONS

LIST OF TABLES

LIST OF NOTATIONS

A_s	=	area of reinforcement (in^2, mm^2)
B	=	width of specimen (in, mm)
D	=	depth of specimen (in, mm)
d	=	diameter (in, mm)
E	=	Young's modulus (ksi, MPa)
f_b	=	bending stress (ksi, MPa)
f'_c	=	cylinder compressive strength of concrete (psi, MPa)
f_{ct}	=	tensile strength of concrete (psi, MPa)
$f_{150, 0.75}$	=	residual strength – the stress value obtained from $P_{150, 0.75}$
$f_{150, 3.0}$	=	residual strength – the stress value obtained from $P_{150, 3.0}$
f_y	=	yield strength of reinforcement (psi, MPa)
h	=	beam height (in, mm)
I	=	second moment area moment of inertia (in^4, m^4)
M	=	moment (kip-ft, kN-m)
MOR	=	modulus of rupture (psi, MPa)
L	=	span length (in, mm)
l_d	=	development length (in, mm)
P	=	load (kip, kN)
$P_{150, 0.75}$	=	residual load corresponding to a net deflection equal to 1/600 of the span (or 0.75 mm- (0.03in) using a specimen with a width and depth of 150 mm (6 in.) and span of 20 in.

$P_{150, 3.0}$	=	residual load corresponding to a net deflection equal to 1/150 of the span (or 3.0 mm- (0.12in) using a specimen with a width and depth of 150 mm (6 in.) and span of 20 in.
P_u	=	load at failure (kip, kN)
P_y	=	load at yield (kip, kN)
V	=	shear (kip, kN)
ϕ	=	strength reduction factor
θ	=	angle between axis of strut and tension chord
α	=	angle between axis of strut and reinforcing bars
γ_c	=	unit weight of concrete (lb/ft^3)
ν	=	Poisson's ratio
δ	=	deflection, displacement (in, mm)
δ_p	=	peak-load deflection (in, mm)
δ_1	=	first peak deflection (in, mm)
ϵ	=	material strain (in/in, mm/mm)
σ	=	standard deviation

CHAPTER 1

INTRODUCTION

1.1 Introduction

Deep beams serve many uses applications in buildings and other structures. In buildings, a deep beam or transfer girder is used when for architectural purposes a lower column on the exterior façade is removed. A deep beam, sometimes the full depth of the floor-to-floor height is used to transfer the high axial forces of columns above to the supporting columns below (see Figure 1-1). Foundation walls are sometimes also termed deep beams. In highways, pile caps are classified as deep if the span-to-overall depth ratio (a/h) is greater than four.

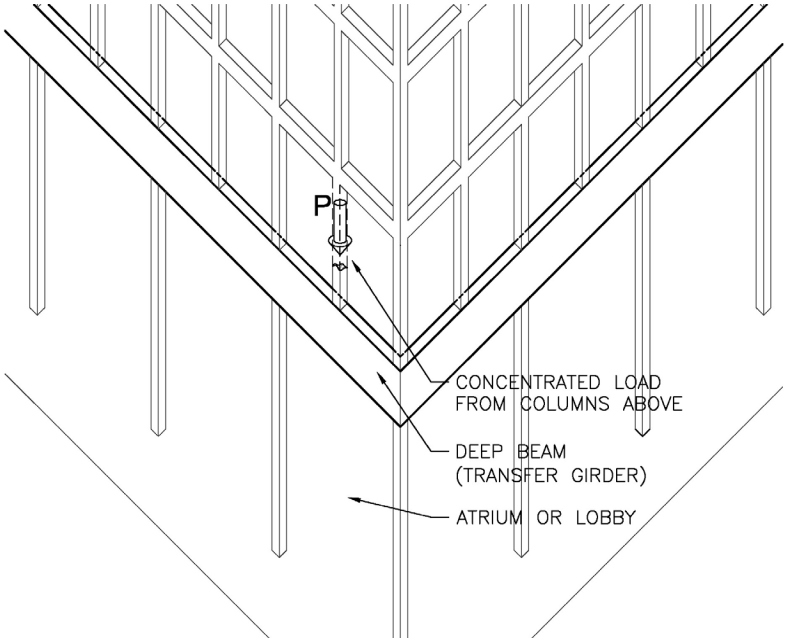

Figure 1-1 Deep beams found in multi-story buildings

Because of the complexity of today's buildings, openings through structural members are frequently required for mechanical, electrical or even for means of passageways such as openings for doors and hallways (see Figure 1-2).

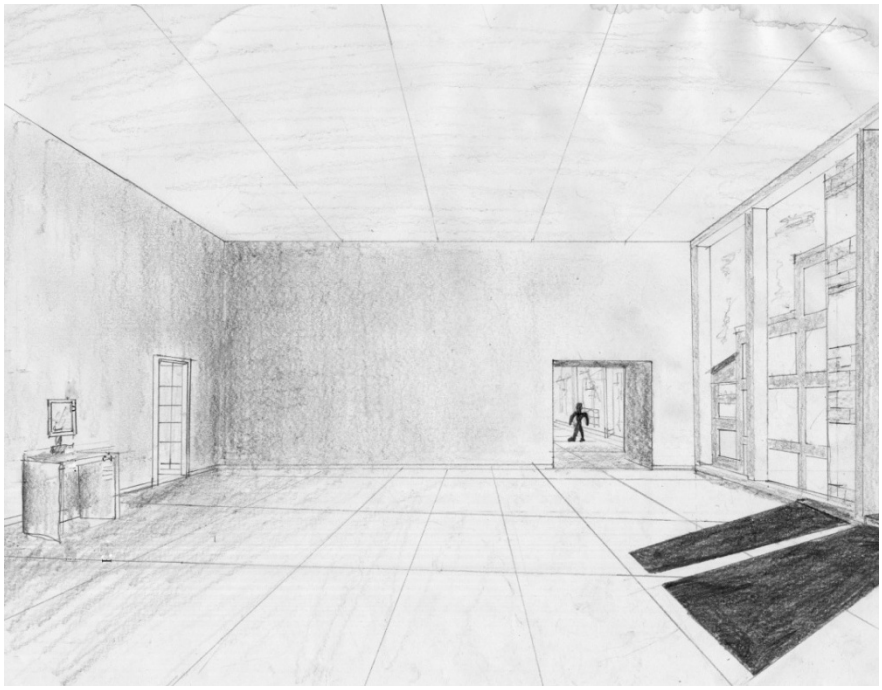

Figure 1-2 Deep beam with opening for circulation used in a high rise building

1.2 Literature Review

The ACI Building Code (ACI 318- 08, 2008) Section 11.7.1 defines deep beams as those beams where the clear span (l_n) is equal to or less than 4 times the overall member depth or beams with concentrated loads within a distance equal to or less than two times the beam depth from the face of support. Many column corbels also fall under this category. In the past, these members were designed based on empirical formulas that were based on experimental data. These deep beams are designed using the so-called "truss analogy" as described by Ritter (Ritter, 1899) and Mörsch (Mörsch, 1909). From St. Venant's principle, stress trajectories are not uniform at loading points and around openings as illustrated in Figure 1-3 (Hibbeler,

2005). Bernouilli equations are not applicable to the D-regions of structural elements where discontinuity of stress trajectories occurs.

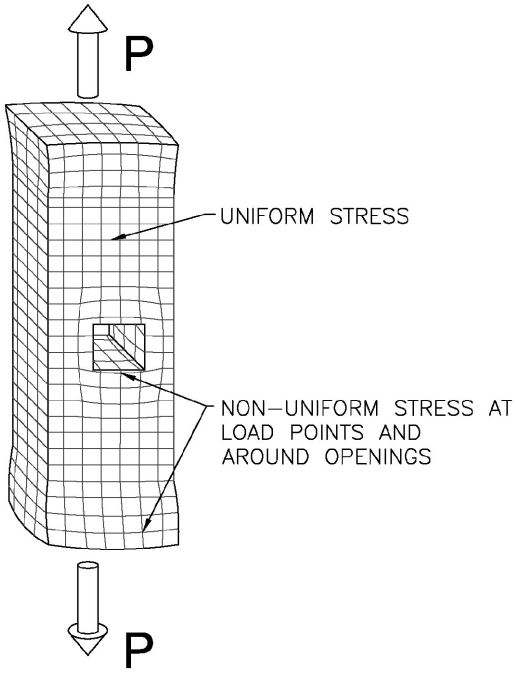

Figure 1-3 St. Venant's principle at loading point and around openings

The empirical-based formulas in the codes however, do not address issues such as designing D-regions (see Figure 1-3 and Figure 1-4) with openings. Historically, structural designers have used “rules-of-thumb” to design. Over the past decades, codes have adopted the use of strut-and-tie models for designers’ aid to designing D-regions.

AASHTTO (AASHTO, 1994) introduced strut-and-tie model (STM) in 1998 and the ACI Building Code did the same in its 2002 edition (ACI 318-02, 2002.) STM design idealizes a deep member with concrete compressive struts connected with steel tensile ties at nodes, idealized as frictionless “pins.” Essentially, the concrete between the truss is neglected for any design purpose. Furthermore, the truss members are in pure compression or tension. Hence, in STM there is only flow of forces from the loading point to the supporting members. This newly

adopted design methodology allows designers to create statically admissible truss models to design struts, ties and nodes using design criteria to design structural members.

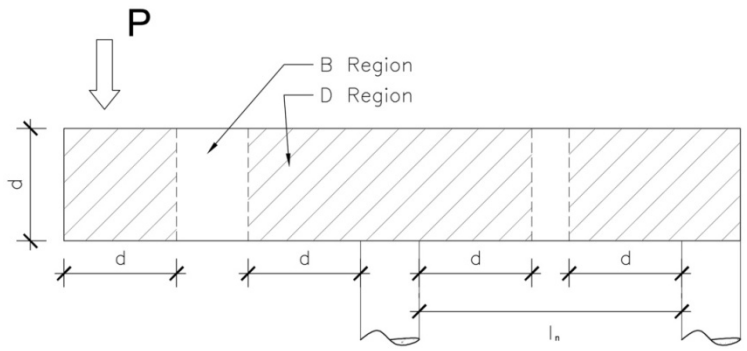

Figure 1-4 D - and B - regions in deep beams

Many times, openings must be located through the structural elements to provide access for conduits or mechanical chases. In doing so, the stress trajectories become disrupted around the openings (see Figure 1-2).

The ACI Building Code (ACI 318-08, 2008) does not give any explicit guidance to designing these elements with openings. Prior studies have been made with deep beams with openings using STM methodology (Breen, et al., 2007; Breen, et al., 2002; Park and Kuchma, 2007; Zhang and Tan, 2007; Maxwell and Breen, 2000; Kuchma. et al., 2008; Breña and Morrison, 2007). These various studies used small-scaled test specimens with different configuration and location of openings designed by STM to validate the usefulness of STM. These experiments showed that the strut-and-tie model gives consistent and conservative results in terms of ultimate strength. It is recommended that the designer first employ a finite element model of the member to help aid in the member load path (Breen, et al., 2007). Designers must at some time face the dilemma of using the correct strut-and-tie model. Inexperienced designers might have doubts about their chosen model. This is because no single model is the correct one for a given structure, provided it meets the criteria for lower-bound theory (see Figure 1-5). In fact, two designers can come up with completely different

models, yet both are statically admissible. Hence, both are adequate based on current design methods. Also, some tests have shown that large differences occur between calculated forces from STM and actual instrumented experimental specimens (e.g. Breña and Morrison, 2007). This implies that the model does not behave as designed. To be effective, the designer assumes that all steel yields in the model; this assures a safe, ductile failure.

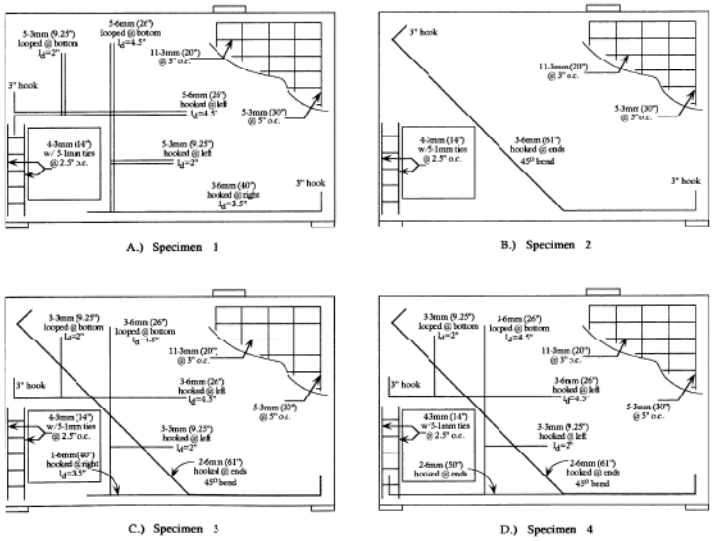

Figure 1-5 Reinforcing layout and detailings developed using various STM models for the same geometry. (Adapted from Maxwell and Breen, 2000)

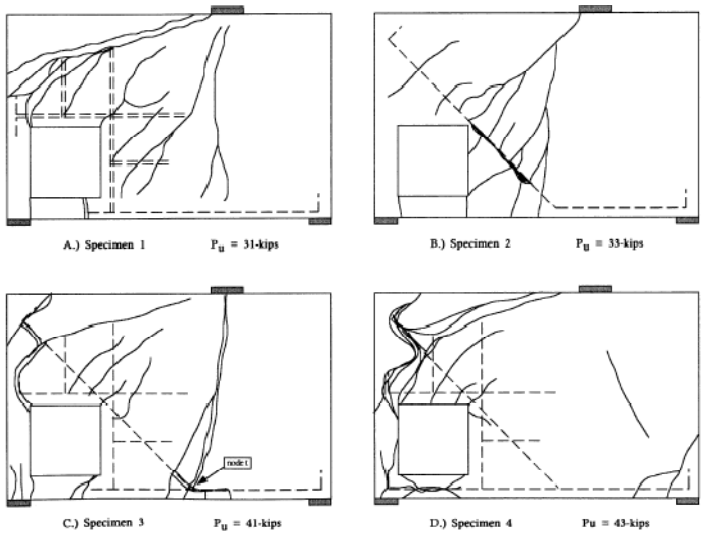

Figure 1-6 Crack patterns for the reinforcement layout shown on Figure 1-5. (Adapted from Maxwell and Breen, 2000)

Another difficulty in using STM is anchorage and congestion. Constructability becomes an issue when there is a large amount of reinforcing bars and the spacing between each is very small.

Recently, there have been concerns and investigations in performance of structural members with complex D-regions under service loads using STM. A poorly selected and detailed STM model can lead to the member cracking and damage and having limited ductility under service loads. Furthermore, these studies concluded that members typically have little post-peak ductility. That is, the envisioned STM structures do not behave as plastic trusses (Kuchma, et al, 2008.)

With STM, it is not possible to determine the actual failure mode using STM. Ideally, the steel ties must yield, but the possibilities of a brittle failures due to improper detailing are not discarded. Tests have shown that even though the ultimate loads are much higher than the design load, ductility is not guaranteed. Other D-region structural elements such as beam-to-column joints designed with STM might exhibit brittle behavior if subjected to cyclic loading such as in an earthquake where forces increase rapidly and ductility is of major concern. Research shows that brittle failures are more pronounced for elements where higher concrete strength is used (Kuchma, et al. 2007). ACI 318-08 and the Canadian (CSA, 1984) codes do not give guidance to these conditions, although ACI does limit the compressive strength of concrete struts to 6,000 psi. However, if the designer specifies a compressive strength in the upper range, the actual compressive strength used in structure may be higher. This is usually the case because the concrete suppliers aim for a higher strength than specified by the designer to be on the “safe side," not knowing of the detrimental effect of using higher compressive strength.

Due to the topic of world-wide energy consumption and CO_2 gas increasing in the atmosphere, advancements in “green” materials becomes more and more important. Materials that are made from recycled materials, more durable, and consume less energy to produce are the preferred sustainable choice. It is known that concrete requires high amount of energy to

produce. However, the efficiency of the material is lost as concrete cracks. In the Ritter and Mörsch “truss analogy” previously described, the concrete between the model is neglected. In essence, the material is, to some extent, wasted.

Another aspect of green materials is the long-term performance when exposed to the environment. “Green” concrete has superior serviceability characteristics, and requires less rehabilitation and gives infrasctructure longer service life (Chao, 2008). Buildings with the United States Green Building Council’s Leadership in Energy and Environmental Design’s (LEED) certification, which uses green technology has increased 62% in 2007 alone (DePillis, 2008).

The concept of reinforcing brittle material with fibers is as old as the pyramids built by the ancient Egyptians (Mehta and Monteiro, 2006). Steel Fiber Reinforced Concrete (SFRC) has gained increased popularity in the lab and in the field. Reinforcing concrete with steel fibers has been used to reduce material in structural slabs (ACI 544-96, 1996). Since their its introduction in the mid 1960s, (ACI 544-96, 1996) SFRC has many advantages over conventionally-reinforced concrete. Tests have shown that SFRC is tougher and more ductile (ACI 544-96, 1996).

Research must be done in this topic, as higher strength concretes become more and more common. Many failure modes include: anchorage failures, local concrete crushing, shear compression or concrete spalling (ACI544-96, 1996). Adding fibers to concrete has shown to resist higher shear forces and prevent concrete from spalling. Shear tests on steel fiber reinforced concrete (SFRC) beams without stirrups have shown that if the fiber dosage is sufficient no other transverse reinforcement is necessary to achieve the desired shear capacity (Dupont, et al. 2003). Furthermore, SFRC beams show a more ductile behavior and have reduced crack widths (Dupont, et al. 2003). It is generally agreed that the fiber bridging effect limits crack width and mitigates or eliminates the brittle failures encountered in previous experiments. Studies have been done on deep beams using different dosages of fibers, varying

concrete compressive strengths, shear span-to-depth ratios. Those tests showed that adding steel fibers reduced crack width in deep beams by four times at steel fiber ratio of 1.25 by weight (Darwish, et al., 1988) (In some cases, adding an opening interrupts the concrete compressive strut. Tests have shown that failure occurs in shear where the strut is interrupted.) However, to the best of the author's knowledge, there is no experimental data on FRC deep beams with web openings.

Eliminating shear reinforcement practically eliminates congestion and potentially reduces construction costs. In addition, FRC offers a multidirectional reinforcement and higher post-cracking residual stress. Unfortunately, FRC is rarely used in structural applications (Casanova and Rossi, 1999)

The basis was to eliminate the conventional steel reinforcing and secondary steel and use steel fiber in the concrete matrix. The only conventional reinforcement used in the experimental program was flexural reinforcement. Simply-supported beams where initially tested to verify the results with the beams tested previously using the strut-and-tie model. These beams where approximately one-fourth scaled beams originally tested by Schlaich, et al. (Schlaich, et al., 1987). It has been argued that experimental data becomes skewed when small diameter reinforcement is used in small-scaled beams and bearing plates are not scaled down (Zhang, et al., 2007). Care was used when determining the reinforcing layout to preclude the small-scaled beams failing by anchorage.

1.3 Overview of Chapter II, III and IV

Chapter II on Material Testing discusses the testing of materials used in the experimental program. Material testing was conducted following appropriate American Standard for Testing and Material (ASTM) standards. All testing was conducted for the reinforced concrete specimen and for the SFRC specimen. Concrete compressive strength was determined from cylinders. Concrete flexural strength was determined using beam third-point

loading. Tensile testing was conducted on the deformed reinforcing steel to determine the actual yield strength.

Chapter III titled, Experimental Program, discusses the procedure for casting the large-scale test specimens, as well as the instrumentation used for testing. The observed cracking, and other measured data from instrumentation are presented for the RC specimen, followed by the same data obtained from the SFRC specimen. Finally, the two specimens are compared using data obtained from Acoustic Emission (AE.)

Chapter IV explains the analysis using Computer Aided Strut and Tie (CAST) and experimental data is compared for the reinforced concrete test specimen and an analysis with same beam with only a single reinforcing tie. Graphs and tables quantify the comparisons between the two specimens.

Chapter V closes with conclusions from the research project, as well as recommendations for future work. References used in this research are listed also listed.

1.4 Appendices A and B

Appendix A includes information about analysis of CAST such as how the specimen's geometry, material properties, strut types, and other aspects essential to STM.

Appendix B and C includes the output files of the specimens analyzed. This data includes element forces, stresses and stress limit/yield force ratios.

CHAPTER 2

MATERIAL TESTING

2.1 Introduction

The purpose of material testing is to determine the actual material properties used in the experiment in order to estimate the strength of the specimens as well as evaluate the performance of the materials used. Typically, structural members are designed using assumed material properties; it might not ever be known the actual properties due to fabrication, environmental, or construction variations, among others. Therefore, it is important that actual material properties be known.

Figure 2-1 Casting of large-scale specimens and ASTM beams and cylinders

2.2 Concrete Mix Design

Mix design was done such that the optimum quantity of materials and similar proportions were used for both plain concrete and SFRC mixes. Chemical admixtures were not used in any specimens in this project.

Table 2-1 Concrete mixture composition by weight and total weight per specimen

Material	SFRC Mix (lb.)	RC Mix (lb.)
Portland Cement (Type I)	360	444
Fly Ash (Class C)	180	222
Fine Aggregate (Sand)	612	754
Coarse Aggregate (1/2 in.) Limestone	360	444
Water	216	266
Superplasticizer (SP)	0	0
Viscous Modifying Agent (VMA)	0	0
Steel Fiber	89 (1.5% in vol.)	0
Total Weight	1817	2131

Table 2-2 Steel fiber mechanical properties

Type	Length (mm)	Diameter (mm)	Aspect Ratio (L/d)	Tensile Strength (N/mm^2)	Coating
Cold-drawn, hooked ends*	60	.75	80	1050	None

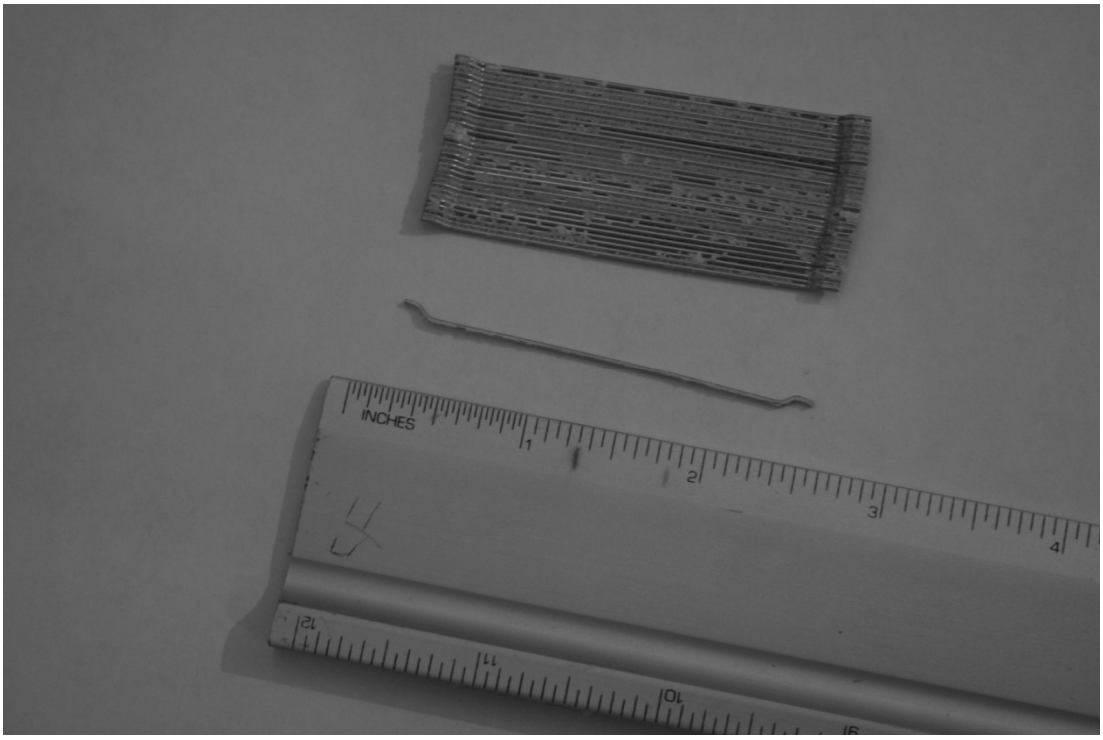

Figure 2-2 Steel fibers used in this study

2.3 Compressive Strength

Concrete cylinders were cured under the same environmental conditions as the large-scaled specimens. All specimens were covered with a sheet of polyethylene for twenty-four hours. The cylinders were capped in accordance with ASTM 617-98, "*Practice for Capping Cylindrical Concrete Specimen*" (ASTM, 2005). The cylinders were tested the same day when the large-scale specimen was tested. The average compressive strength for the six plain concrete specimens was 6185 psi. The test showed typical results for unconfined, plain concrete in cylinders. All cylinders had Type I failure modes, as described by ASTM C39/ C 39M-05, "*Test Method for Compressive Strength of Cylindrical Concrete Specimens*," (ASTM, 2005). Compressive strength testing showed a brittle failure of the plain concrete specimens. The cylinders suddenly exploded and were no longer able to resist load. Severe spalling occurred on the top portion of the cylinders (Figure 2-4). Concrete completely separated after the load was removed.

(a) (b)

Figure 2-3 Capped plain concrete cylinder (a) and steel fiber reinforced concrete cylinder before testing (b)

Testing of SFRC was the same as plain concrete cylinders. The average compressive strength for the six SFRC specimen was 5867 psi. Testing was done 35 days after casting, the same day that the large-scale specimens were tested. Tests showed that the concrete crushed under load. All cylinders were severely cracked, but none had concrete separation, even after load was removed. The failure mode was much more ductile compared to the plain concrete tests (Figure 2-4)

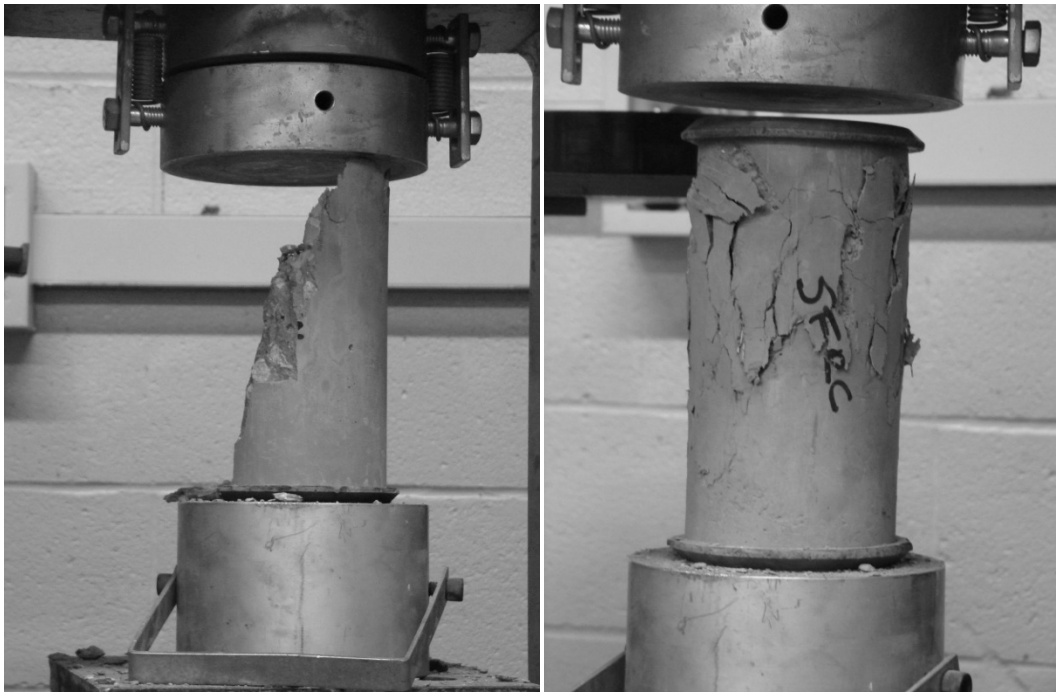

(a) (b)

Figure 2-4 Typical plain concrete cylinders after testing (a) and steel fiber reinforced concrete cylinder after testing (b)

Table 2-3 Plain concrete compressive cylinder test results

Sample No.	Load (k)	Diameter x Height (in.)	Area (in^2.)	$f'_c = P/(\pi/4)d^2$ (psi)
1	70830	4.00 x 8.00	12.56	5636
2	80360	4.00 x 8.00	12.56	6395
3	74300	4.00 x 8.00	12.56	5912
4	74290	4.00 x 8.00	12.56	5912
5	83280	4.00 x 8.00	12.56	6627
6	83290	4.00 x 8.00	12.56	6628
			Average f'_c	6185
			Standard Deviation σ	371

Table 2-4 SFRC concrete compressive cylinder test results

Sample No.	Load (k)	Diameter x Height (in)	Area (in^2)	$f'_c = P/(\pi/4)d^2$ (psi)
1	75180	4.00 x 8.00	12.56	5983
2	77670	4.00 x 8.00	12.56	6186
3	76620	4.00 x 8.00	12.56	6102
4	75200	4.00 x 8.00	12.56	5989
5	63760	4.00 x 8.00	12.56	5078
6	73590	4.00 x 8.00	12.56	5861
			Average f'_c	5867
			Standard Deviation σ	401

2.4 Flexural Strength

The plain concrete specimen used for flexural testing had nominal dimensions 6 in. x 6 in. x 20 in. width, height and length, respectively, with a clearspan length of 18 in. They were tested in accordance with ASTM C78-02, "*Test Method for Flexural Strength of Concrete using Simple Beam with Third-Point Loading.*" (ASTM, 2007). LVDTs measured displacement on each side of the beam, so that an average displacement value could be taken. Loading rate, as prescribed by ASTM standard is 0.002 to 0.005 in./min of net deflection up a total deflection of L/600; after this point, the loading rate is 0.002 to 0.010 in./min. until a deflection of L/150 is reached, or 0.12 in. of deflection. This procedure applies to the size of the beams used throughout this study.

Peak load was measured at 4175 lb. The modulus of rupture, was calculated as follows:

$$MOR = PL/BD^2 \quad \text{(Eq. 2-1)}$$

where MOR = modulus of rupture, psi

P = ultimate applied load, lb

L = specimen span, in

B = specimen width, in

D = specimen height, in

The modulus of rupture for the specimen was 348 psi. The cracking load was the failure load.

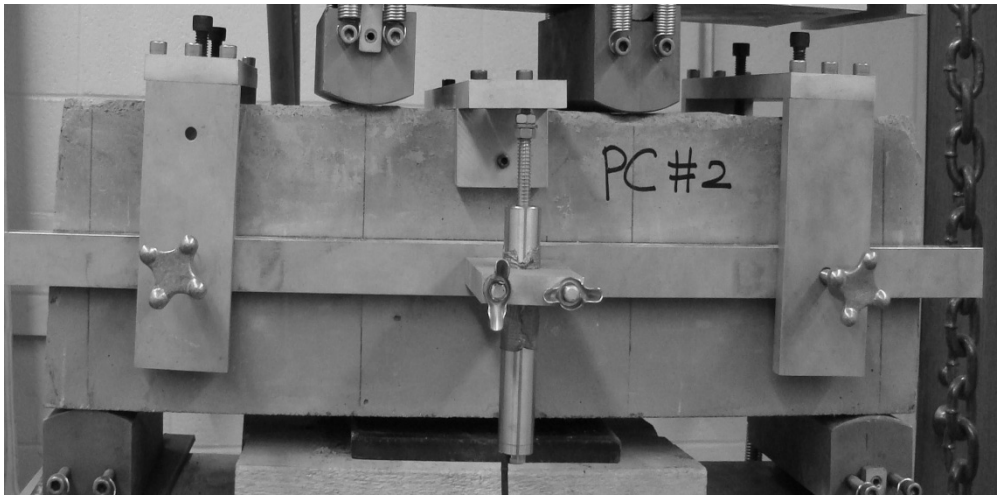

(a)

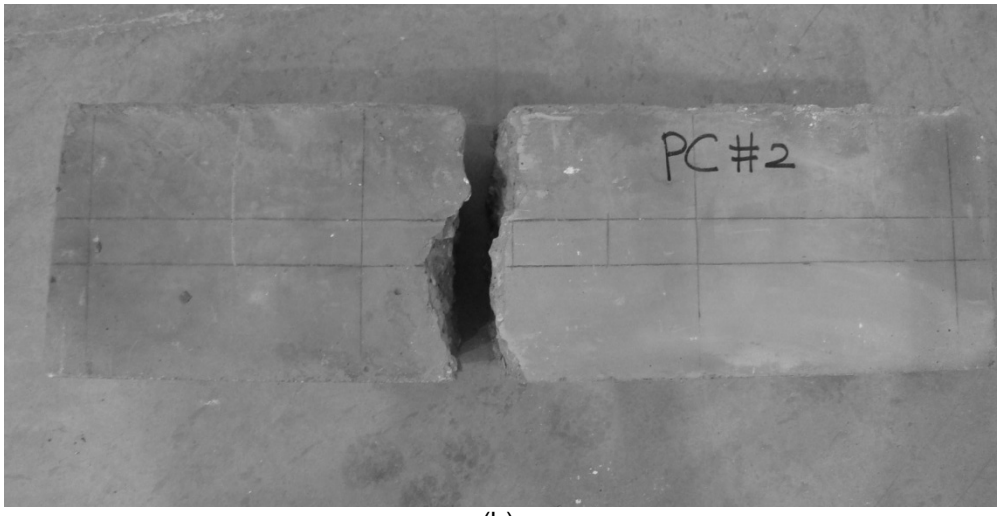

(b)

Figure 2-5 ASTM C78 plain concrete beams in testing machine (a) before failure and (b) after removing from testing machine due to failure

The SFRC specimens were tested in accordance with ASTM C 1609/C 1609M – 06, "*Test Method for Flexural Performance of Fiber-Reinforced Concrete Using Beam with Third-Point Loading,* "(ASTM, 2007). Deflection was with linear Variable Differential Transducers on each side of the specimen located at midspan. The values were taken as the average between the two. Although the ASTM standard was different for SFRC specimens, the setup was the same for both plain concrete specimen and SFRC specimen. The loading rate was also the same for both. As a result, instrumentation was the same as for the plain concrete beam. The

first SFRC beam's first peak load was equal to peak load. The second SFRC beam had a peak load greater than the first peak load. In both SFRC beams, after the first crack formed, smaller micro-cracks formed branching out from the initial crack. Those cracks opened as load continued to increase. The fibers were observed pulling out and cracks opening wider as the test neared the end (Figure 2-7b).

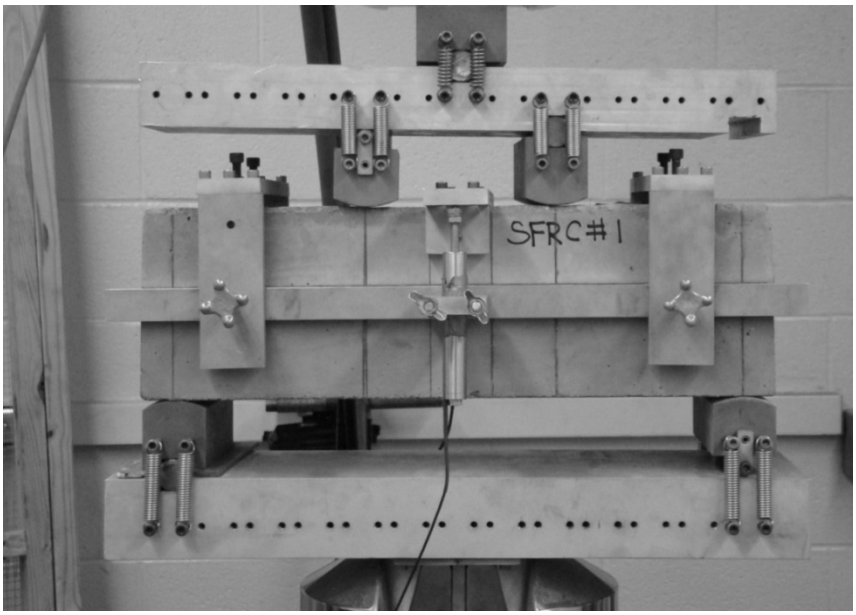

Figure 2-6 ASTM C1609 SFRC test beam 1 in loading position

(a) (b)

Figure 2-7 First crack in bottom of beam (a) and crack at end of test (b) for SFRC test beam 1

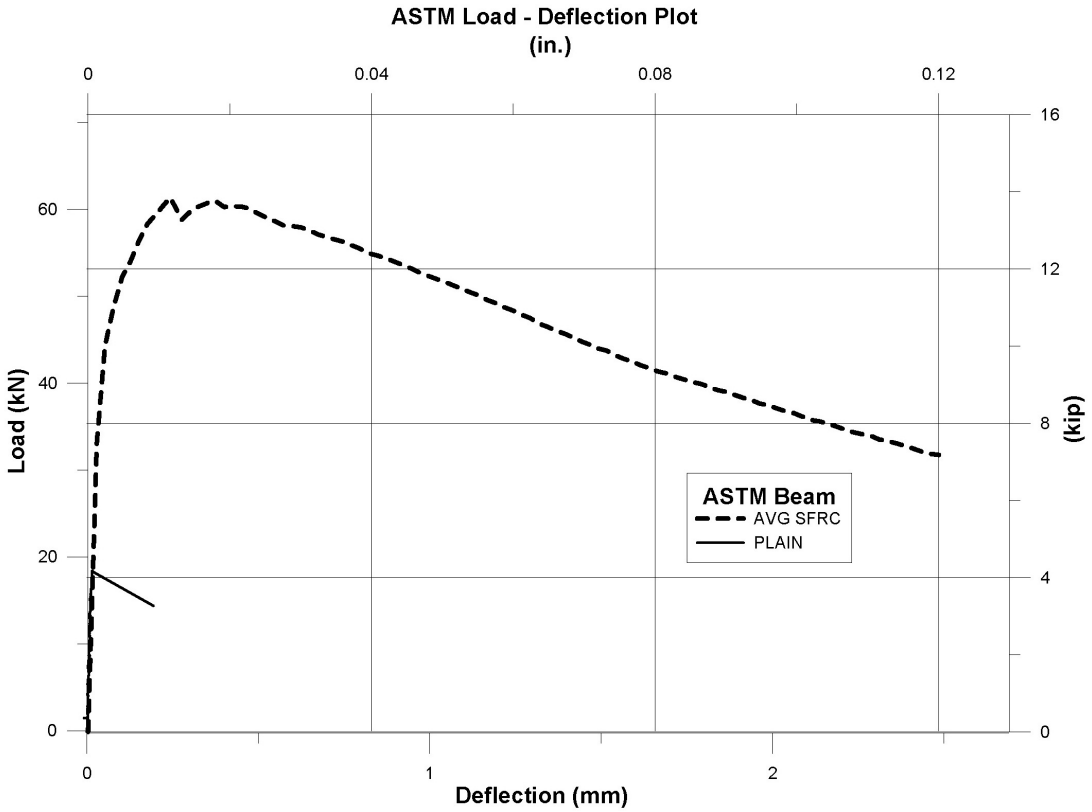

Figure 2-8 Load-displacement plot of ASTM test beams

Table 2-5 Performance of ASTM test beams

Test Specimen Summary				
Specimen Number	Plain 1	Plain 2	SFRC 1	SFRC 2
Span Length, L (in)	----	18	18	18
Modulus of Rupture, MOR (psi)	----	348	n/a	n/a
First Peak Load, P_1 (lb)	----	n/a	14, 365	13,315
Peak Load, P_p (lb)	----	n/a	14, 365	14, 075
Peak-Load Deflection, δ_p (in)	----	n/a	0.2730	0.2672
First-Peak Deflection, δ_1 (in)	----	n/a	0.2730	0.2531
Peak Strength, f_p (psi)	----	n/a	1,200	1,175
First- Peak Strength, f_1 (psi)	----	n/a	1,200	1,110
Residual Load at L/600, $P_{150,0.75}$ (lb)	----	n/a	12,181	13,990
Residual Strength at L/600, $f_{150,0.75}$ (psi)	----	n/a	1,015	1,160
Residual Load at L/150, $P_{150,3.0}$ (lb)	----	n/a	4,416	9,882
Residual Strength at L/150, $f_{150,3.0}$ (psi)	----	n/a	370	825

Remarks:

1. All beams tested were 6” by 6” by 20” on 18” span.
2. No data for Plain 1 due to operator error.

3. Plain concrete beams tested in accordance with ASTM C-78
4. Steel fiber reinforced concrete beams tested in accordance with ASTM C-1609

2.5 Reinforcing Bar Tensile Strength

Reinforcing bars used in test beams were No. 3, deformed bars having nominal yield strength of 60 ksi. Actual average yield strength from tensile test was 97.7 ksi. Since the test was stopped at 2% strain, the ultimate stress and strain were not calculated.

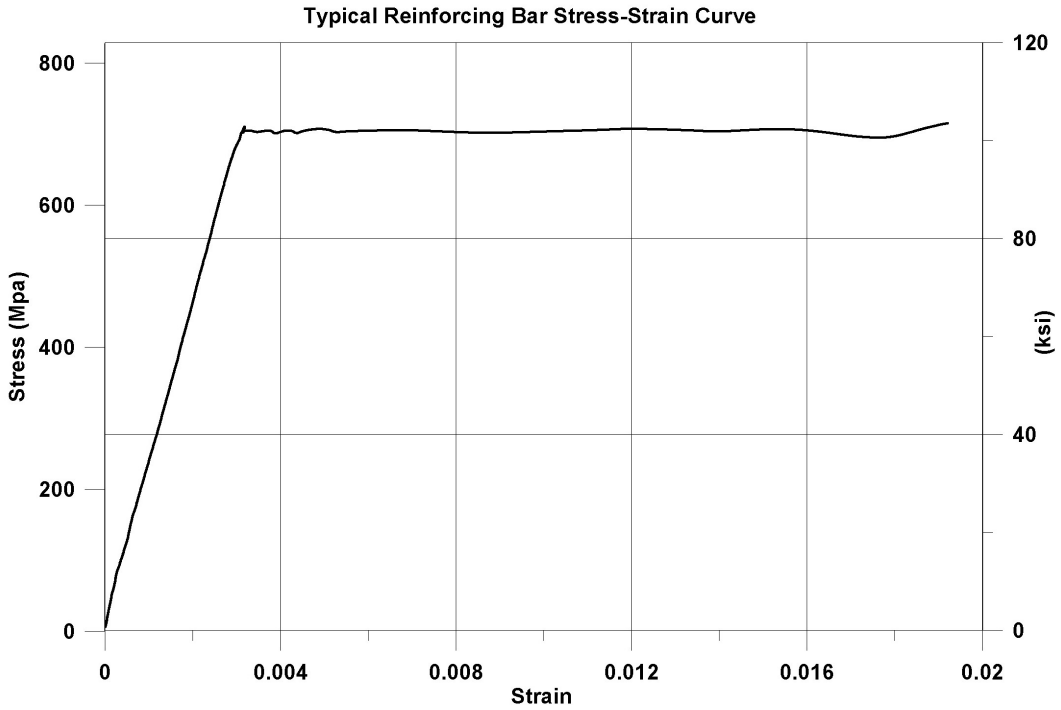

Figure 2-9 Typical stress-strain graph of reinforcing bars (No.3)

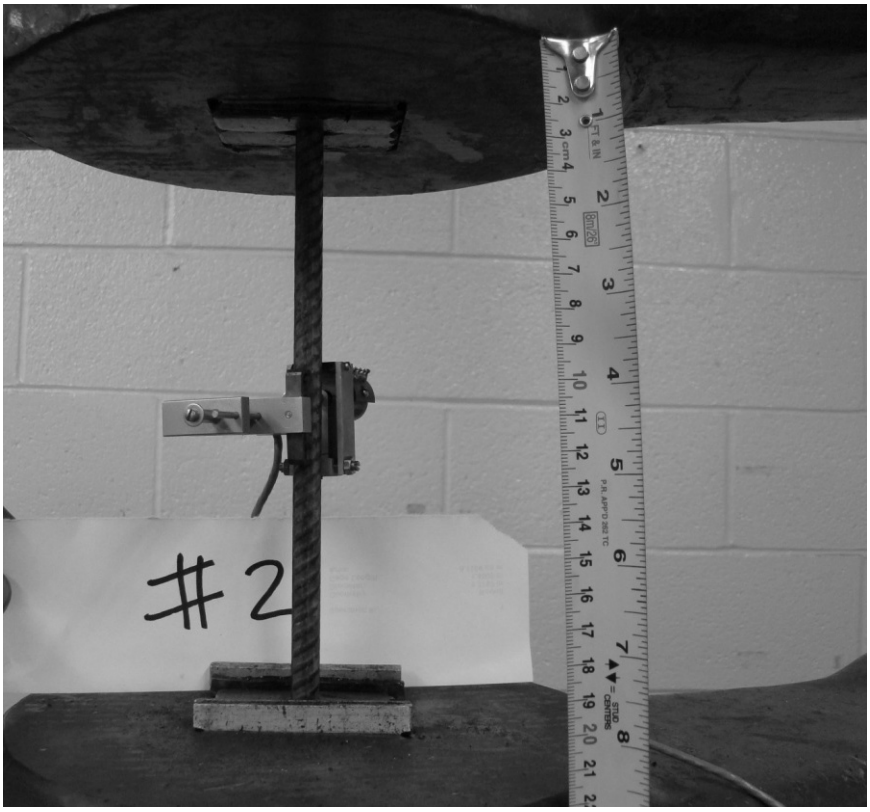

Figure 2-10 Typical reinforcing bar testing setup

CHAPTER 3

EXPERIMENTAL PROGRAM

3.1 Beam 1 – Conventional Reinforced Concrete

Beam 1 was a modification of the specimen tested by other researchers (Breña and Morrison, 2007). This test beam was approximately a one-quarter scaled beam based on landmark paper published by Schalaich, et al. in 1987. The beam is 74 in. long, 47 in. in. depth and 4.4 in. thick. There is a 15 in. by 15 in. opening near one of the reactions, interrupting the concrete compressive strength. A point load is applied on the side opposite to the end of the opening (see Figure 3-1).

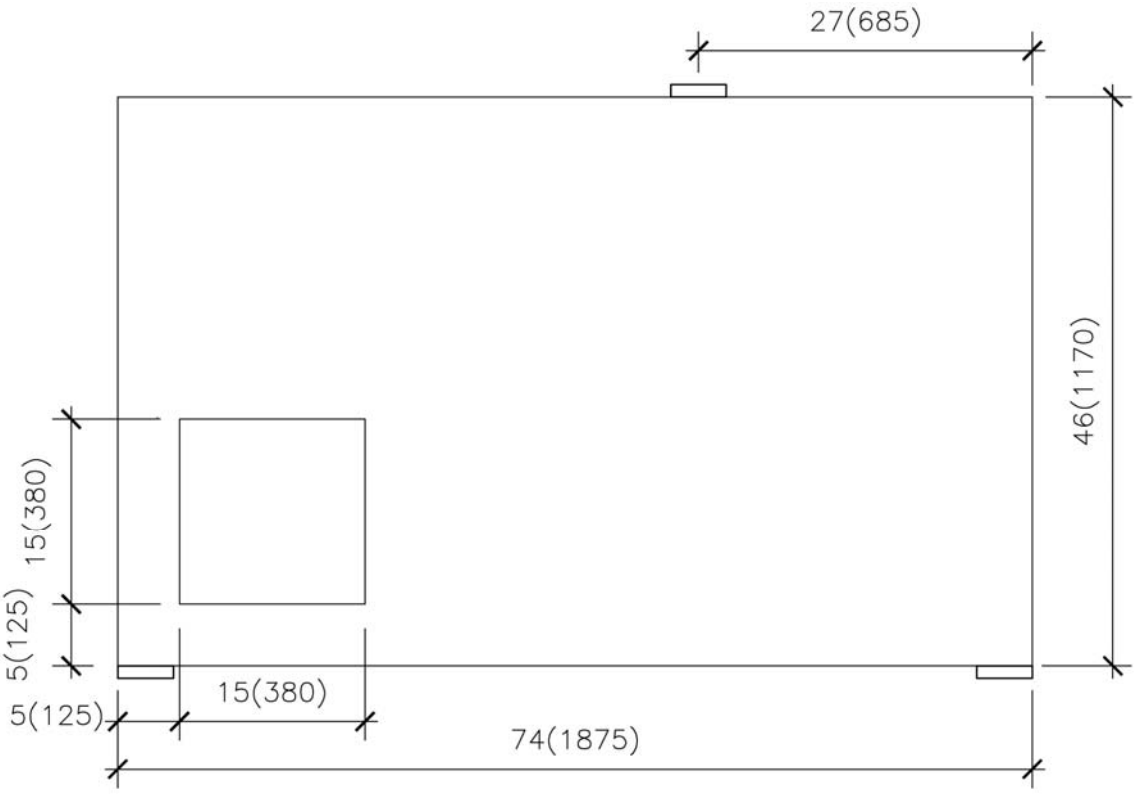

Figure 3-1 Geometry of beam with opening. Units in inches and (mm)

As mentioned previously in Chapter 1, beams with similar geometry have been used by other researchers. The testing performed by Breña and Morrison (2007) showed that STM yields conservative results. One significant modification in this study was that secondary reinforcement used for temperature and shrinkage cracking was not used in the RC specimen. This is due to the fact that the secondary reinforcement increased load capacity by 37%, up to 86%, as observed by Breña and Morrison (2007). Also, the same researchers concluded that ACI 318, Appendix A does not give guidance to provide confinement reinforcement in regions of high stress.

Figure 3-2 Rotary concrete mixers. Two batches were made per mixer for each test

The concrete mixture with a nominal 28-day expected compressive strength f'_c equal to 5,000 psi was used. The measured compressive strength was 6185 psi at the day of testing, 35-days after casting. The maximum aggregate size used was ½ in. Concrete mixing was done using two 9 cubic foot concrete mixers. Two batches were mixed per mixer for each beam. Consolidation was accomplished using a concrete vibrator with a 9 in. head as concrete was

placed in the form (see Figure 3-7). All cast fresh concrete was covered with a sheet of polyethylene for 24 hours for curing, along with the ASTM beams and cylinders. ASTM beams and cylinder were demolded within 48 hours.

Standard No. 3 rebar having nominal area of 0.11 in^2 was placed within the wood form leaving approximately 1 in. cover on each side. Anchorage was accomplished with standard hooks in the beam's longest directions (see Figure 3-3) which were needed for development. This was based on the suggestion by Breña and Morrison (2007).

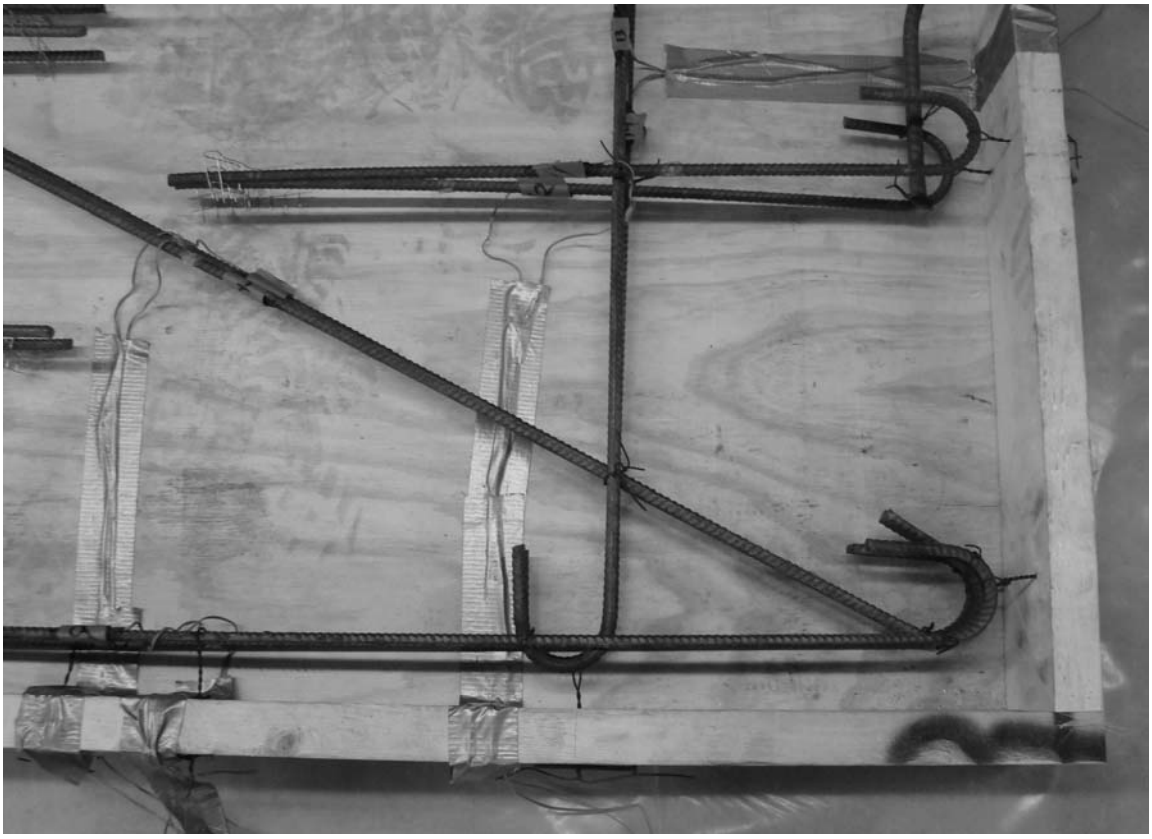

Figure 3-3 Reinforcing steel detail at right support. Note strain gages bonded to steel bars

Internal strain gages were carefully affixed to the reinforcing bars to record tie strains. The beam was cast horizontally on the ground. Two rebar hooks were also cast on the face of the beam to facilitate hoisting the beam into position (see Figure 3-5). Secondary reinforcement was not used due to reason discussed previously.

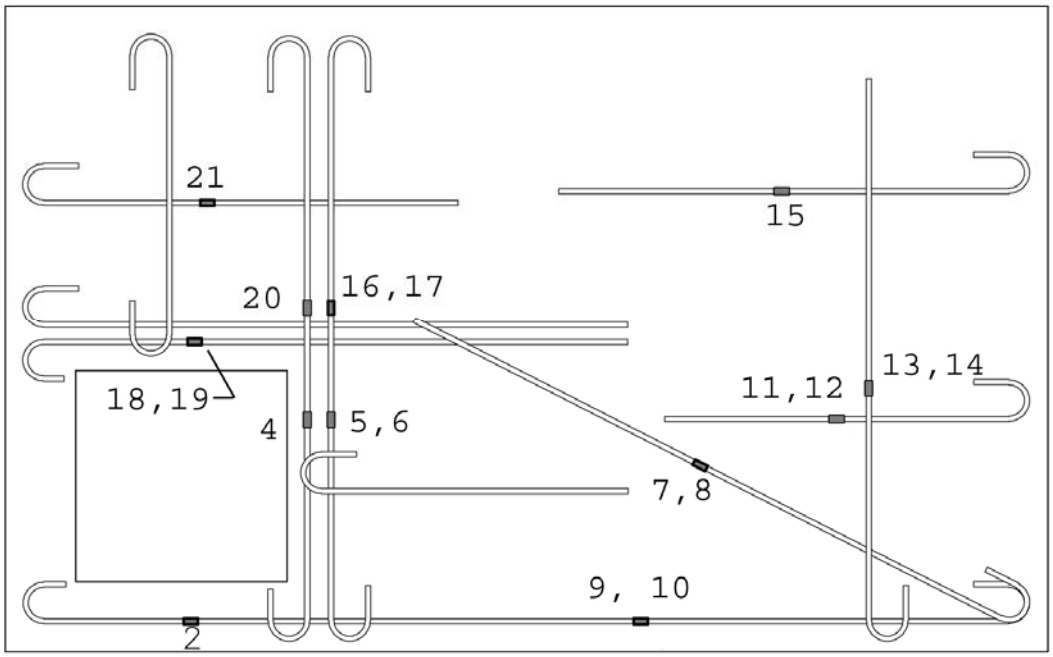

Figure 3-4 Reinforcement layout of RC specimen. Numbers indicate strain gage number

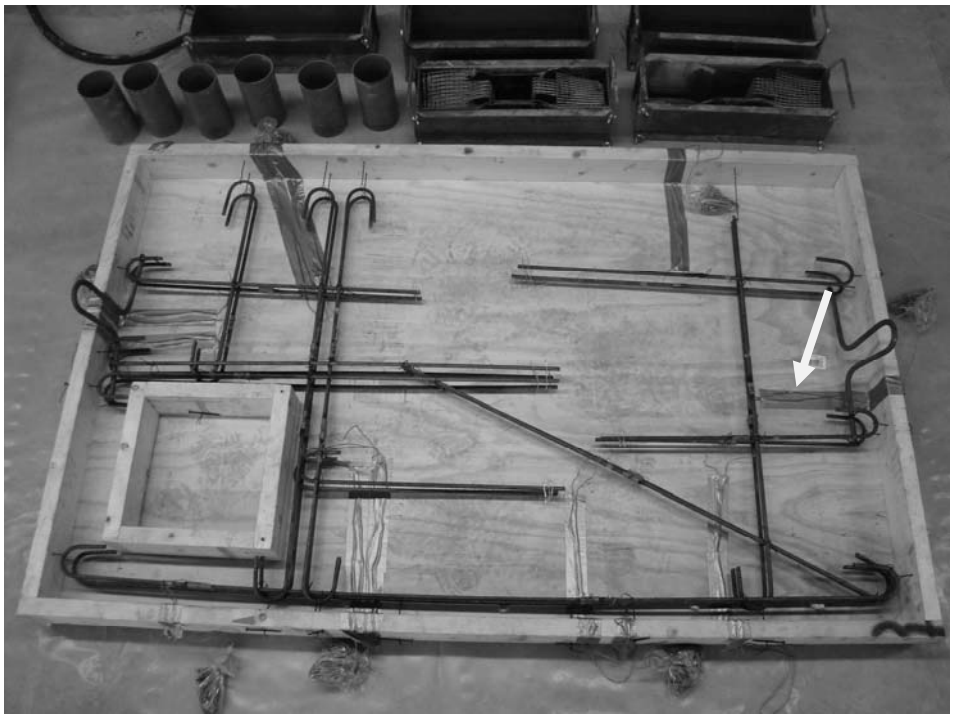

Figure 3-5 RC test specimen and material testing forms before casting. Arrow shows rebar hooks cast for lifting purposes

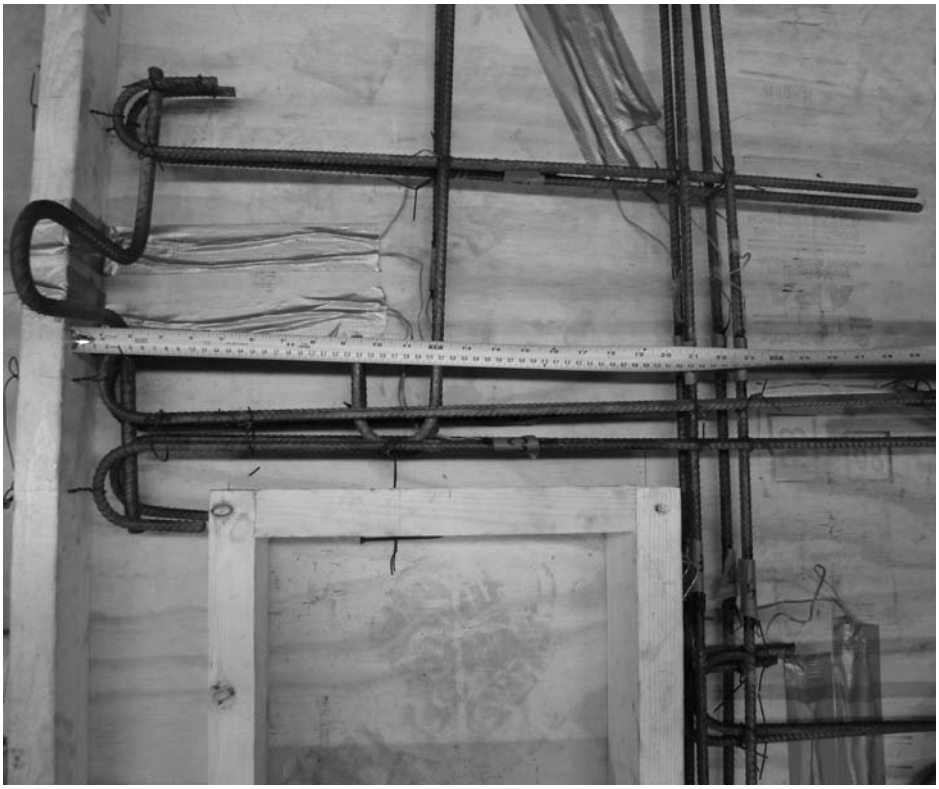

Figure 3-6 Detail of reinforcement above opening

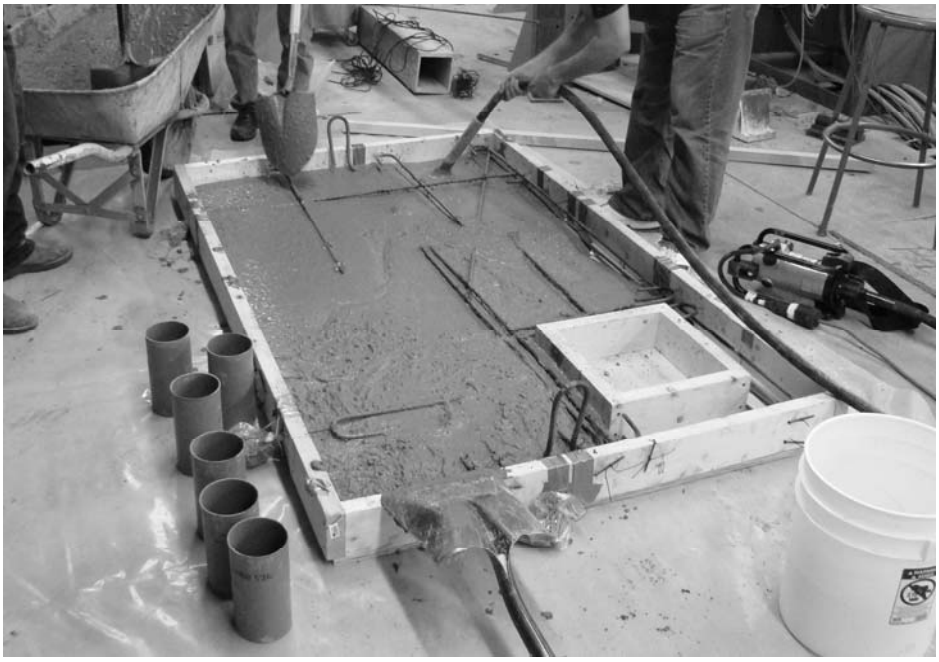

Figure 3-7 RC specimen during placing and consolidation of plastic concrete

3.1.1 Instrumentation

The performance of the two specimens required precise electrical instrumentation to be recorded and latter analyzed. The instrumentation consisted of strain gages to monitor reinforcing steel strains. Linear Variable Differential Transducers (LVDTs) were used to measure concrete strains. Potentiometers were used to calculate the maximum net deflection. Finally, Acoustic Emission (AE) was used to help identify internal crack formations that were not visible to the naked eye under loading. Except for AE, which had its own computer, all instruments were connected to a data acquisition system and connected to a computer for storage.

(a) (b)

Figure 3-8 Data acquisition system (a) and scanner box (b)

3.1.1.2 Strain Gages

Post-yield strain gages having a gage length of 5 mm. were affixed to the rebar after carefully leveling the surface enough to obtain a flat surface for the strain gage. Attention was given so that the bar cross sectioned was not reduced (see Figure 3-9b). The ground surface was thoroughly cleaned and neutralized to ensure proper bonding. After adhesive dried, the strain gages were covered with thin plastic rubber to protect it during concrete placing (see Figure 3-9c).

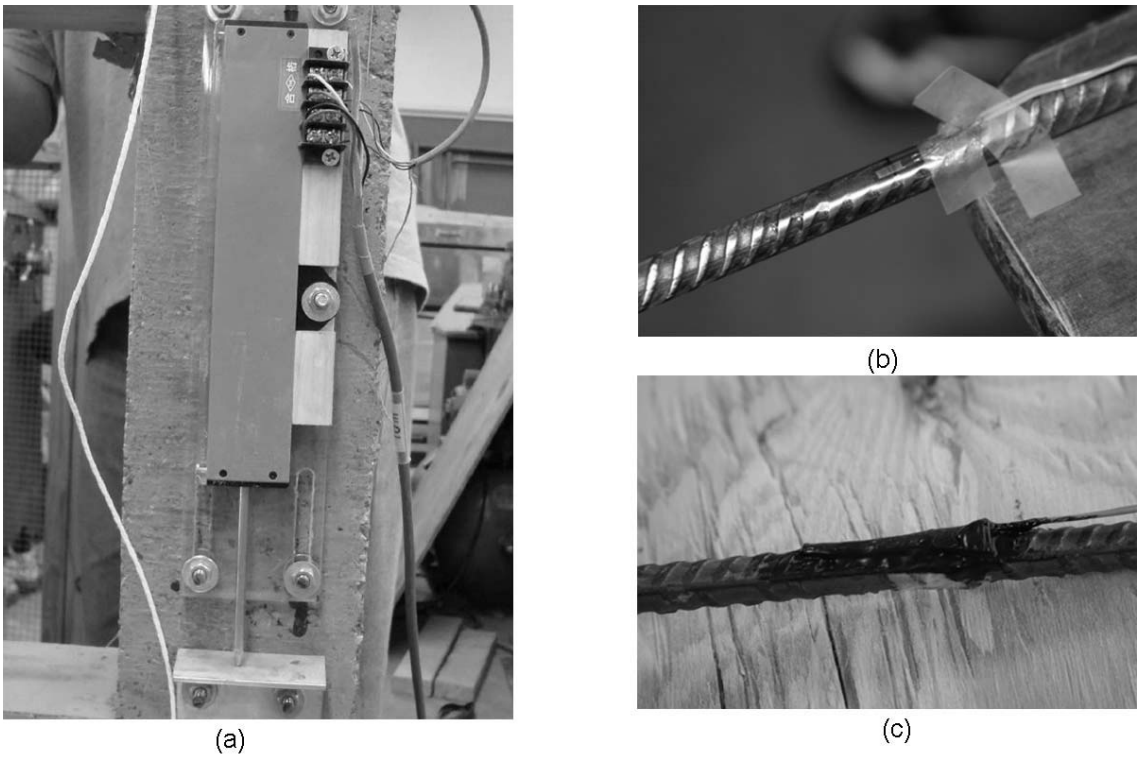

Figure 3-9 Typical LVDT used to measure concrete strains during monotonic testing (a) Typical strain gage bonded to reinforcing bar (b) and after protective coating (c)

Linear Variable Differential Transducers (LVDTs) were installed to measure concrete deformations as load was applied (see Figure 3-9a). LVDTs were located to monitor deformation in areas susceptible to concrete crushing, namely in the support areas. Also, LVDTs were positioned in the concrete strut regions (see Figure 3-15 for LVDT locations). All LVDTs were connected to a data acquisition system. A total of 24 internal strain gages and 4 LVDTs were used.

3.1.1.4 Acoustic Emission

Acoustic Emission (AE) is a non-destructive evaluation method, was used to measure crack propagation. Acoustic emission uses sensors that detect acoustic waves created during cracking. It served as a very valuable tool, as it allowed analysis of energy dissipation in the form of crack formation, crack propagation and reinforcing slippage and yielding (Colombo, et. al, 2003). AE sensors were bonded with hot glue to the surface of the RC and SFRC specimens before testing (see Figure 3-13). A total of 7 sensors were used, each having a radius of

influence of approximately 30 in, as determined by the so-called lead pencil break test. This test consists of breaking a 0.3 mm in steps to determine the effective radius of influence. Beyond this radius of influence, the system does not detect signals. These sensors were connected to a central scanner box with in-line pre-amplifiers. The pre-amplifiers were set at 40 dB boost, which was determined before testing that this setting was most effective on eliminating unwanted noise associated with loading the concrete specimen. A computer was used to store the data from AE during testing (see Figure 3-11). The shear wave velocity was calculated as 1.10×10^5 ft/s for reinforced concrete. This was done by recording the time between the detection of two sensors and dividing by the known distance between the sensors (see Figure 3-10).

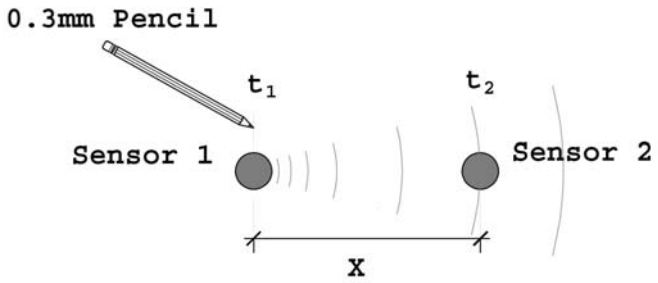

Figure 3-10 Method to determine shear wave velocity

$$v = \frac{x}{\Delta t} \qquad \text{(Eq. 3-1)}$$

where:

v = shear wave velocity (ft/sec)

$\Delta t = t_2 - t_1$ (s)

x = distance (in.)

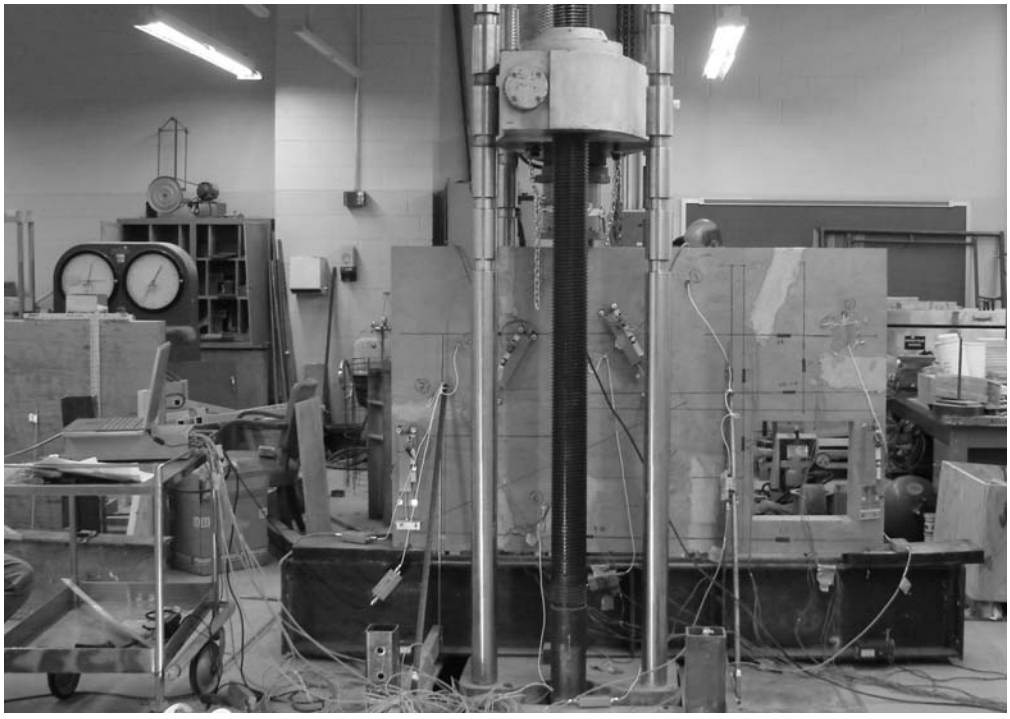

Figure 3-11 Lab setup for specimen testing showing AE data acquisition system on left

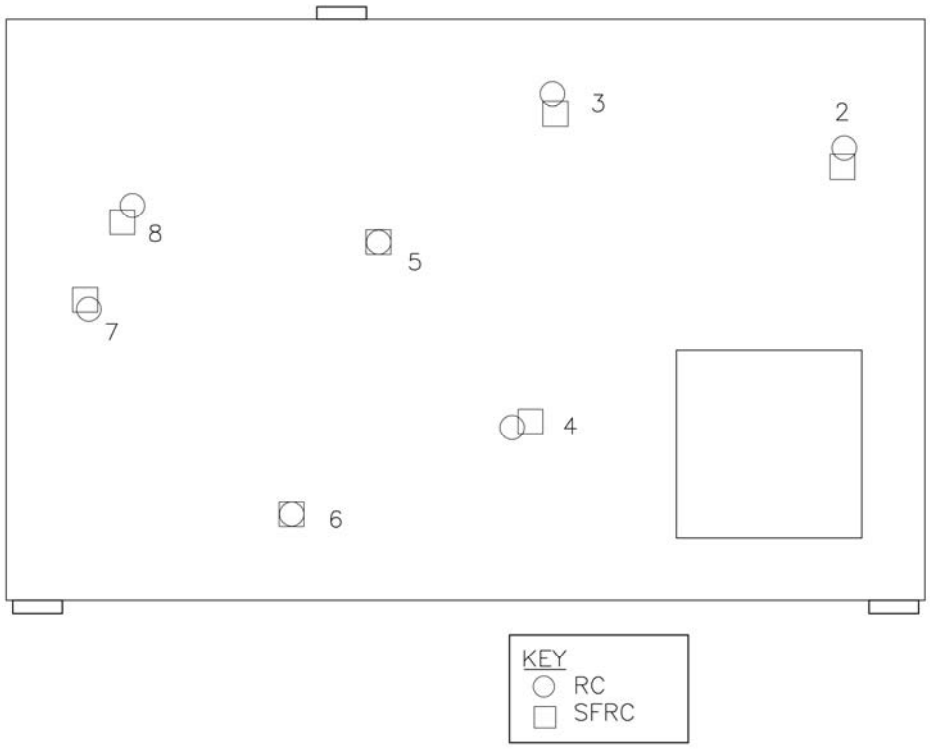

Figure 3-12 Location of AE sensors – back face

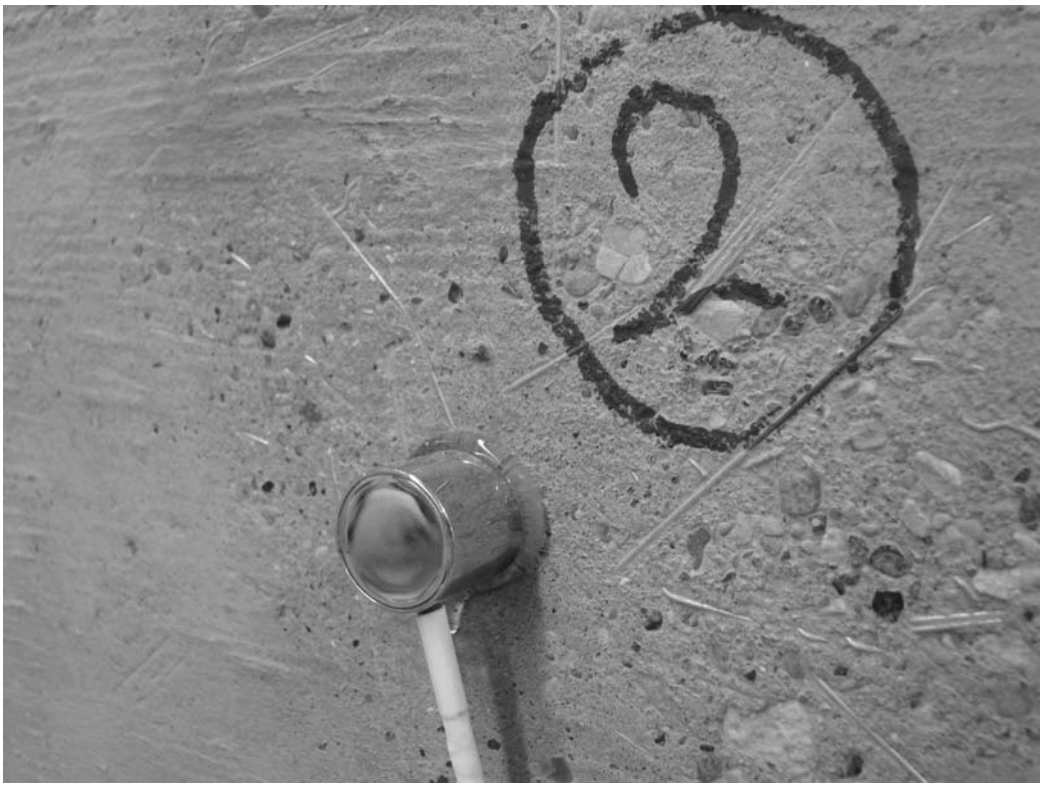

Figure 3-13 Typical AE sensor bonded to test specimen

The point load consisted of a 11 in. diameter by 1 in. thick round steel plate which held the load cell. This bears onto a rectangular bearing plate 5 in. by 1 in. thick which was grouted to the beam to ensure no eccentricity and alignment (see Figure 3-15)

The large beams were demolded and placed vertically. The STM was drawn on one side and the reinforcement layout on the other face of the beam (see Figure 3-14).

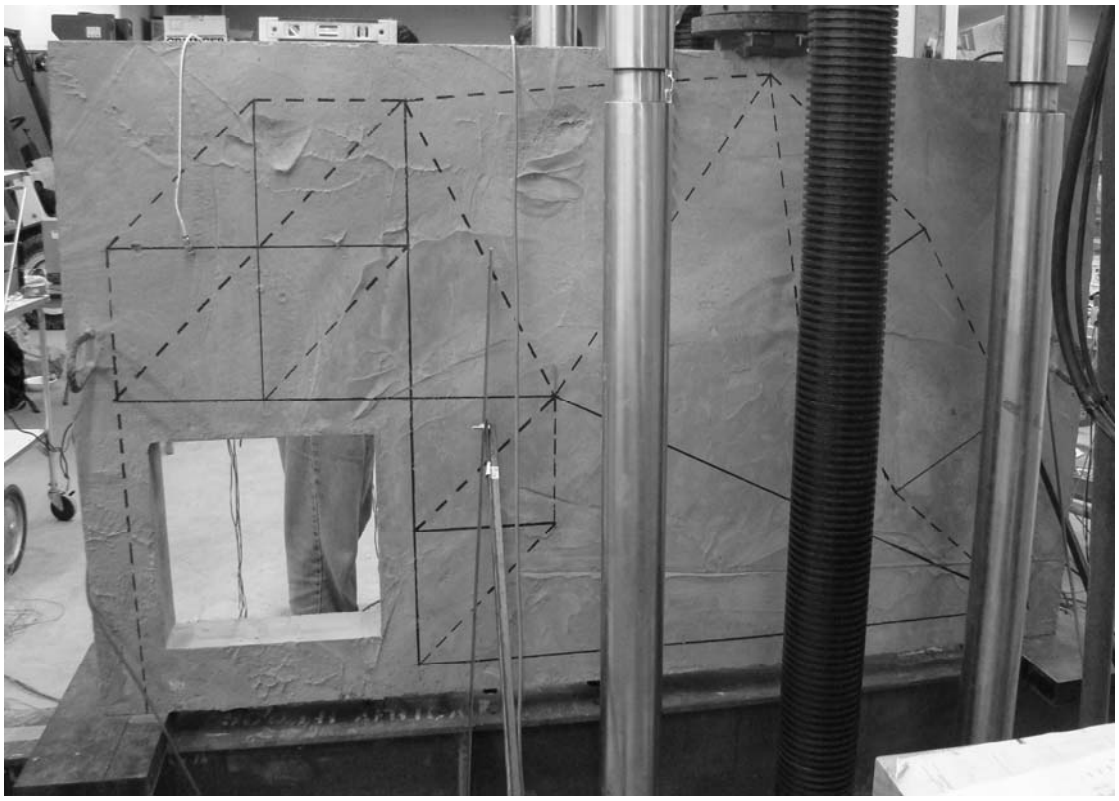

Figure 3-14 STM model marked on RC specimen's front face

Linear potentiometers were placed directly under the loading point, 23 in. from the top of the beam to measure displacement under load, and at the reactions to calculate the deformation of the supports. The deflection of the supports was subtracted from the deflection under the loading to obtain the net deflection under the support (see Figure 3-15 for locations).

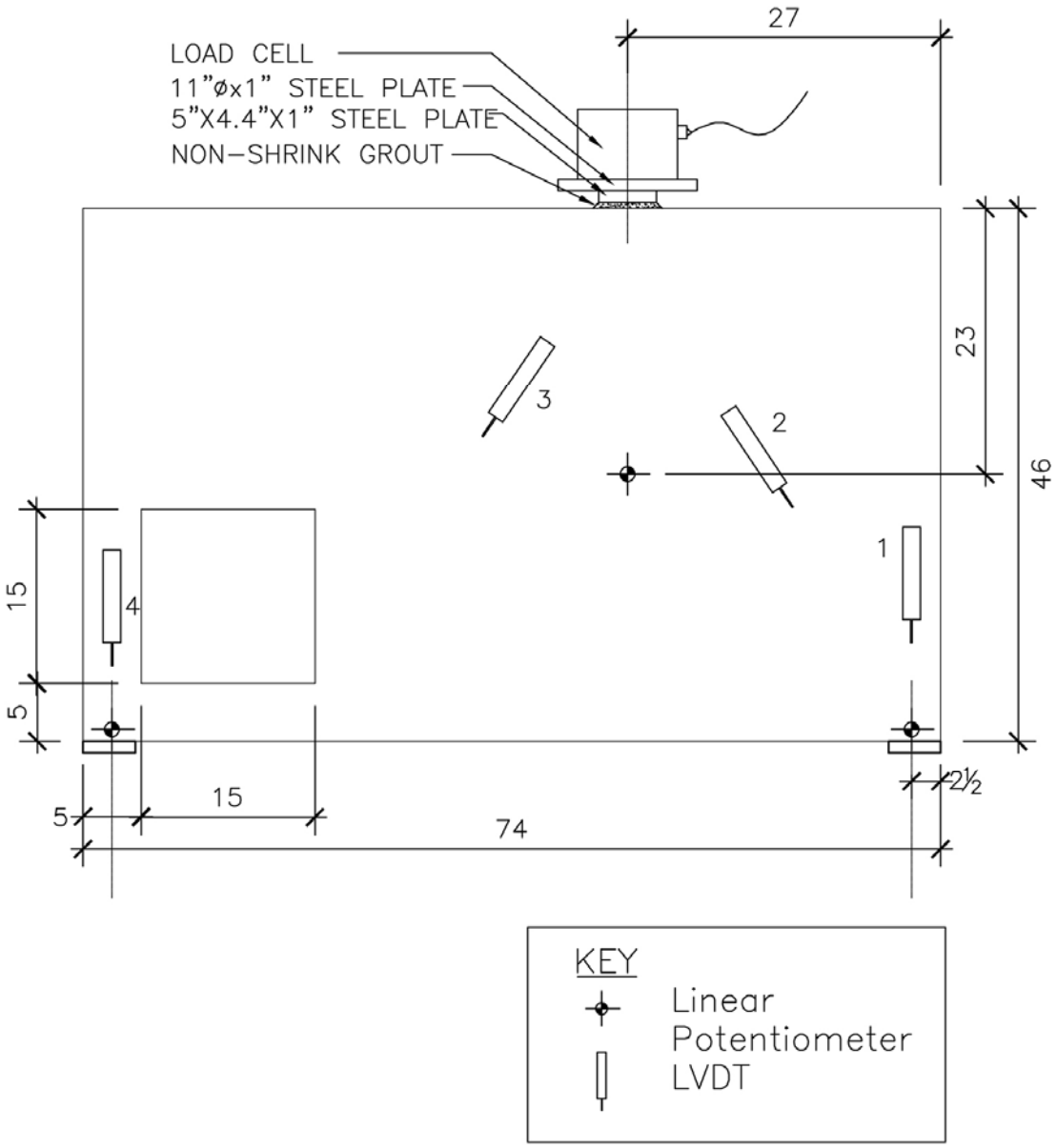

Figure 3-15 Instrumentation of beams. Units in inches

Test specimens were tested using a 400 kips universal testing machine with monotonic loading (see Figure 3-11). The support conditions consisted of 2 in. thick neoprene bearing pads with a bearing length of 5 in. on each side (see Figure 3-16). The test specimen was placed on top of a steel spreader beam that transferred the load to the base of the testing machine.

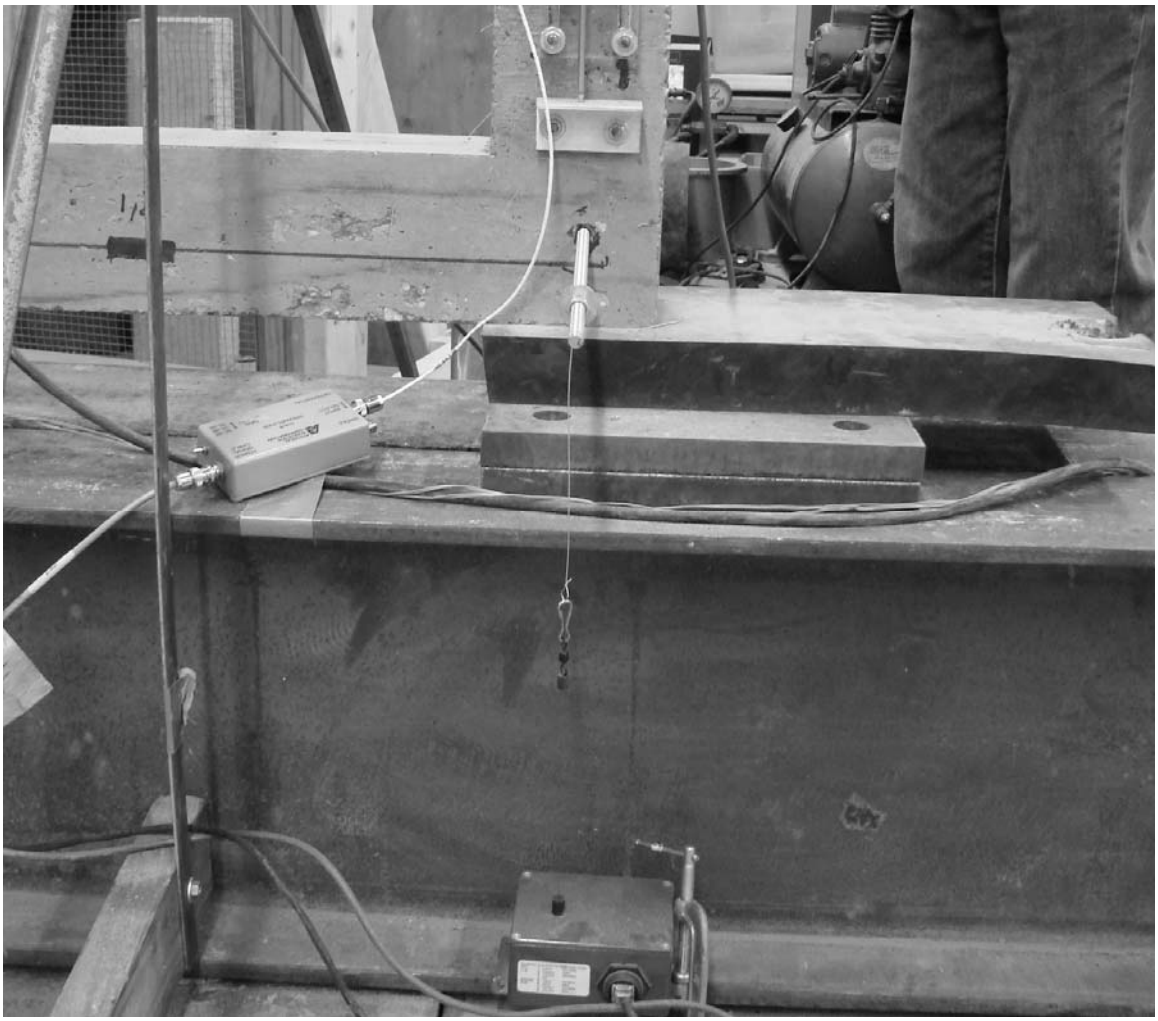

Figure 3-16 Typical support condition showing bearing pad and threaded rod attached to linear potentiometer below. The device shown on the left is the AE pre-amplifier

3.2 Test Results – Conventional Reinforced Concrete

3.2.1 Observed Cracking - RC Specimen

Loading was stopped at 5 kips intervals to document crack propagation and width. The first crack appeared on the right support(support closest to loading point) at 25 kips. At 35 kips, a small spall was formed on the right support. Diagonal cracks started to appear at 35 kips. These cracks generally grew as load continued to be applied. A popout of concrete was created on the left and right support at 40 kips and 45 kip, respectively. At 35 kips, a small portion of the right support separated from the beam. At 60 kips same region had larger pieces of concrete

separated (see Figure 3-19). The crack from the top left corner of the opening running to the loading point opened to 0.40 mm at 65 kips. Other diagonal cracks formed in the 50-65 kips load range. At 70 kips, flexural cracks formed under the point of load. One crack formed running almost the full width of the beam, followed by a smaller crack on each side. The long crack measured 0.40 mm and the two shorter cracks measured 0.10 mm. At this point, the beam became unstable due to the severe damage at the support regions and testing was stopped.

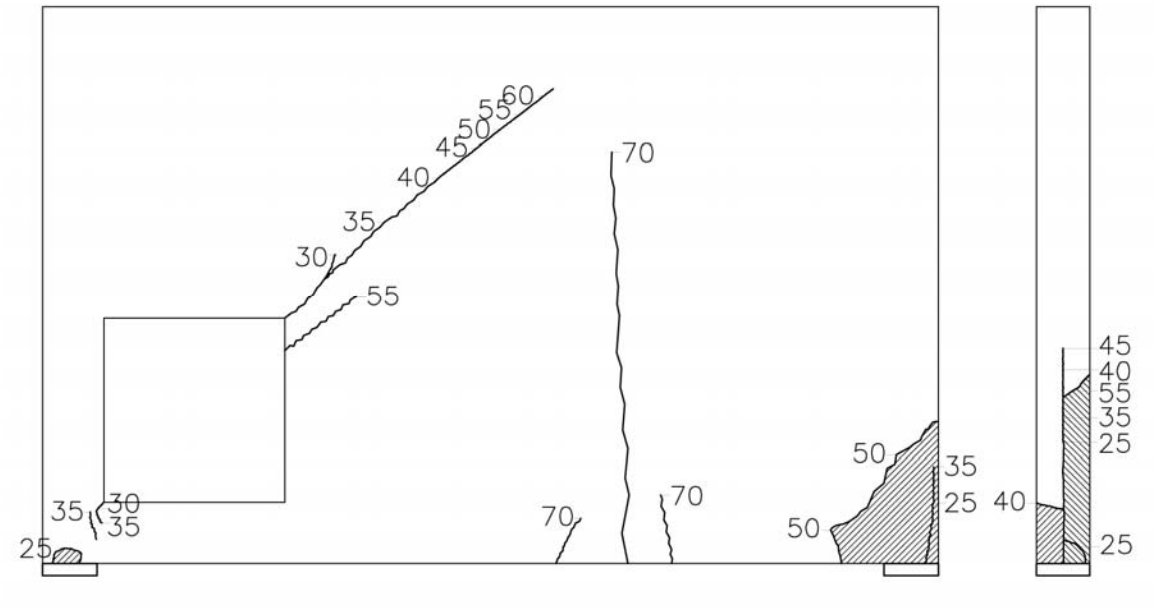

Figure 3-17 RC specimen cracks – front face. Numbers indicate loading steps in kips (shaded areas indicate spalling)

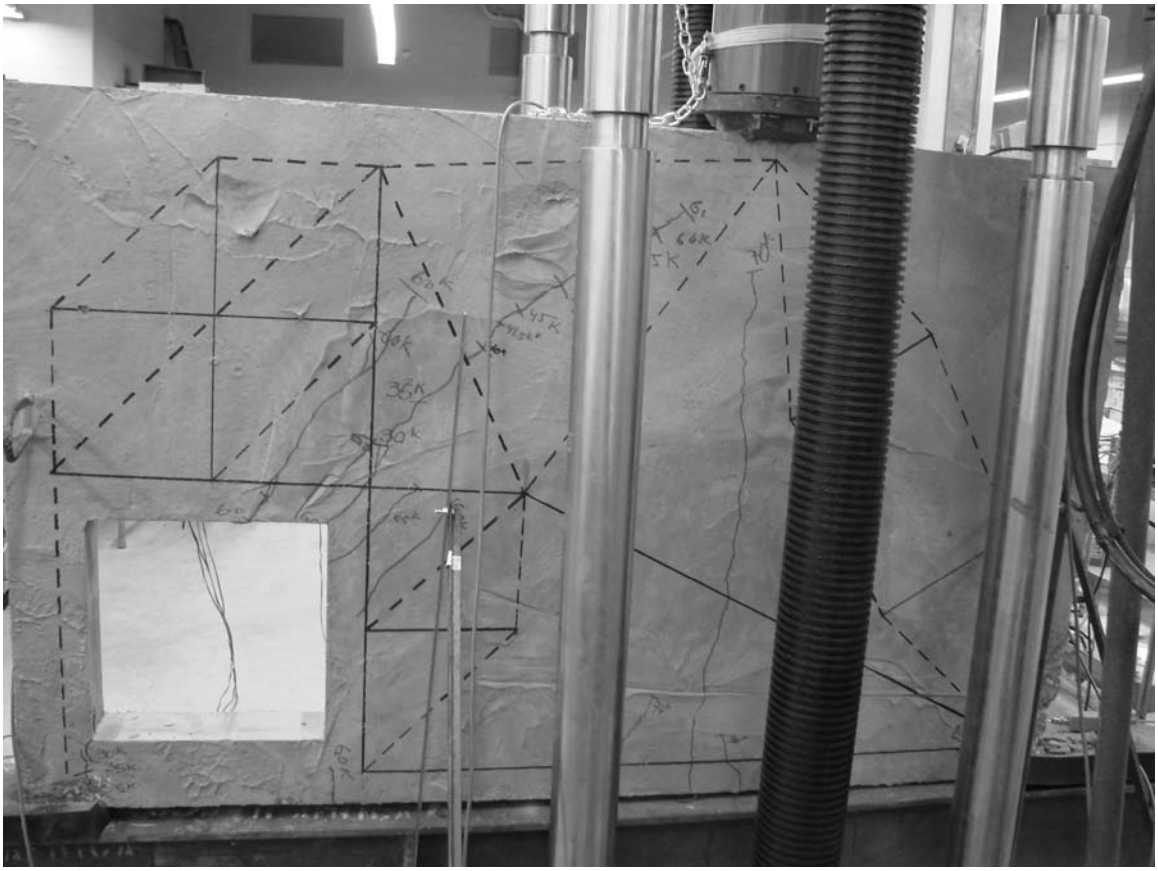

Figure 3-18 RC specimen at 70 kip – front face

Figure 3-19 Right support of RC test specimen at 60 kip

3.2.2 Load-Deflection Response

As previously mentioned, there were several blowouts at the supports of the RC specimen during the loading stages. This caused the instrumented threaded rod to break lose from the supports at 25 kips and 45 kips, for the right and left support respectively. As a result, the data acquisition system was unable to record data beyond this loading. Therefore, a net displacement graph was now plotted. However, the gross displacement under the load is presented here to graphically illustrate the load-displacement response under the point load (see Figure 3-20).

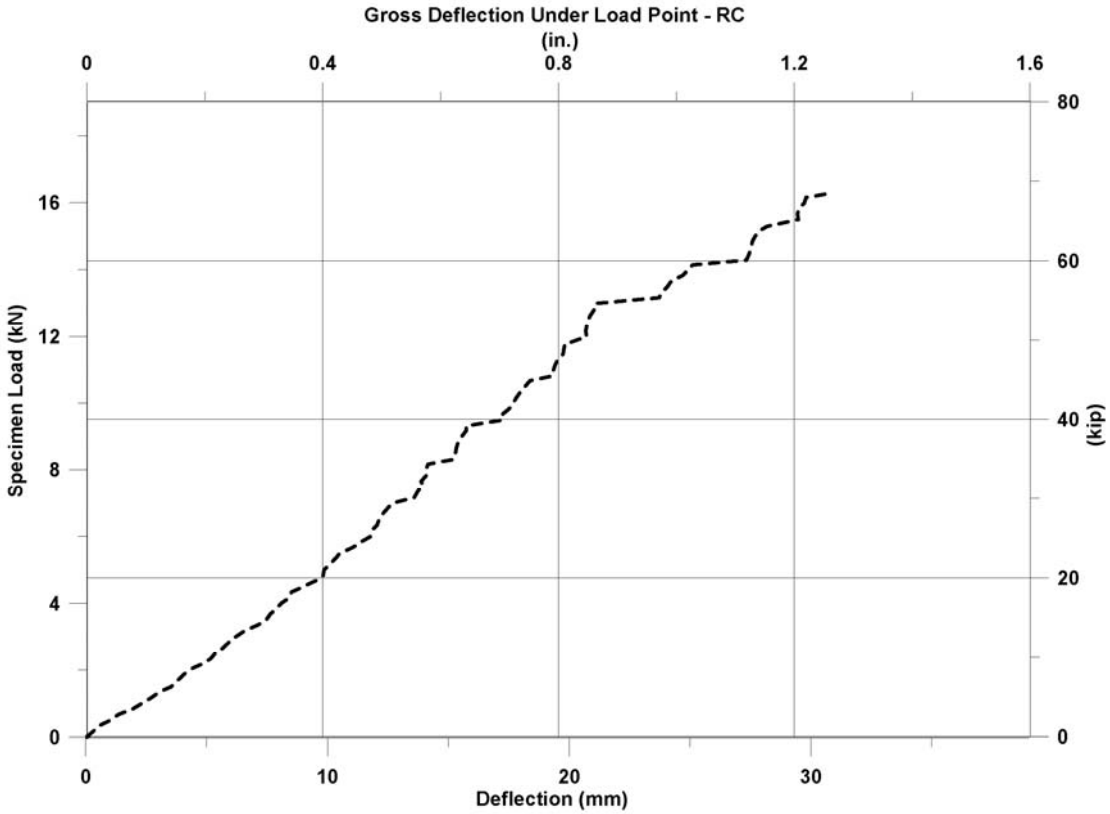

Figure 3-20 Gross load – displacement response for RC specimen under loading point

This load-displacement plot shows a linear response up to 55 kips. Since this is the gross load-deflection plot and not the net load-displacement plot, this reference is for the general response and not for the actual magnitude of the deflection.

3.2.3 Concrete Strains

Concrete strains recorded showed a linear behavior up to 10 kips. Concrete strain measured by LVDT 1, 2, and 3 were 250×10^{-6} in/in (deformation measured/gage length) at ultimate. The strain measured by LVDT 4 increased rapidly between 20 and 40 kips. It increased slightly up to 60 kips, where strain was recorded at 0.00125 in/in. It suddenly became negative (see Figure 3-21). This was due to the support being split and one side taking load while the other unloaded and actually settled so that the concrete was literally stretched after being compressed.

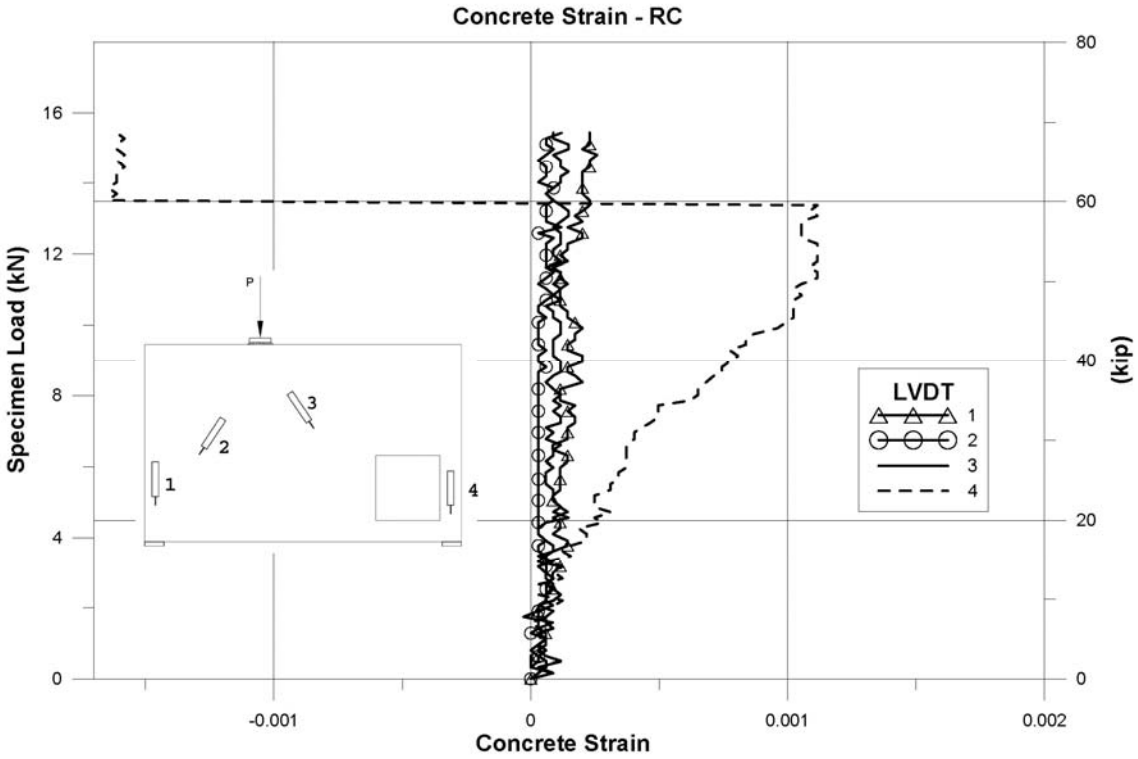

Figure 3-21 Concrete stains in R/C concrete (compression shown as positive, tension shown as negative)

3.2.4 Reinforcing Steel Strain

Reinforcing steel strains related the tie forces to the applied force. The tie at the bottom of the specimen showed the largest force. Strain gage 10 recorded the largest strain during testing. Strain gages 11, 12 and 13 (see Figure 3-23 and Figure 3-24) deformed about 0.0001 at ultimate strength. These are very small strains in spite of the forces generated by the strut and tie model. It is important to note that most reinforcing bars deformed the same amount in the same location. Strain gages 9 and 10 have nearly identical load-deformation curves (Figure 3-23). This is not the same, however, for all strain gage pairs. This phenomenon is due to unequal force sharing by the reinforcing bars. The test specimen split nearly in half in the long direction on the left support at 25 kips. This crack widened as load was increased; eventually large pieces of concrete broke lose and separated in this region at 60 kips (Figure 3-19). The crack forced bars on one layer of reinforcement to take larger forces than the other. Strain gage

13 and 14 had maximum strains at about .0001 and 0.002 in/in, respectively. Strain gage 13 was placed on top layer of reinforcement, while strain gage 14 was placed on the bottom layer.

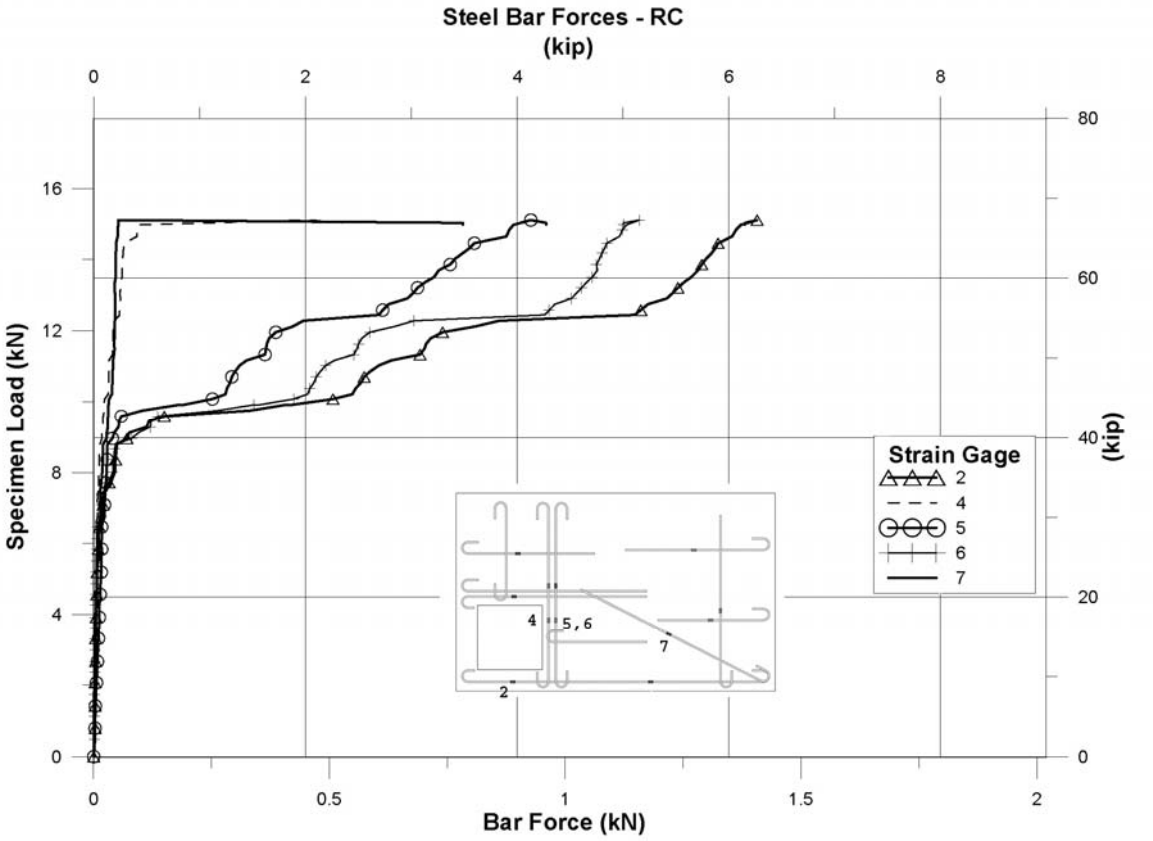

Figure 3-22 Reinforcing bar force in RC specimen (strain gage 2-7)

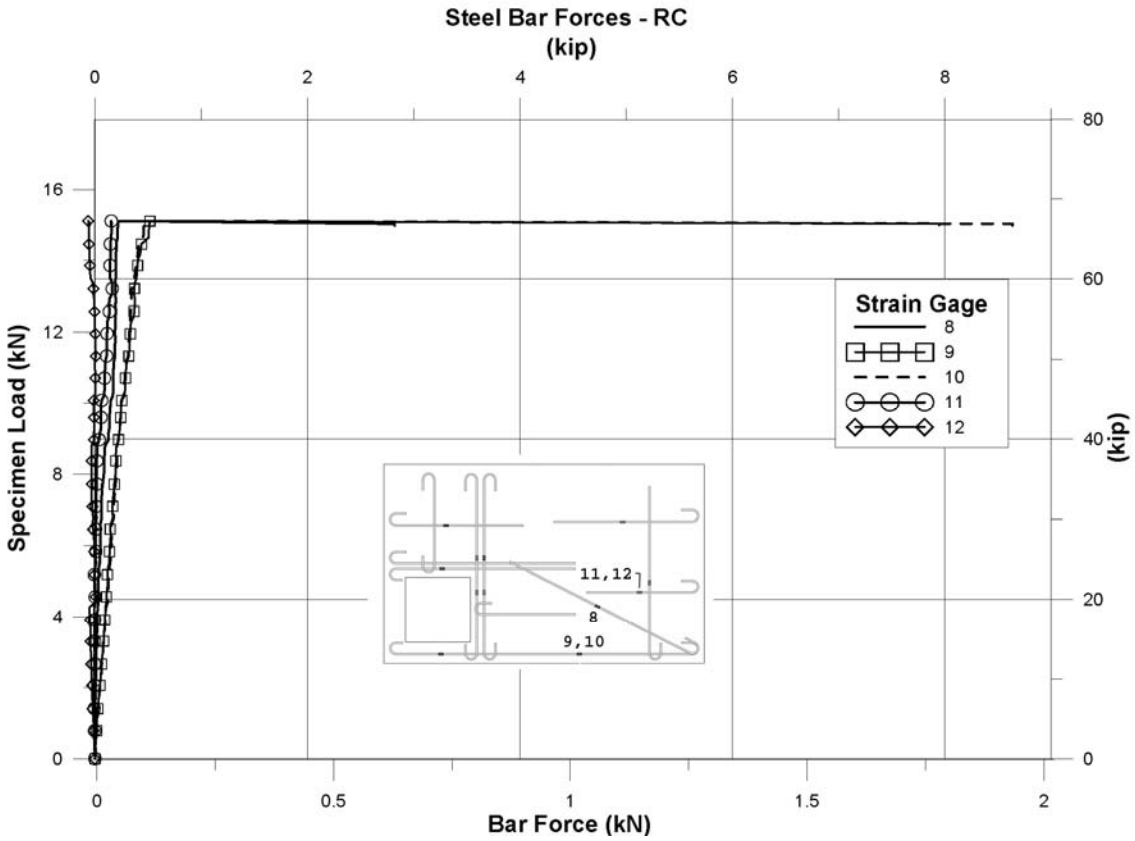

Figure 3-23 Reinforcing bar force in RC specimen (strain gage 8-12)

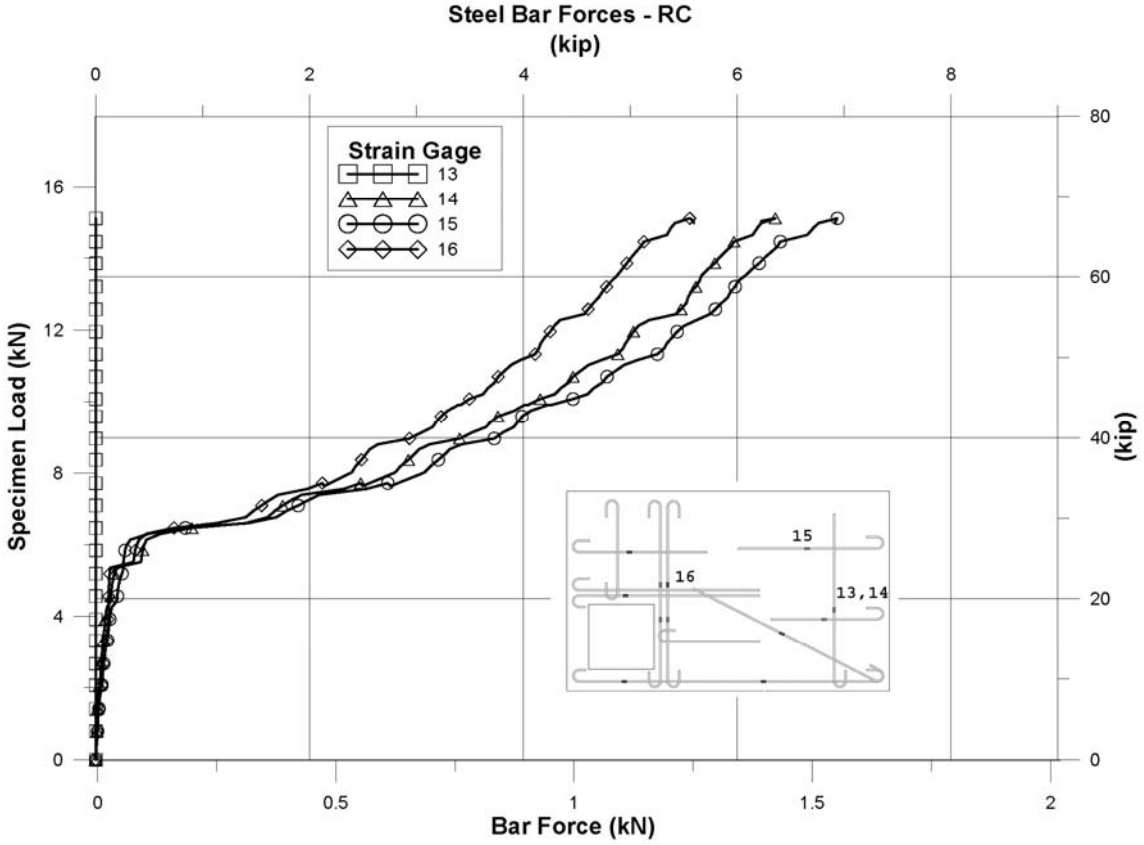

Figure 3-24 Reinforcing bar force in RC specimen (strain gage 13-16)

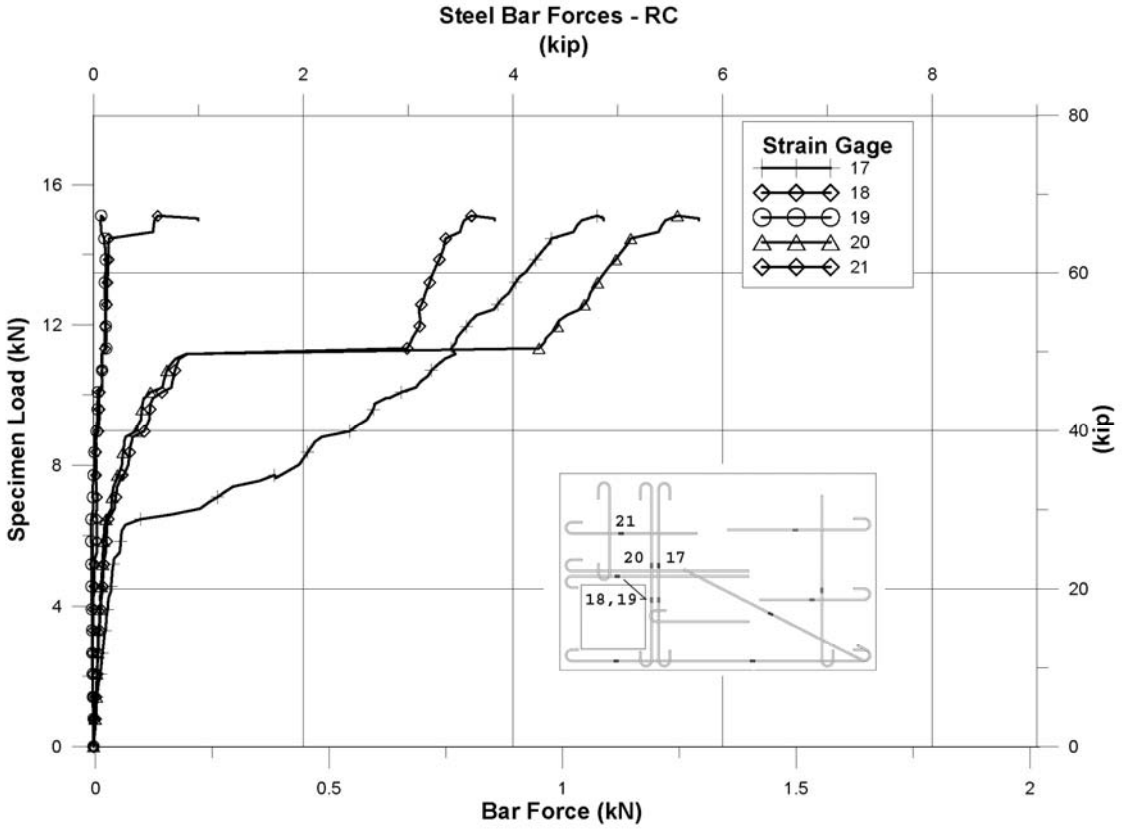

Figure 3-25 Reinforcing bar force in RC specimen (strain gage 17-21)

The next two tables represent the tabulated measured forces compared to the forces found from analysis. Table 3-1 compares the forces measured in the specimen compared to the design load of 31.3 kips. Table 3-2 compares the measured forces in the specimen when testing was terminated at 70 kips to the predicted forces from analysis.

Since some ties were not instrumented with strain gages at every steel bar, the measured strain was assumed to be the same in the next adjacent bar (eg. The vertical tie to the right of the opening's strain was the sum of strains from strain gage 5 and 6 plus two times the strain measured in strain gage 4). Otherwise, the total tie force is the summation of each individual bar force (eg. The tie on the bottom of the opening's strain is two times the measured strain from strain gage 2). Use Figure 3-25a and Figure 3-25b with Table 3-1 and Table 3-2.

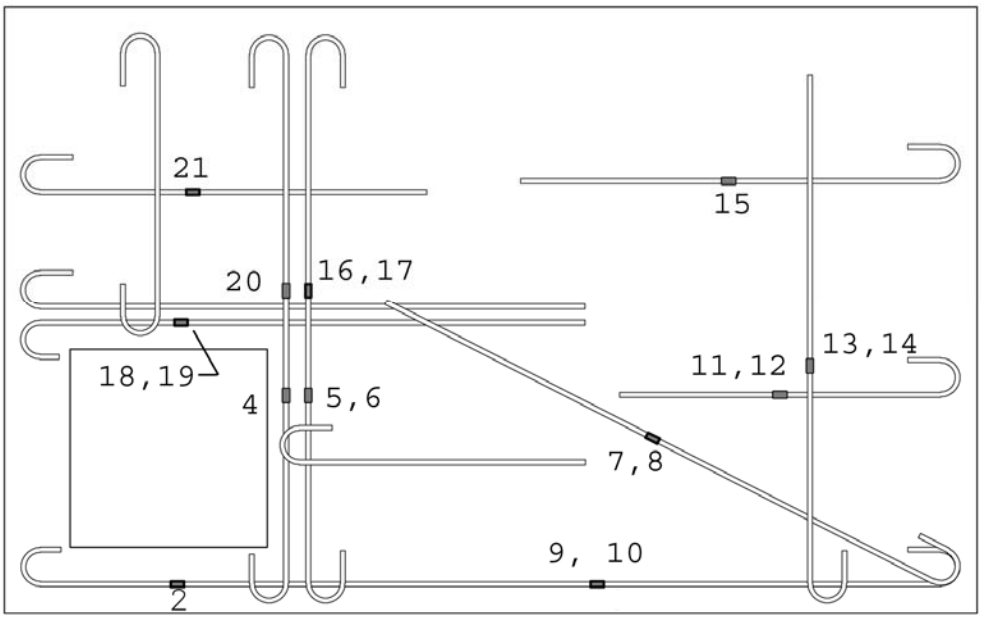

(a)

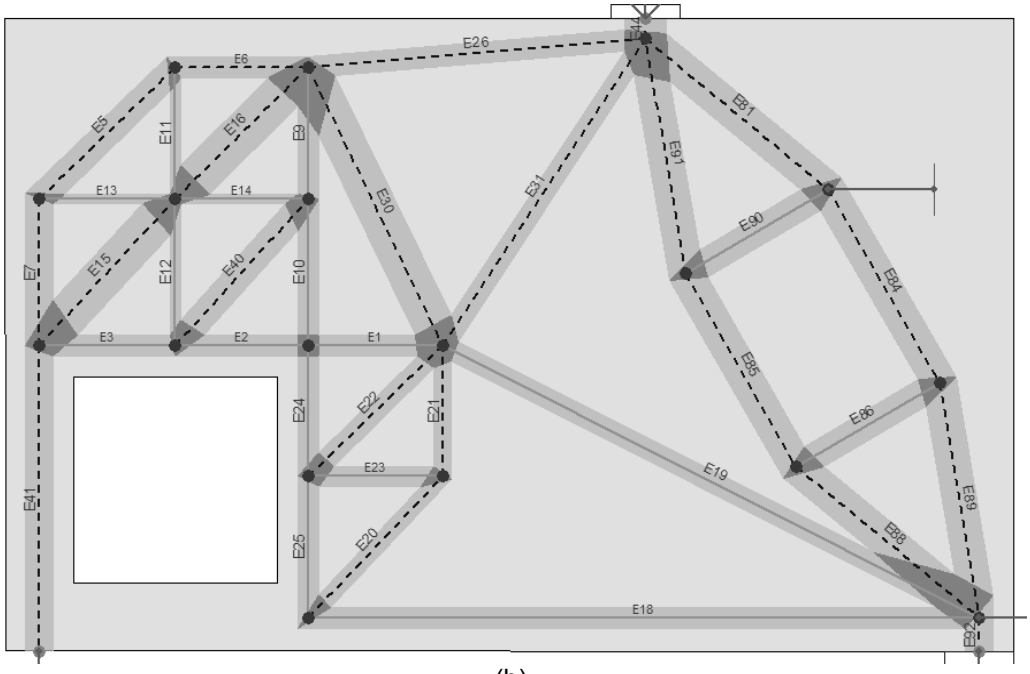

(b)

Figure 3-26 Location of strain gages (a) and STM element identification (b)

Table 3-1 Tie forces at predicted design specimen capacity – RC

(1) Tie ID	(3) Strain Gage	(4) Bar Area, in^2	(5) $Calc_0$:Tie Force from Analysis (kip)	Tie force at design capacity				
				(6) Strain (in/in)	(7) Stress (ksi)	(8) Force per bar (kip)	(9) Total $Force_0$ (kip)	(10) $Force_0$/ $Calc_0$
*	2*	0.11	-	0.00001	0.336	0.04	0.07	-
E24	4	0.11	11.43	0.00003	0.824	0.09	0.36	0.03
	5	0.11		0.00003	0.967	0.11		
	6	0.11		0.00002	0.644	0.07		
E19	7	0.11	9.83	0.00002	0.559	0.06	0.13	0.01
	8	0.11		0.00002	0.584	0.06		
E18	9	0.11	5.72	0.00005	1.541	0.17	0.35	0.06
	10	0.11		0.00006	1.640	0.18		
E86	11	0.11	5.36	0.00000	0.112	0.01	-0.01	0.00
	12	0.11		-0.00001	-0.209	-0.02		
*	13*	0.11	-	-0.00001	-0.351	-0.04	1.71	-
	14*	0.11		0.00055	15.886	1.75		
E90	15	0.11	5.16	0.00059	17.187	1.89	3.78	0.74
E10	16	0.11	11.43	0.00049	14.082	1.55	2.80	0.25
	17	0.11		0.00037	10.751	1.18		
	20	0.11		0.00001	0.294	0.03		
E2	18	0.11	10.02	0.00000	-0.056	-0.01	0.34	0.03
	19	0.11		0.00006	1.610	0.18		
E14	21	0.11	4.31	0.00007	1.945	0.21	0.43	0.10

Table 3-2 Tie forces at specimen ultimate load during testing - RC

(1) Tie ID	(3) Strain Gage	(4) Bar Area, in^2	(5) $Calc_u$:Tie Force from Analysis (kip)	Tie force at testing ultimate				
				(6) Strain (in/in)	(7) Stress (ksi)	(8) Force per bar (kip)	(9) $Force_{uf}$ (kip)	(10) $Force_{uf}$/ $Calc_u$
*	2*	0.11	-	0.00077	22.28	2.45	4.90	-
E24	4	0.11	25.58	0.00200	57.97	6.38	20.42	0.80
	5	0.11		0.00138	40.12	4.41		
	6	0.11		0.00164	47.42	5.22		
E19	7	0.11	22.0	0.00096	27.73	3.05	5.42	0.24
	8	0.11		0.00074	21.57	2.37		
E18	9	0.11	12.79	0.00240	69.64	7.66	15.75	1.23
	10	0.11		0.00254	73.53	8.09		
E86	11	0.11	11.98	0.00005	1.45	0.16	0.12	0.01
	12	0.11		-0.00001	-0.36	-0.04		
*	13*	0.11	-	0.00003	0.93	0.10	6.50	-
	14*	0.11		0.00201	58.17	6.40		
E90	15	0.11	11.55	0.00223	64.65	7.11	14.22	1.23
E10	16	0.11	25.58	0.00180	52.20	5.74	12.76	0.50
	17	0.11		0.00157	45.46	5.00		
	20	0.11		0.00032	9.16	1.01		
E2	18	0.11	24.66	0.00003	0.91	0.10	11.86	0.48
	19	0.11		0.00183	53.01	5.83		
E14	21	0.11	9.66	0.00121	35.02	3.85	7.70	0.80

From the tie forces tables, it can be observed that the tie forces at the predicted design load capacity based on STM are lower than calculated, hence all ratios of actual force/calculated are less than one (column (10) in Table 3-1). At the predicted ultimate load capacity, again, all ties, except the horizontal tie with strain gage 15, were lower than expected. In fact, the strain measured by strain gage 15 was greater than expected by 23% (column (10)

in Table 3-2. The diagonal tie with strain gage 7 and 8 and horizontal tie with strain gage 11 and 12 were at 24% and 1% of the expected tension force (column (10) in Table 3-2). The bottom tie instrumented with strain gage 9 and 10 experienced a large strains near ultimate. This corresponds to the observed crack down the loading point, at the bottom of the test specimen (see Figure 3-16). When the concrete cracked, the large force was transferred to the reinforcing steel.

3.3 Beam 2 – Steel Fiber Reinforced Concrete

Beam 2 had the same geometry as Beam 1. It is hypothesized that SFRC has a higher shear capacity due to the superior performance in tension compared to plain concrete (ACI 544-96, 1996). Beam 2 was designed such that only flexural reinforcement was used to carry predominately flexural forces. Hence, only the bottom No. 3 bars that extend from support to support used in Beam 1 were used in Beam 2 (see Figure 3-27). These reinforcing bars also had the identical strain gage layout as the one used in Beam 1, although only four strain gages were used.

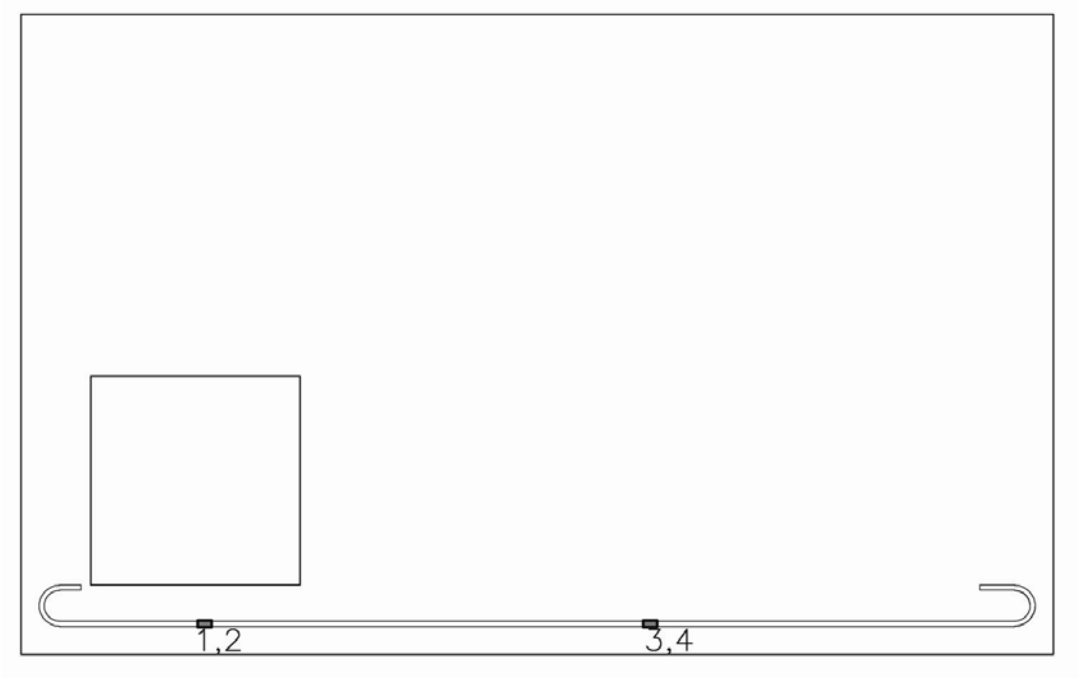

Figure 3-27 Steel reinforcing bar layout of SFRC specimen – Front face.
Numbers indicate strain gage number

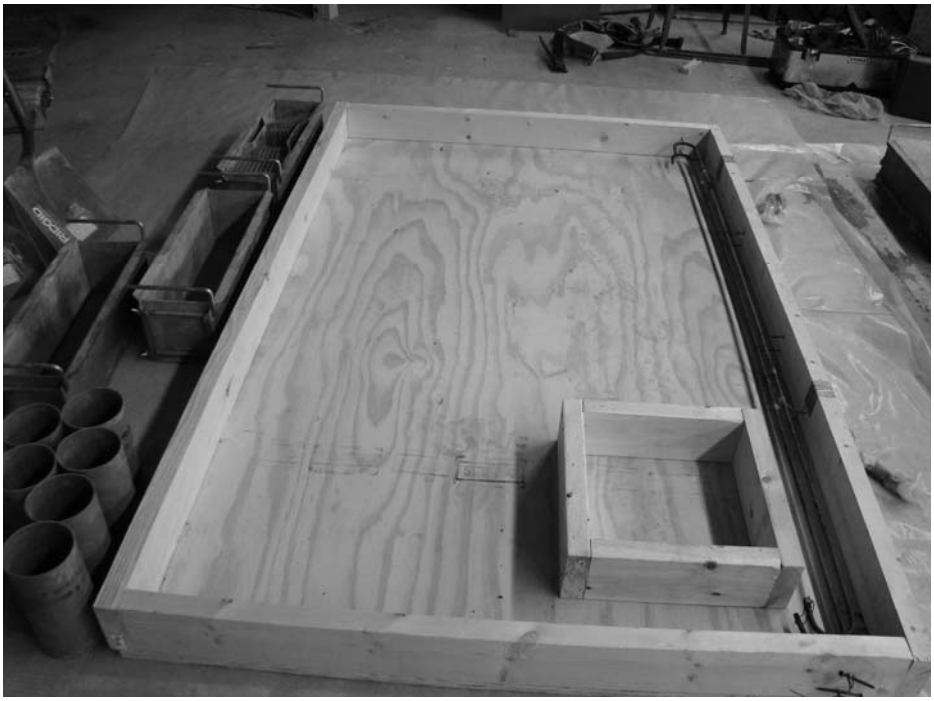

Figure 3-28 SFRC test specimen before casting

Figure 3-29 SFRC test specimen during placing and consolidation of plastic concrete

Fibers used were RC-80/60-BN manufactured my Bekaert with hooked ends, and an aspect ratio of 80. A fiber volume fraction of 1.5% (or 200 lb. per cubic yard of concrete) was used. The same procedure was used to mix and consolidate the concrete as mentioned in the procedure for Beam 1 (see Figure 3-29). The concrete mixture was observed having steel fibers well dispersed in the plastic concrete state, with no segregation (see Figure 3-30).

Figure 3-30 Close-up of plastic SFRC during casting

3.4 Test Results – Steel Fiber Reinforced Concrete

3.4.2 Observed Cracking

Cracks were drawn on the back face in blue and red in the front face to distinguish the sides. The first observed crack occurred on the support closest to the point load at 15 kips. This crack was short and increased slightly as load increased. At 20 kips, a small crack measuring

0.10 mm was formed near the bottom middle span of the beam, about 4 inches long. At 25 kips, many microcracks, less than 0.10 mm in width were observed close to the top of the beam in the vicinity of the point load. There was a small blowout in the area were the first crack occurred during the load increase to 30 kips. A small diagonal crack formed on the top corner of the opening running in the direction towards the loading point at 30 kips (see Figure 3-31a). The crack measured less than 0.10 mm in width.

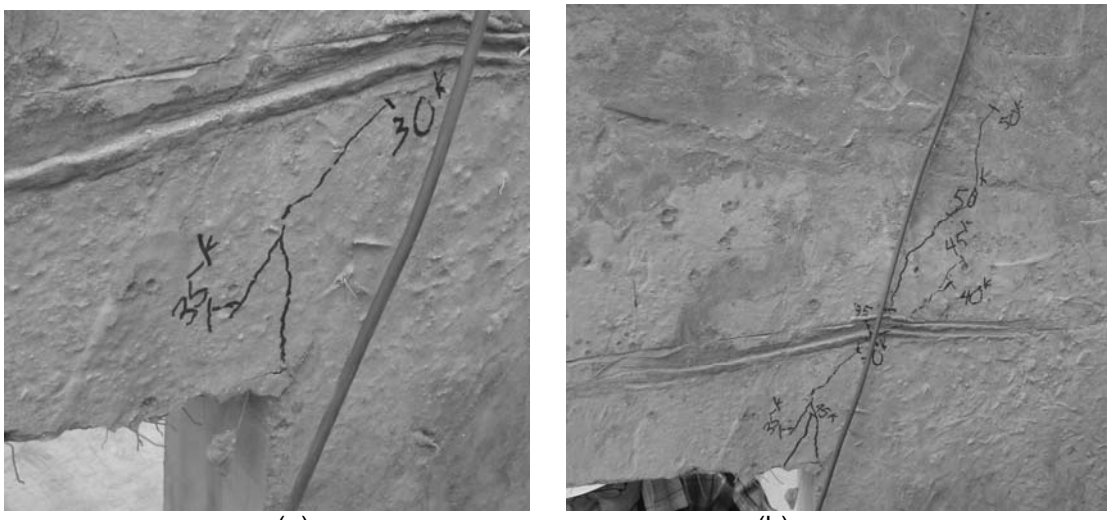

(a) (b)

Figure 3-31 Diagonal crack at 35 (a) and 50 kip (b) on the front face

During the next loading steps, there were no major cracks formed and cracks generally did no open measurably. Many small cracks were observed after the 50 kip loading step. A crack formed in the support near the opening 0.25 mm in width. Other cracks formed emanating from the opening during this stage. The diagonal crack opened to 0.40 mm and extended to about halfway between the corner of the opening and the loading point as loading increased (see Figure 3-31b). More cracks were observed in the support near the load after 55 kips. These cracks were formed in the area that had cracked and spalled initially. The fibers limit the propagation and widening of cracks; even though the concrete in this region had multiple cracks, overall it looked in good condition. At this stage, cracks opened to about 0.15 mm.

(a)

(b)

Figure 3-32 Multiple cracks in back (a) and front (b) face around opening at ultimate load

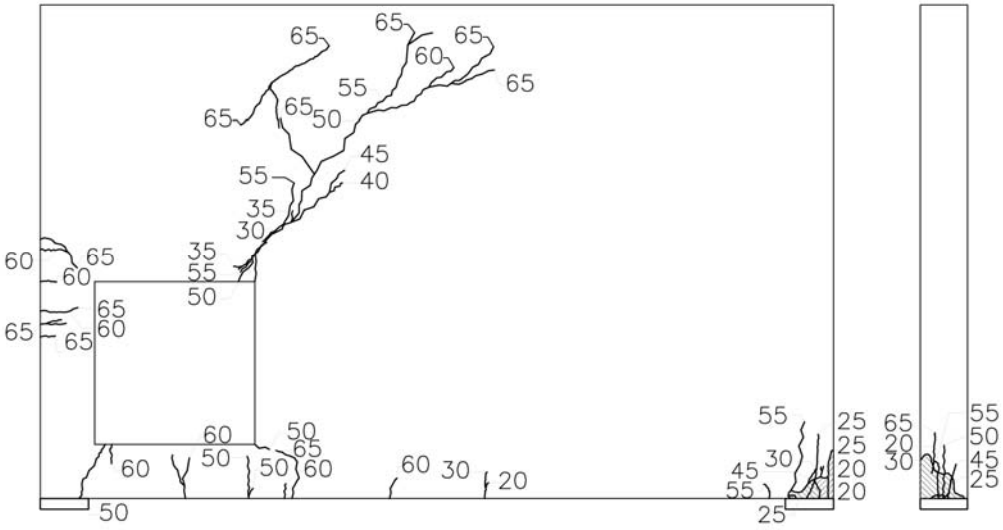

Figure 3-33 SFRC Cracks – Front face. Numbers indicate loading steps in kips (shaded area indicates spalling)

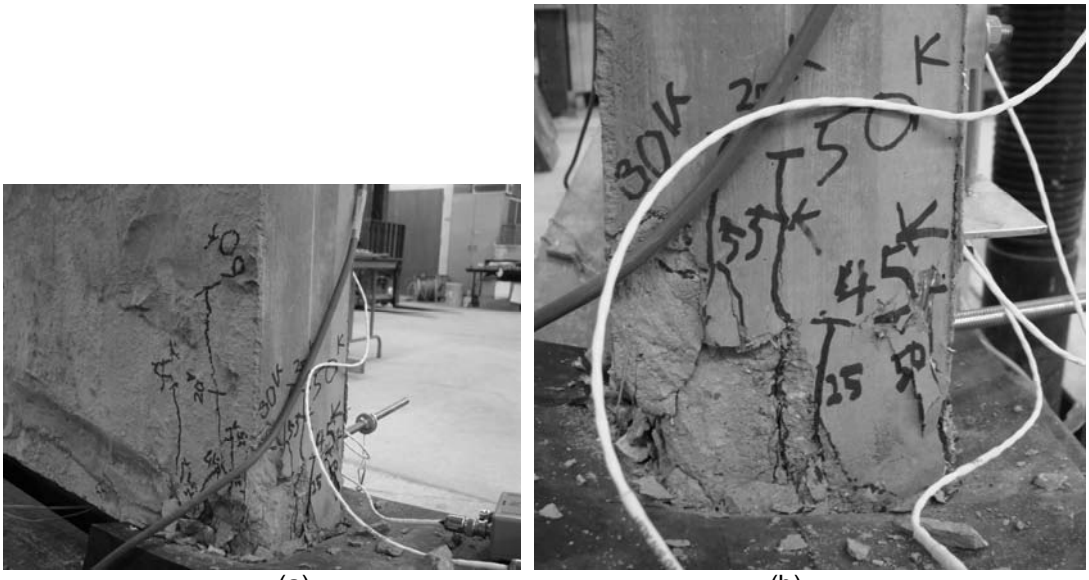

(a) (b)

Figure 3-34 Right support of SFRC specimen at 60 kip – oblique view (a) and end view (b)

After 60 kips, cracks previously formed near the opening generally opened; more cracks about 0.10 mm in width were formed. Horizontal cracks also formed on the back corner of the beam at about the height of the opening. These cracks formed about half the thickness of the beam in each direction around the corner. The diagonal crack opened to about 0.15 mm and grew closer to the loading point. Also, additional microcracks formed, branching away from

the diagonal crack. The beam failed at 65 kip. The loading dropped slowly as the diagonal crack was seen open further. Testing was stopped due to the inability of the beam to take additional load. The diagonal crack opened as the steel fibers were observed pulling out of the concrete between the diagonal crack (see Figure 3-35 and Figure 3-36).

Figure 3-35 Diagonal crack of SFRC specimen at ultimate load (back face)

Figure 3-36 Steel fibers pulling out of the diagonal crack at ultimate load (front face)

3.4.3 Load-Deflection Response

As previously mentioned, the net load-displacement data for the RC specimen was not usable after testing. Although that data for the SFRC specimen was successfully recorded, for comparison purposes, the gross load-displacement plot under the loading point is presented here (see Figure 3-37). The load-displacement plot of the SFRC shows a linear response up to 25 kips. The plot also shows linear behavior between 30 to 50 kips. This agrees with the fact there were no major cracks observed between these loading stages and the specimen deformed proportionally to the load being applied.

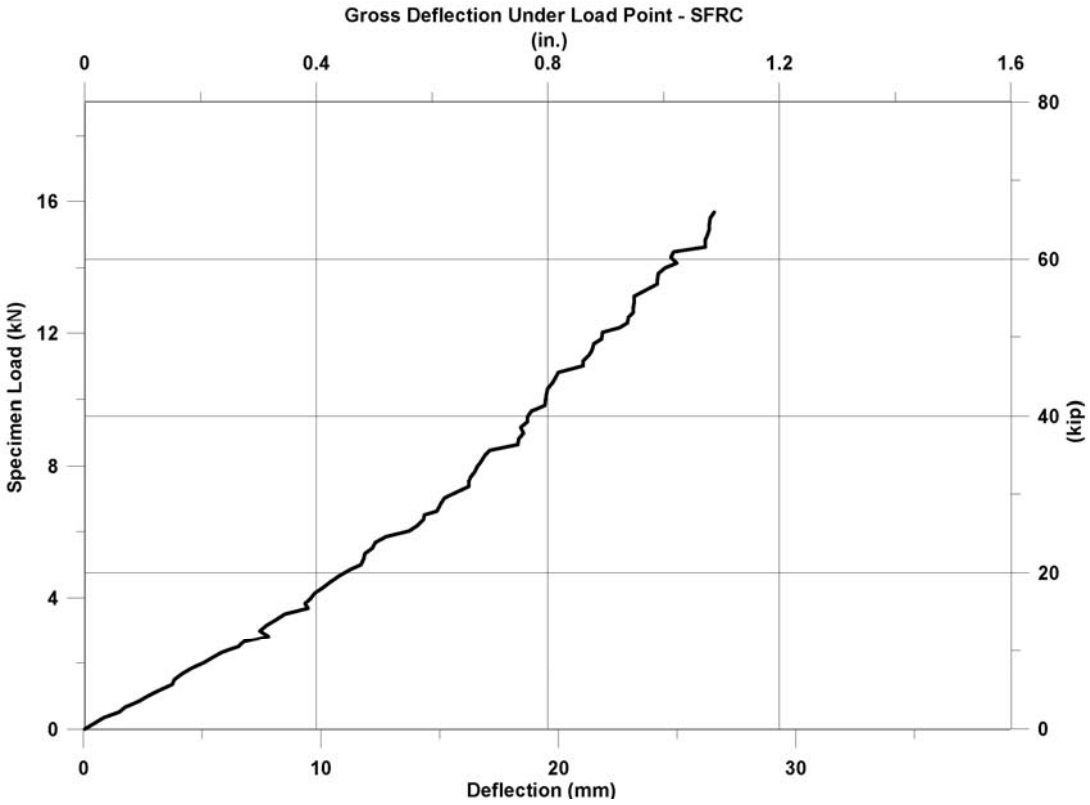

Figure 3-37 Gross load–displacement response for SFRC specimen under loading point

The comparison of the two plots shows similar load-displacement response for the applied load (see Figure 3-38). The SFRC specimen deformed slightly more than the RC specimen up to 55 kips, where the RC specimen deformed significantly more up to ultimate.

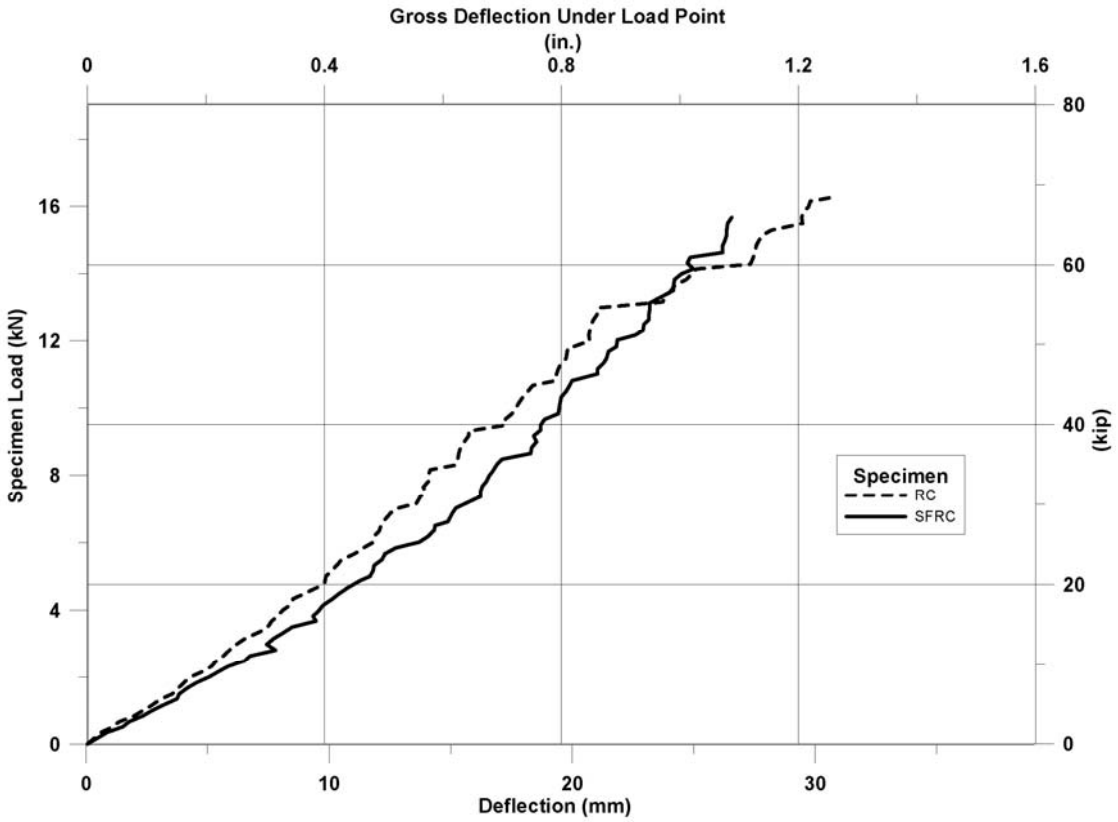

Figure 3-38 Gross load–displacement response for RC and SFRC specimen under loading point

3.4.4 Concrete Strains

Concrete strains were recorded using four LVDTs. LVDT 2 and 3 measured very small deformations. These deformations were measured on axis with the compressive struts from the loading point. The response was linear; however, strains (deformation/gage length) were measured at 125×10^{-6} in/in. Concrete near the left support compressed significantly more. The response was linear until 40 kip. Strain was measured at 0.0015 at ultimate load on the right support. The strain on the right left support was much lower (see Figure 3-39).

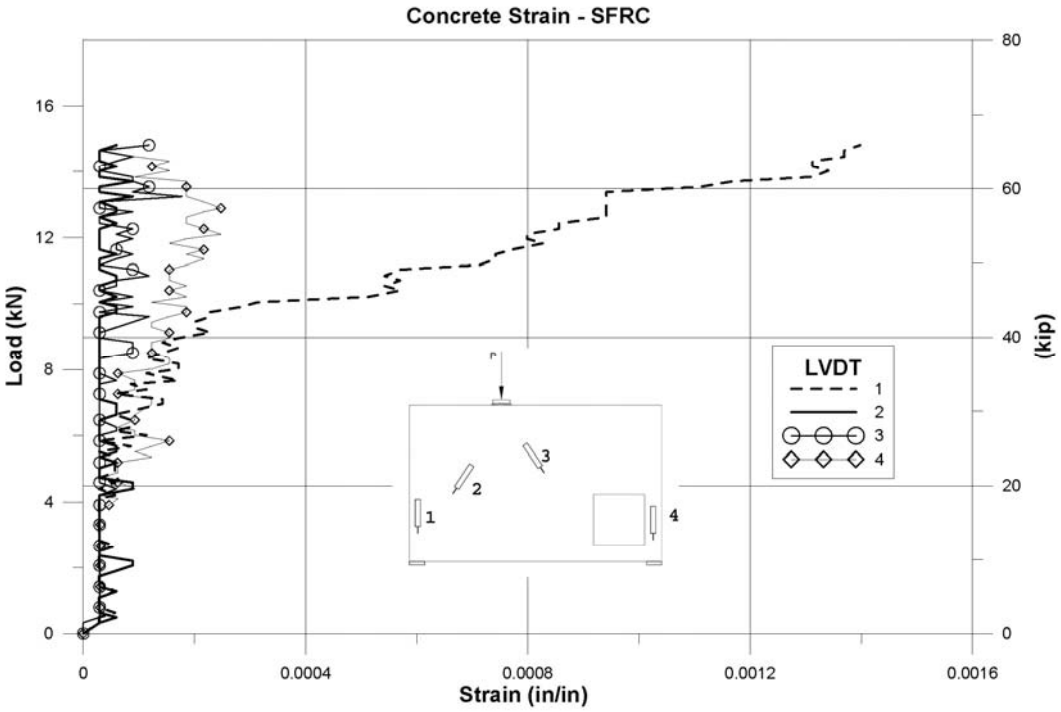

Figure 3-39 Concrete strains in SFRC beam

3.4.5 Reinforcing Steel Strain

Reinforcing steel strain was linear up to 25 kips and 45 kips for the locations under the opening and middle, respectively. The middle location showed a constant force as the load reached 60 kips, followed by a constant strain with no increase in force. After this, the bar took more load as the beam failed. Location 1 and 2 showed a more proportional increase of strain as load was applied. Comparing to the STM, the reinforcement bar in SFRC was strained much less, indicating the higher force-resistance ability of fiber reinforced concrete. At 70 kips, strain gage 10 for the RC specimen was near the 3% elongation, while at 65 kips, SFRC strain gage 4 (same location for both) was strained less than 1%. Compared to the RC test specimen, the SFRC specimen's reinforcing bars load-deformation curves were very similar. This means that both layers of reinforcement resist forces equally (see Figure 3-40). Considering fiber bridging effect, steel fibers were effective in transferring stress uniformly across the cross section of the beam. In the RC specimen the steel is effective in transferring stress, provided the crack occurs

in the vicinity of the bar. Otherwise, it is likely that since that there are large areas of plain concrete not confined by steel reinforcement, stress could not be transferred once cracks occured.

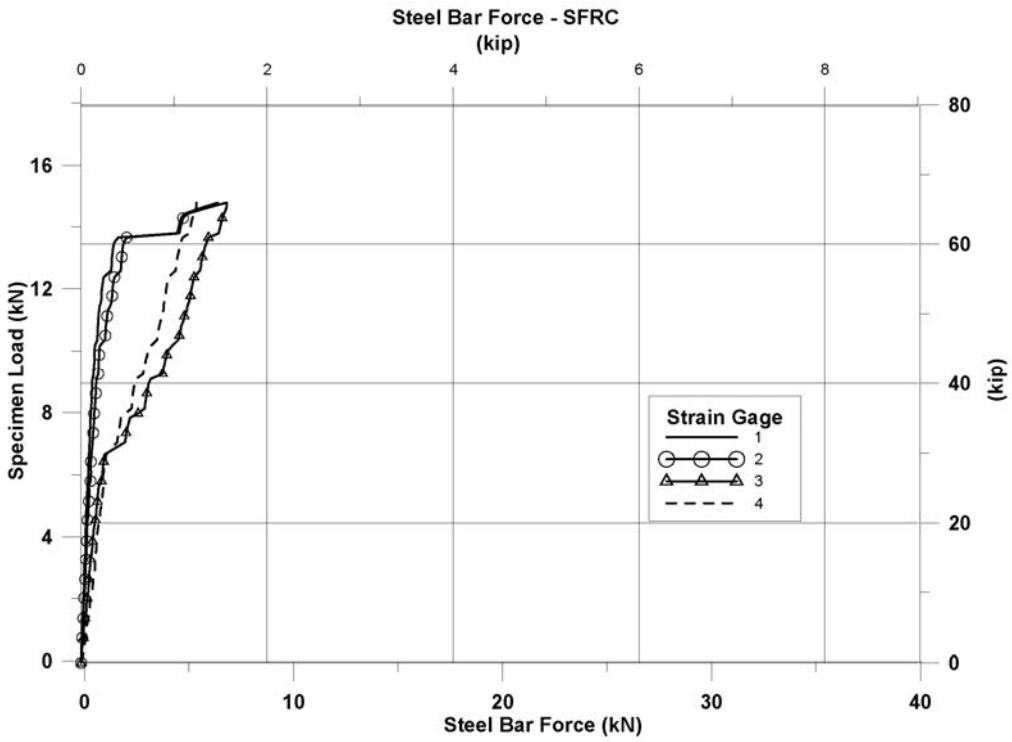

Figure 3-40 Plot of reinforcing bars strains in SFRC beam

3.5 Acoustic Emission Results

Acoustic Emission results showed where strain energy was released relative to the location of the test specimens. Time-versus-hits were synchronized with loading increments to determine at the specific time when energy was released within the specimen. The shear wave velocity was calculated as 1.10×10^5 ft/s for steel fiber reinforced concrete, based on the method described previously. Because of the opening on the specimen AE was less effective between the piezoelectric sensors and concrete mass in the direction of the void by the opening (Figure 3-41 to Figure 3-47).

AE results show that the SFRC test specimen had more hits than the RC specimen. The cracked area around the diagonal crack from the opening is much more in SFRC than in RC specimen. This indicates that the SFRC specimen was effective in resisting and redistributing internal strains so that greater concrete strut was utilized to resist the force (see Figure 3-40 to Figure 3-45).

The RC specimen showed little activity at the support near the loading point, although this was the region that caused the beam to fail. Since the beam split in the thickness side in this region, the AE sensors could not capture all of the events in this area. The sensors were located on one face of specimen. For hits that occurred on the other face, waves could not travel in empty space between the void caused by the crack in the specimen.

However, AE revealed that more energy was dissipated on the area between the opening and the loading point of the SFRC specimen. Compared to RC, the SFRC specimen showed many more hits in this area (see Figure 3-45). Extending the fiber bridging effect, it is apparent that the concrete compressive strut is widened during loading. Where in the RC specimen the compressive strut is effective only up to a certain width, the SFRC expands the width of damage in the strut. Comparing the RC and the SFRC specimens in Figure 3-47, the SFRC shows energy dissipated in a more wide area.

The inclusion of steel fibers in the concrete mix causes energy to be dispersed into smaller, discrete amounts, which AE captures as hits. The RC specimen had the same amount of energy dissipated, although in more concentrated amounts. Hence, the figure shows fewer hits in the same region than the SFRC specimen. This agrees with crack observations that the SFRC specimen had smaller, thinner cracks that branch out in random directions. The steel fibers serve as a “bridge,” that enables forces to be redistributed from one area to the next. This overcomes concrete’s weak tensile strength capacity and brittle nature.Also, the splitting cracking along a compressive strut could be delayed due to the higher tensile strength of SFRC compared to plain concrete.

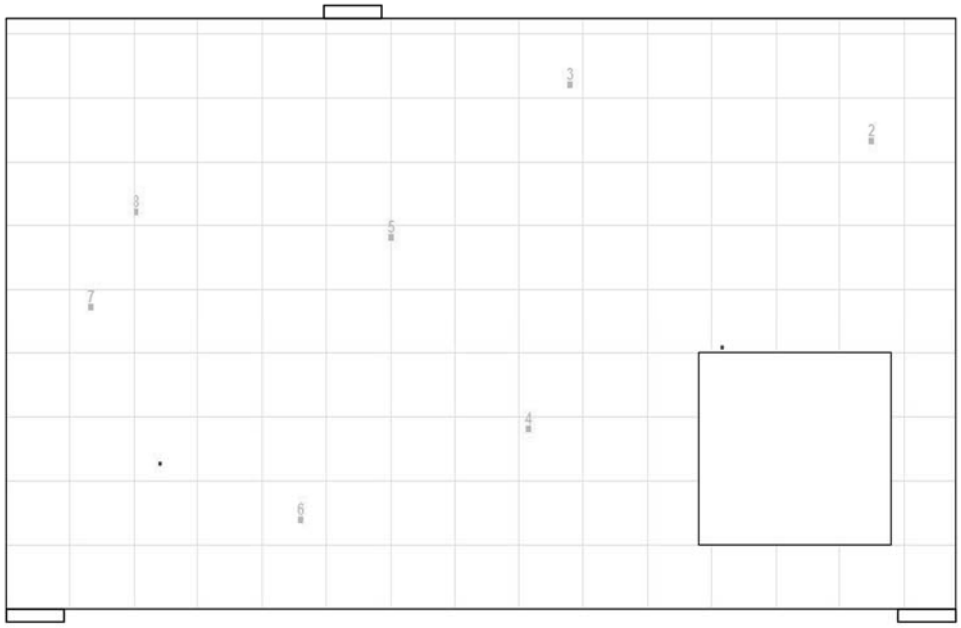

(a)

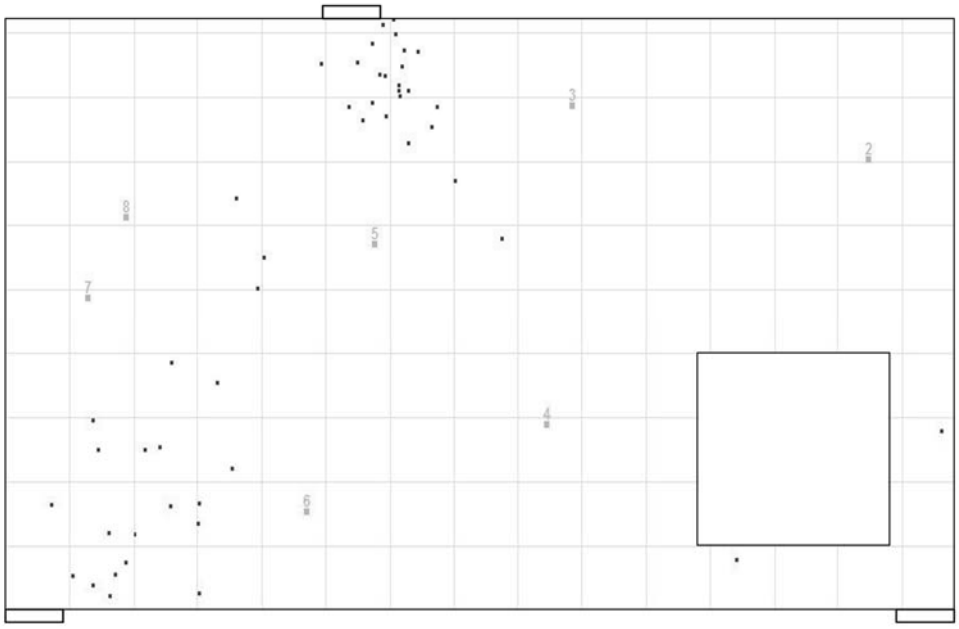

(b)

Figure 3-41 Acoustic Emission cumulative events at 15 kips of RC (a) and SFRC (b) specimens

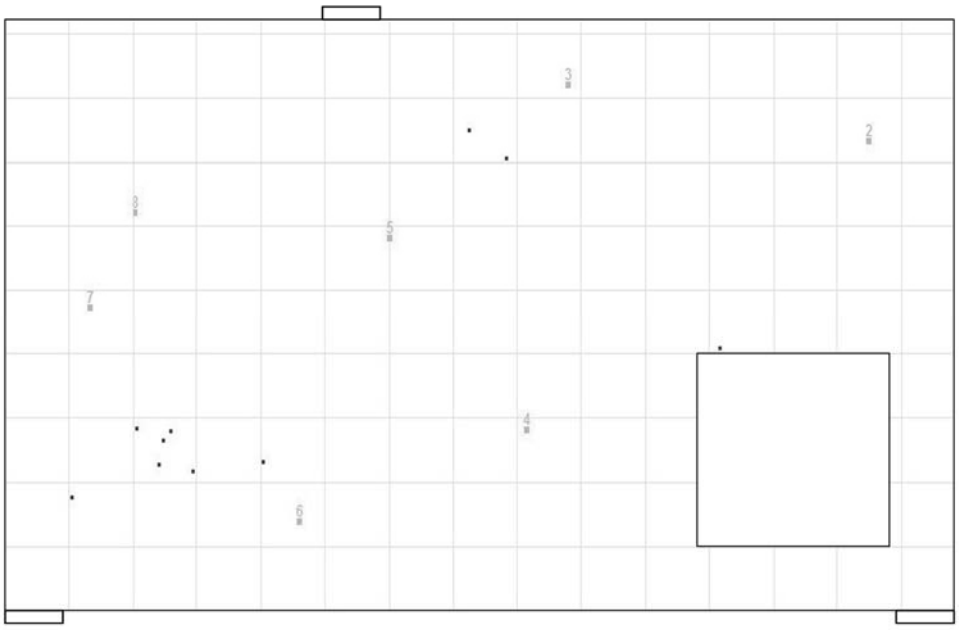

(a)

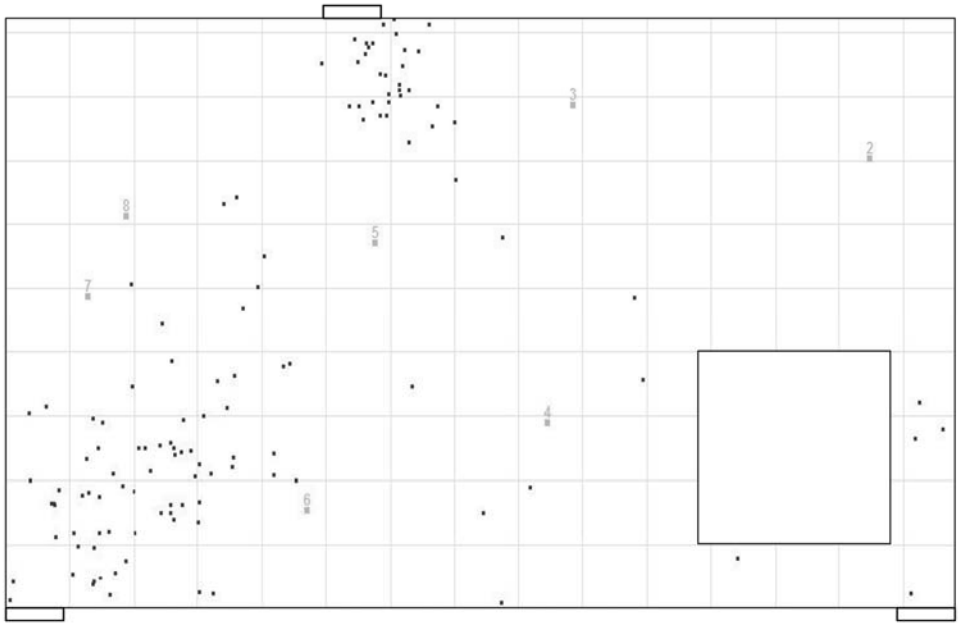

(b)

Figure 3-42 Acoustic Emission cumulative events at 25 kips of RC (a) and SFRC (b) specimens

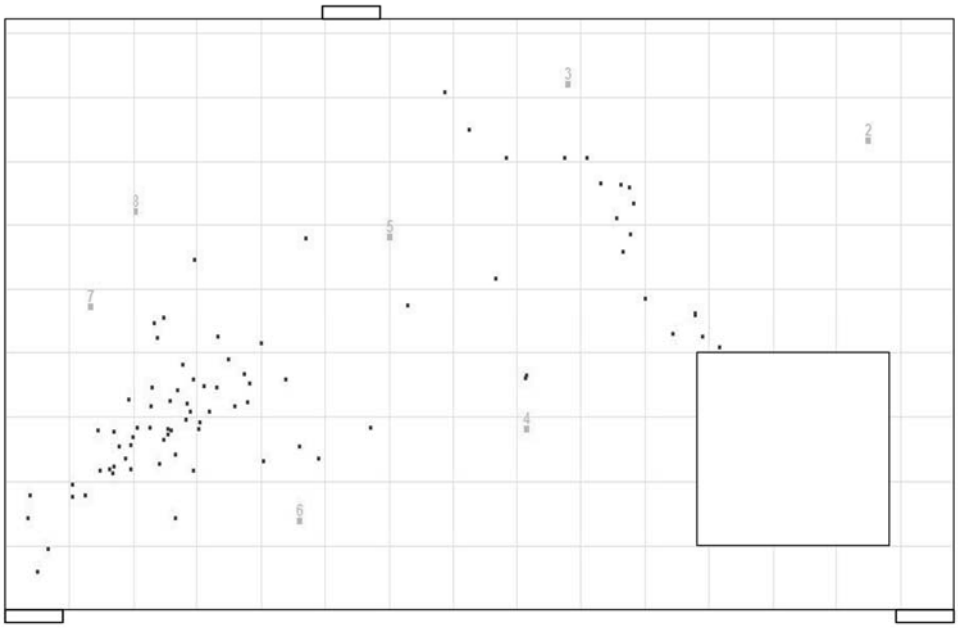

(a)

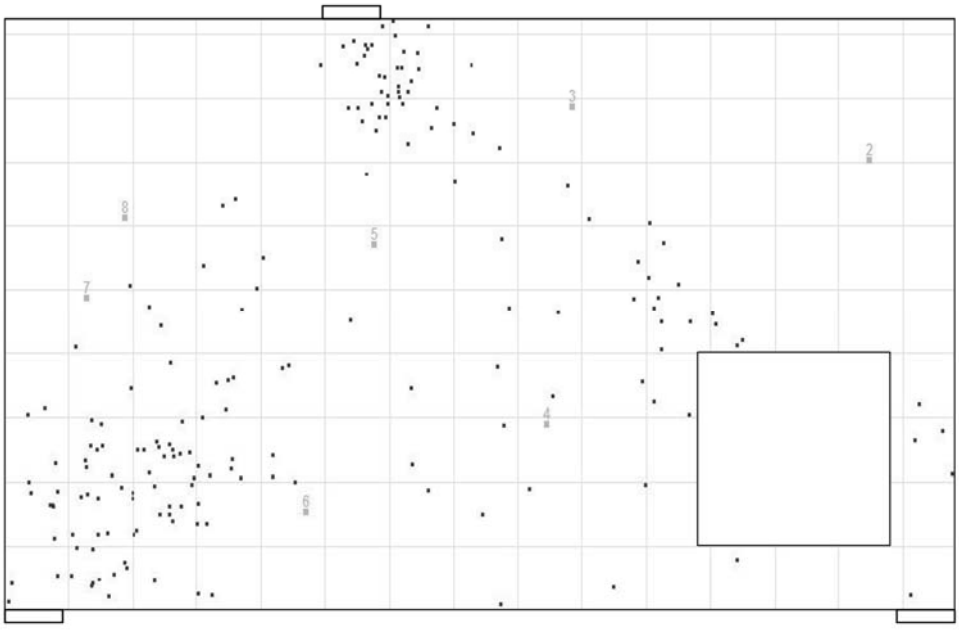

(b)

Figure 3-43 Acoustic Emission cumulative events at 35 kips of RC (a) and SFRC (b) specimens

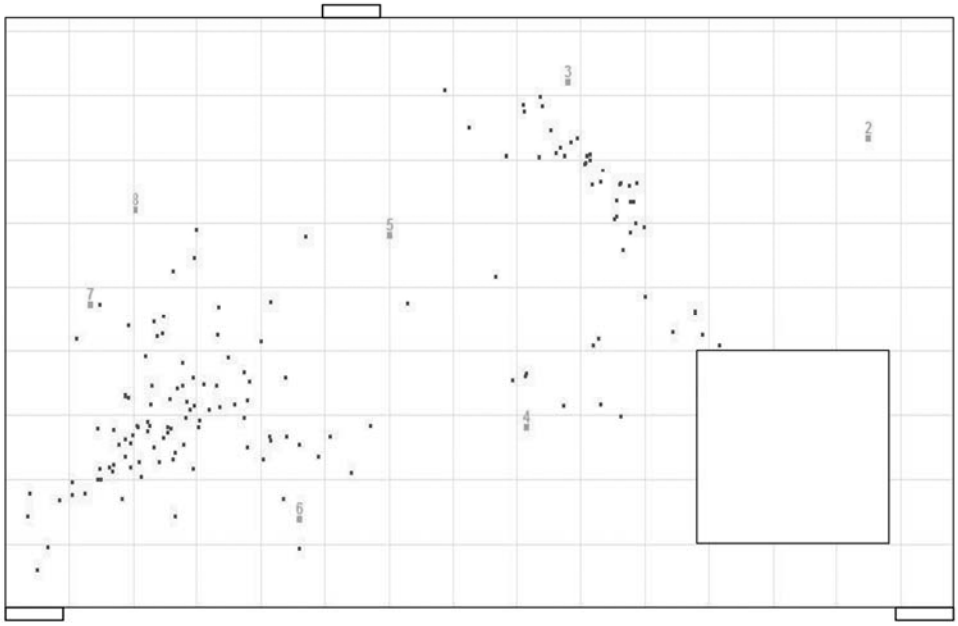

(a)

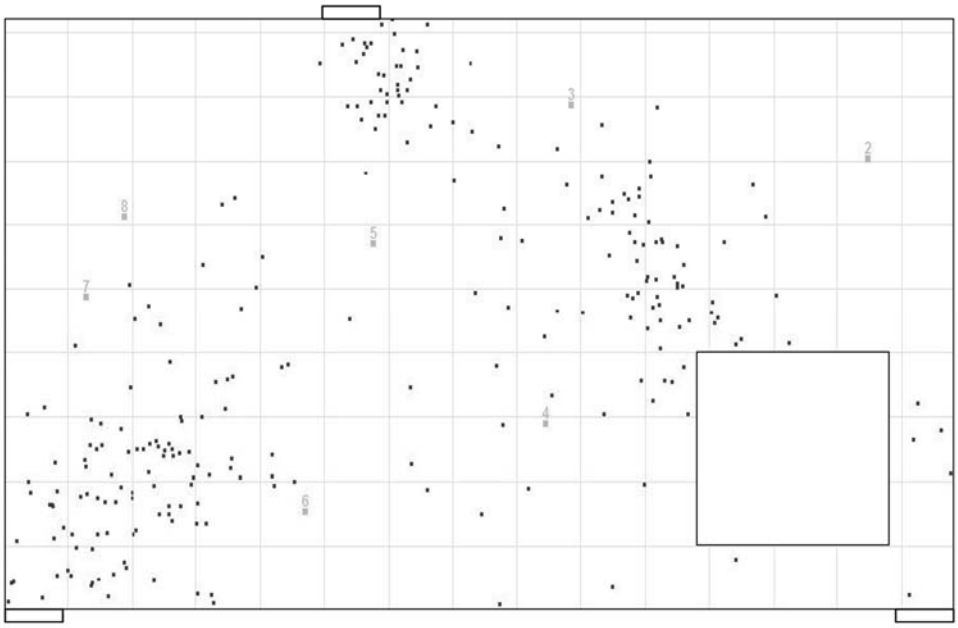

(b)

Figure 3-44 Acoustic Emission cumulative events at 45 kips of RC (a) and SFRC (b) specimens

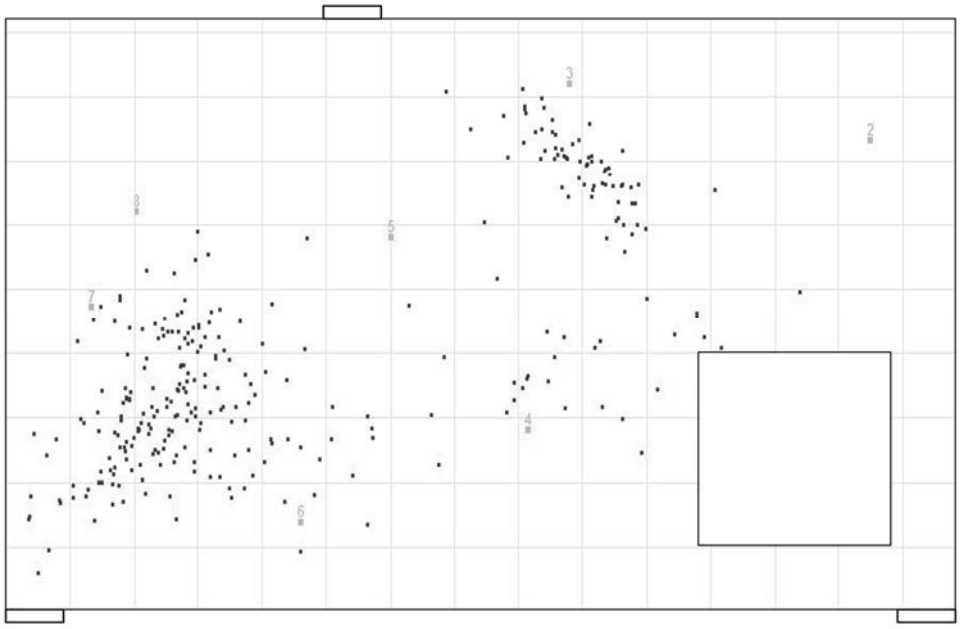

(a)

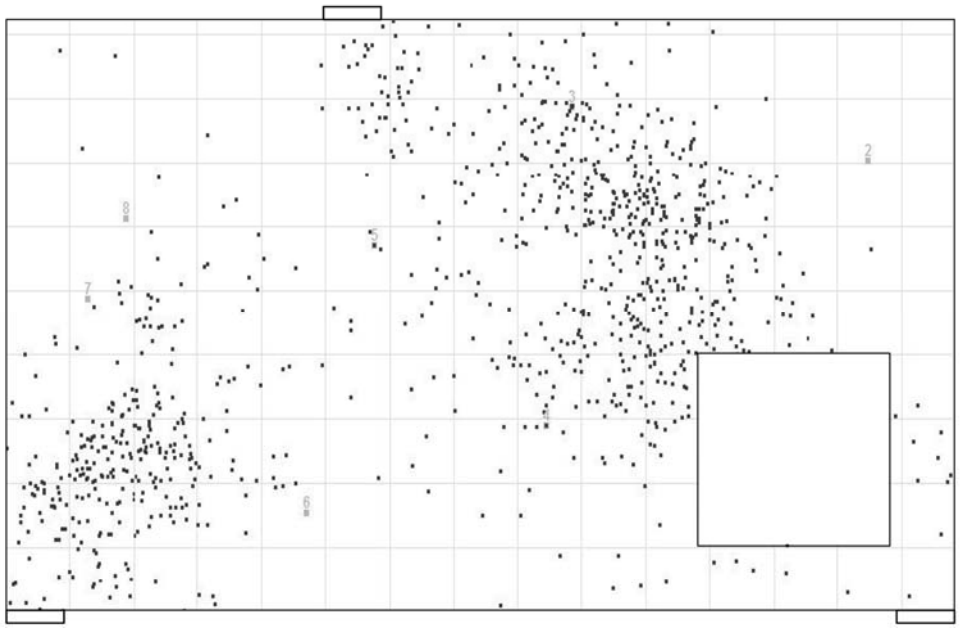

(b)

Figure 3-45 Acoustic Emission cumulative events at 65 kips of RC (a) and SFRC (b) specimens

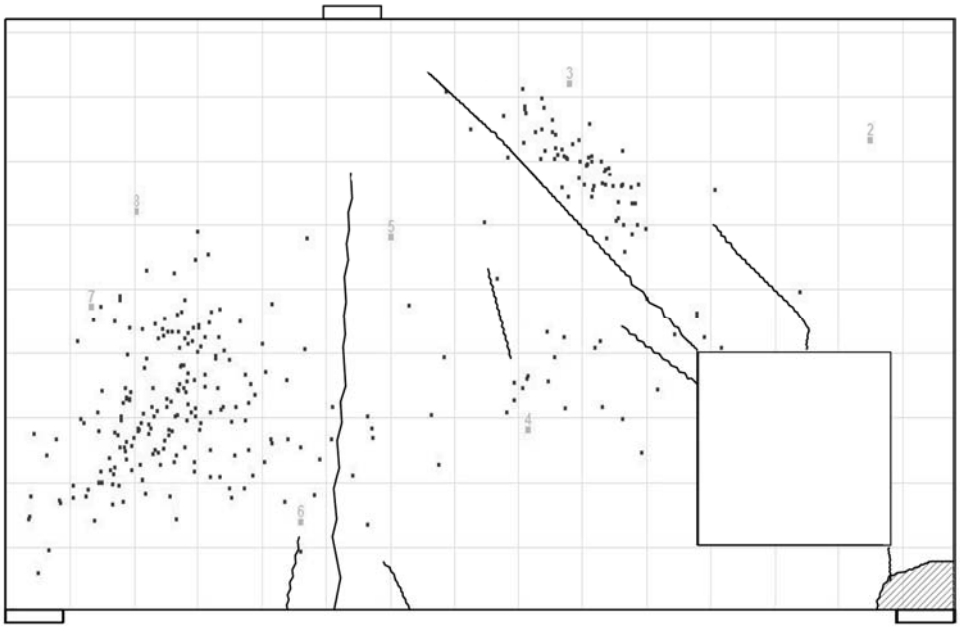

(a)

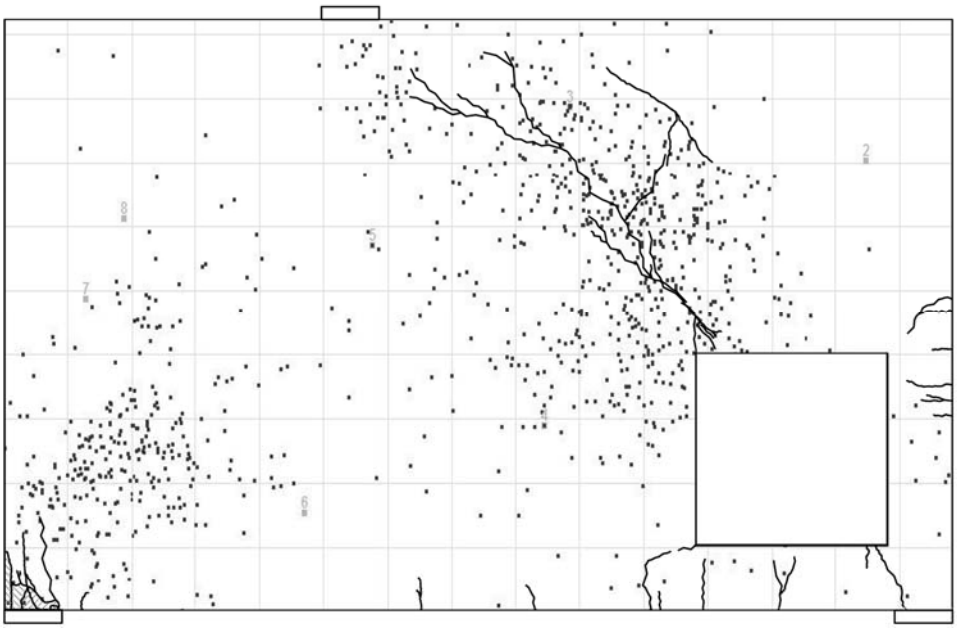

(b)

Figure 3-46 Acoustic Emission cumulative events at 65 kips of RC (a) and SFRC (b) specimens with cracks superimposed

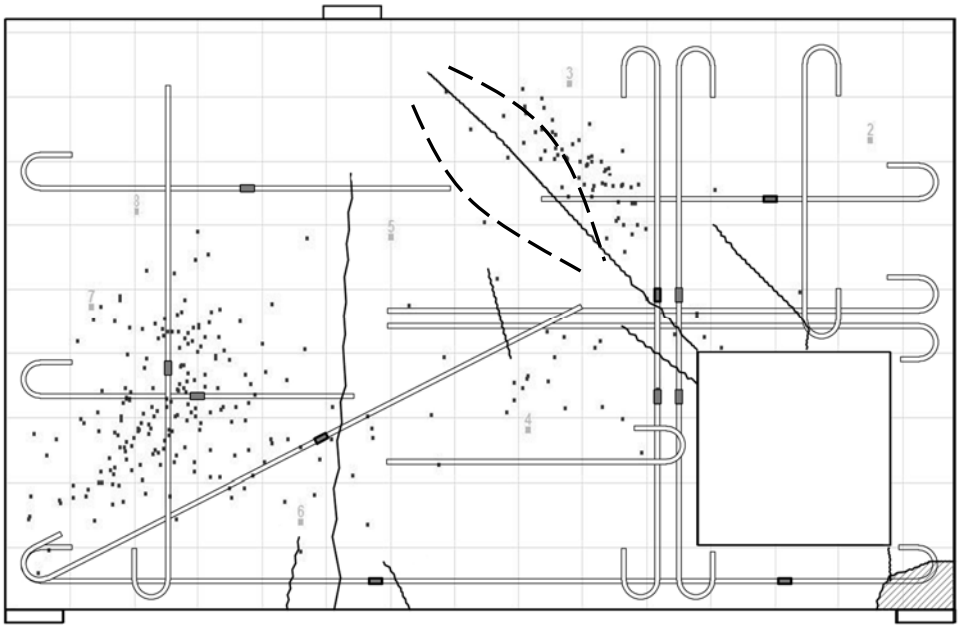

(a)

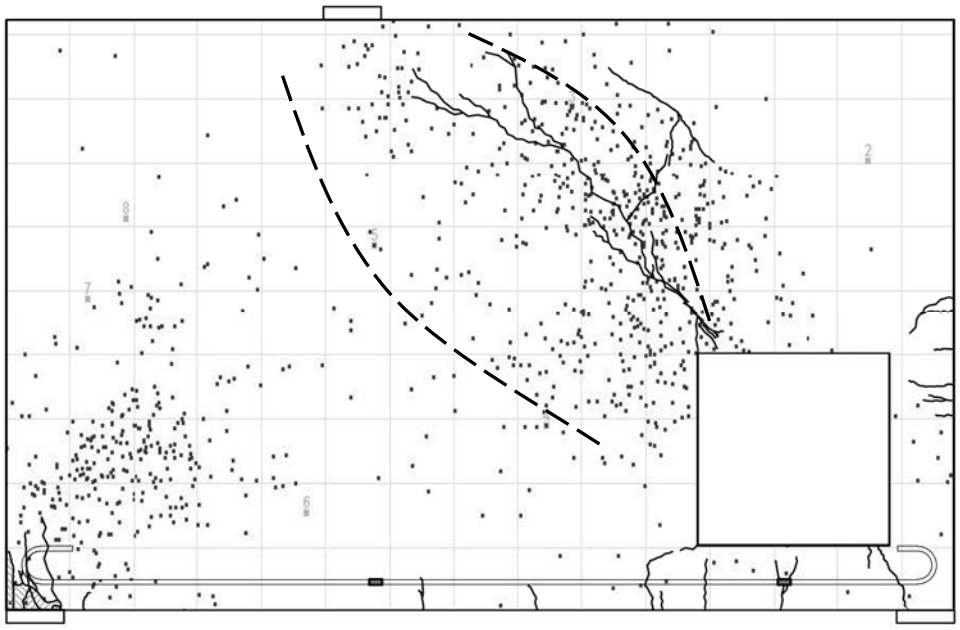

(b)

Figure 3-47 Acoustic Emission cumulative events at 65 kips of RC (a) and SFRC (b) specimens with cracks and reinforcing steel superimposed. Dashed lines indicate approximate extents of effective concrete strut

CHAPTER 4

COMPUTER AIDED STRUT-AND-TIE (CAST) ANALYSIS

4.1 Computer Aided Strut and Tie (CAST) Analysis – RC Specimen

The strut-and-tie model was analyzed using software developed by Tjhin and Kuchma at the University of Illinois at Urbana-Champaign (2002). The materials properties obtained from material tests were used for concrete and reinforcing steel in the models. By doing so, the strength reduction factor φ was set to unity. Tie areas of 0.22 in^2 and 0.44in^2 was set for two and four, No.3 reinforcing bars, respectively. The supports where modeled as a vertical reaction on the left support and a vertical and horizontal reaction on the right support

The input procedure, are presented in Appendix A. The output files are presented in Appendix B. The design load was 31.4 kips. The software's capacity prediction feature was used to estimate the capacity using the provided steel reinforcement, concrete struts and nodal zones.

Additionally, the software has a feature that allows analysis of the nodes to ensure that geometry and stress limits are not exceeded. The estimated capacity according to the software was 41.2 kips for the RC specimen using the nominal material strengths (see Figure 4-2). However, since the material strengths were determined by testing, the expected ultimate capacity estimated by the software was 70.3 kips (see Figure 4-3). According to CAST, the failure would occur by yielding of the diagonal tie. This is desirable in STM because it allows the member to fail in a ductile manner as the reinforcing bars yield first before failure, as opposed to brittle failure of the concrete struts.

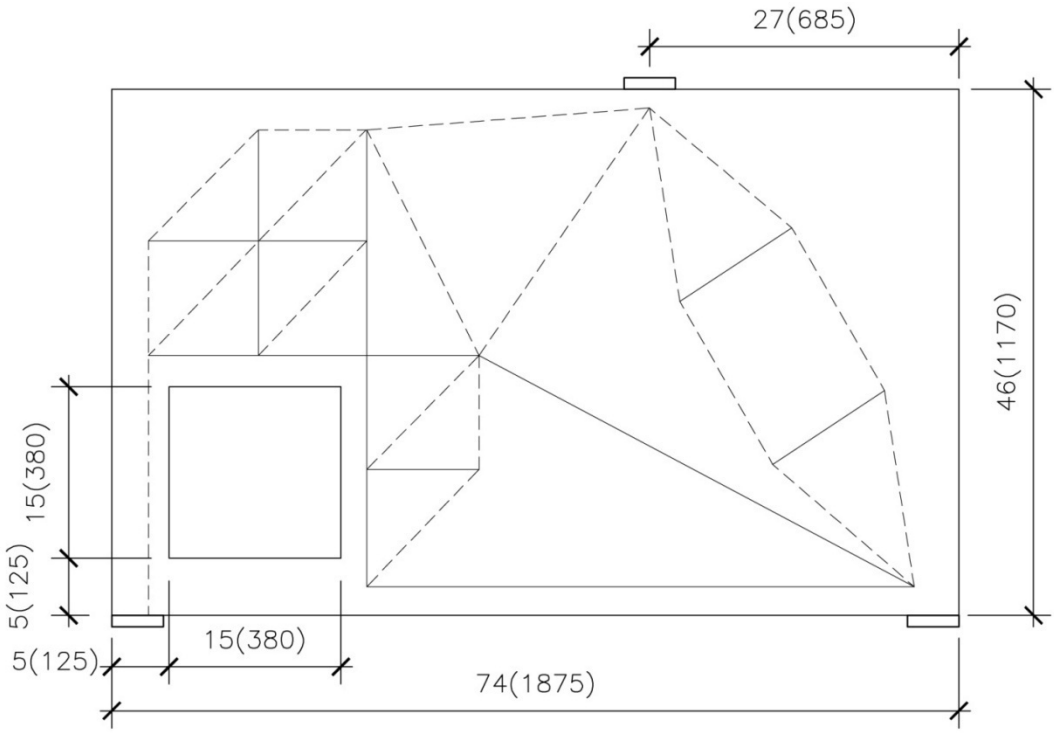

Figure 4-1 Geometry and strut-and-tie model. Solid lines indicate tension tie and dashed lines indicate compressive strut. Units in in. and (mm)

The numbers in parenthesis (O/S) show the actual load divided the demand capacity. For any value greater than one, the actual force is greater than the model allows; therefore, it has failed. Depending on the analysis (predicted strength based on the model or design strength) the program gives the tie that has analytically failed.

CAST precludes analysis if the truss system is not stable. Therefore, a support was added to the right side of bottle-shaped strut from the loading point to the right support (see Figure 4-2). This support is only required for the program to run the design and does not calculate a reaction or calculates a very small reaction. The location was not critical, since other joints that cause stability are also possible. Note that in Figure 4-2 that there are no over strength elements. Therefore, all O/S ratios are less than one.

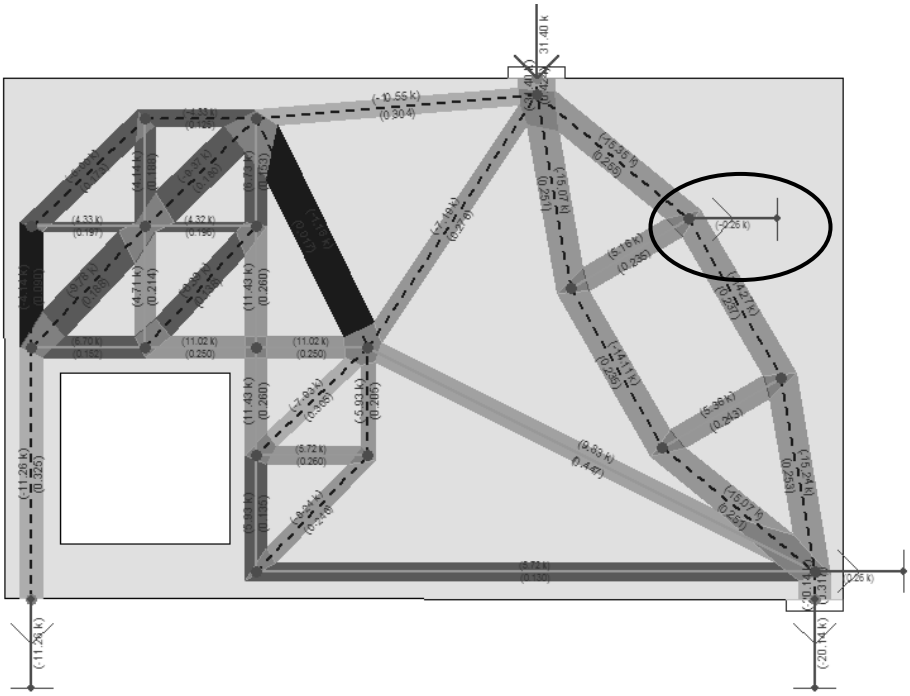

Figure 4-2 Strut and tie model analysis based on CAST at design load (numbers indicate the ratio between demand and capacity of each member; O/S indicated over strength)

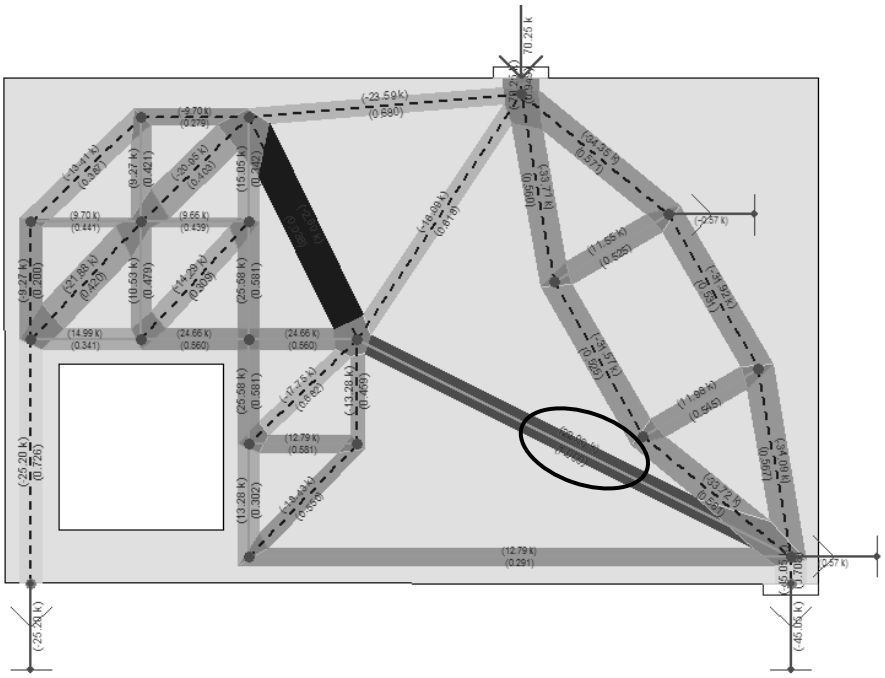

Figure 4-3 Strut and tie model analysis based on CAST at ultimate load (unitless numbers indicate the ratio between demand to capacity of each member; O/S indicated over strength)

4.2 Computer Aided Strut and Tie (CAST) Analysis –RC Specimen with Single Bottom Tie

The same software discussed in the preceding sections was used to predict the ultimate load the specimen would take if only the bottom steel reinforcing tie was used and concrete tensile ties were assumed. The intent was to determine how much capacity the specimen would gain by the inclusion of steel fibers, if any. The concrete tensile strength was calculated using ACI 318-08 equation 9-8 (ACI 318, 2008):

$f'_t = 7.5\sqrt{f'_c}$ (psi), where

f'_t = concrete tensile strength (psi)

f'_c = 28 day concrete compressive strength from the cylinder test (psi)

Researchers have suggested concrete tensile strength of $4\sqrt{f'_c}$ (psi) in a transverse "compression field" stress (Al-Nahlawi, Wight, 1992), although the concrete tensile strength used here is more commonly used in practice. The CAST analysis predicted the specimen would fail at ultimate load of 14.26 kips. The concrete tensile strength was substituted for the steel tensile strength. However, since CAST does not allow two different strengths to be used for the same STM component, an "equivalent" area of steel was used for the bottom steel tension tie used in the actual specimen. Hence, the RC CAST model and the SFRC CAST model were able to develop the same tensile force in the bottom tie.

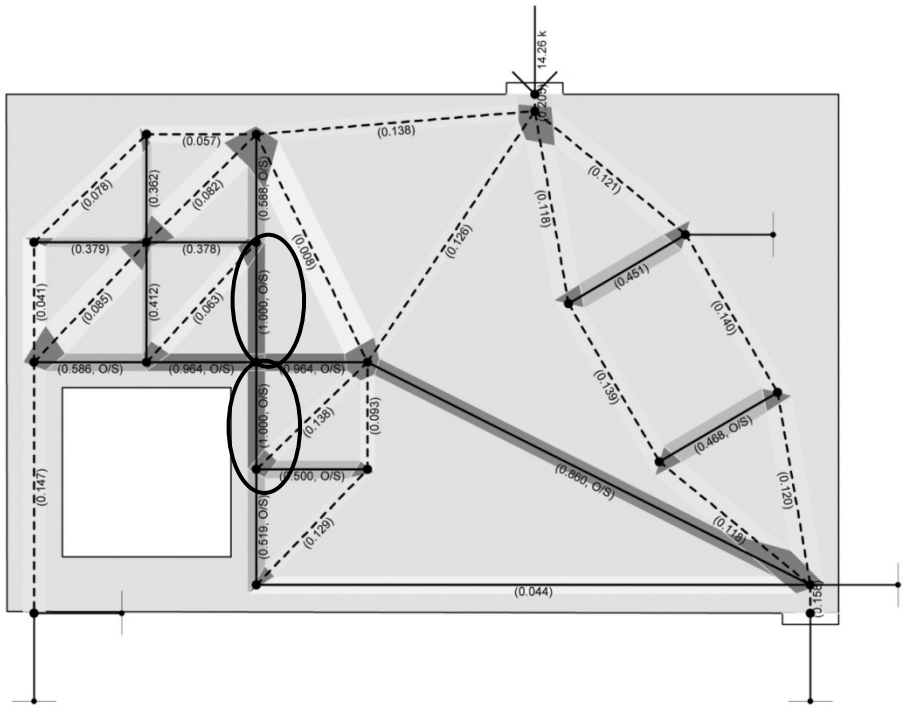

Figure 4-4 CAST model of RC specimen considering concrete's tensile strength (numbers indicate demand/capacity of each member; O/S indicated over strength)

Following the same procedure from the RC specimen, the bottom steel tie was also extended into the left support, although the CAST model does not require this, provided sufficient anchorage is provided.

From the model, one can see that the area on the top-right of the opening would be the first to fail (see Figure 4-4 and Figure 4-5). The concrete tensile ties around this region have a O/S ratio of 1.0, with ratios as previously described. The tie crossing perpendicular to the first failed tie has the second highest force, with a O/S ratio or near one. Since the compressive strength of the concrete was kept the same, the values for the compressive struts was very low, as expected for a corresponding low specimen load. Obviously, the model with the concrete tensile strength was not adequate for the first beam's design load. This is due to plain concrete's very low tensile strength resisted in the ties of the model, although the compressive strength of the concrete struts was very high.

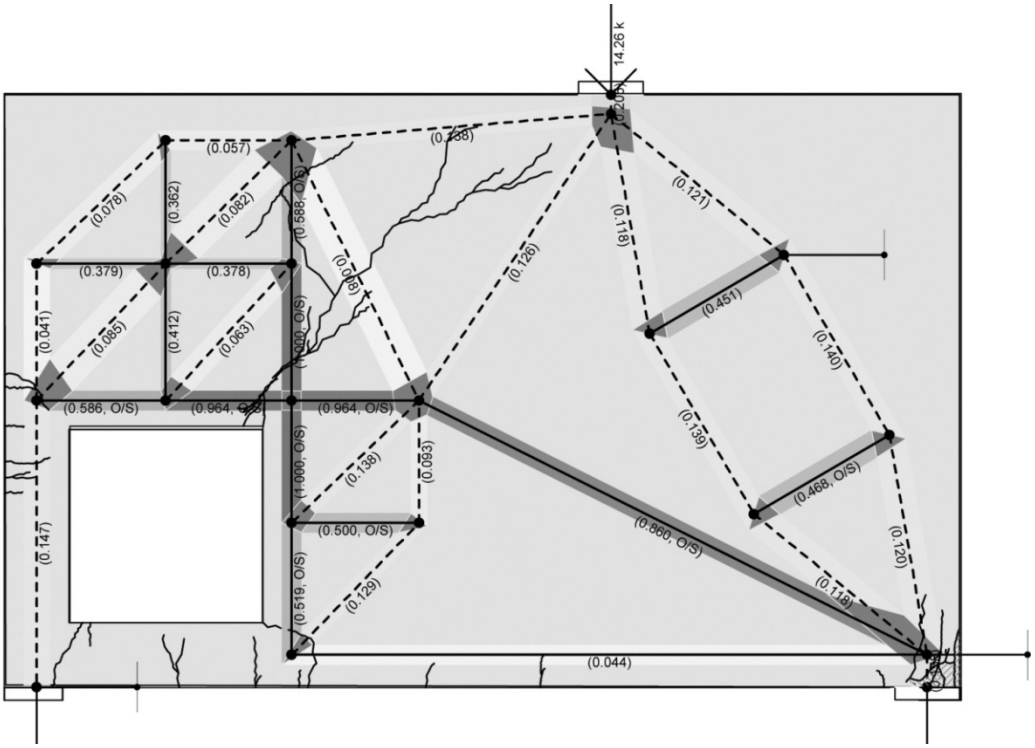

Figure 4-5 CAST model of RC specimen considering concrete's tensile strength with crack mapping overlay

CHAPTER 5

CONCLUSIONS AND RECOMMENDED FUTURE WORK

5.1 Summary and Conclusions

The performance of using steel fiber reinforced concrete was compared to a very widely-used and accepted design method envisioned more than 100 years ago by Ritter and Mörsch, which was further developed by Schlaich, et al. Although the strut-and-tie model is gaining acceptance by the design professions, it is nonetheless cumbersome and at times, ambiguous. Issues such as openings are not explicitly addressed in the ACI 318 Code. Less experienced designers might overlook the importance of proper detailing, leading to unexpected structural behavior due to poor detailing.

The concept of reinforcing brittle material with fibers is as old as the pyramids built by the ancient Egyptians (Mehta and Monteiro, 2006). Reinforcing concrete with steel fibers has been used to reduce material in structural slabs (ACI 544-96, 1996). Developments in the ability to control the characteristics of plastic concrete has facilitated the use of concrete reinforced with various types of fibers.

The performance of the SFRC specimen compared very well to the RC specimen designed using the strut-and-tie model. Generally, the cracks of the SFRC were much smaller in width than those of the RC specimen. The sudden energy release of the RC specimen was mitigated in the SFRC specimen, due to fiber bridging effect, as seen visually and measured by Acoustic Emission. Although there was no steel reinforcing in the area adjacent to the opening in the SFRC specimen, the beam took nearly the same load as the heavily reinforced RC specimen. The SFRC specimen failed as the fibers pulled off in the diagonal crack from the opening to the loading point.

An analysis was performed using the same procedure as the RC specimen, except that concrete's tensile strength, as recommended by the literature, was used in place of tension ties and one steel tie from support to support. The failure mode was in agreement with CAST's analysis that predicted failure near the opening leading to the loading point. The specimen's ultimate load increased by approximately four times as predicted by analysis, due to the inclusion of steel fibers in the concrete matrix.

The concrete strain was more predictive for the SFRC specimen. Although the measured strain was higher for the SFRC specimen than RC near the support with the opening, the SFRC specimen did not have large pieces of concrete spalled. At about 58 kips, the concrete's strain in the left support became negative for the RC specimen. The STM model would not have predicted a tensile stress on the support opposite the opening. In addition, strain gage 14 measured a small compressive stress on the steel tensile tie.

The SFRC steel reinforcement tensile force increased more linearly than in the RC specimen. At the SFRC's ultimate load, the bottom tensile tie's force was 2.81 kips. The same bottom tensile tie's force was 0.97 kips at the same load. However, the RC specimen saw a tremendous strain increase slightly above this load, where as the SFRC specimen failed in diagonal crack splitting.

The true load-deformation response was not presented due to experimental data loss during testing. From the presented load-deformation response, however, it has been shown that the SFRC specimen behaves similarly to the specimen designed with STM. Additionally, from the observed failure of the SFRC specimen, the SFRC specimen failed in a controlled manner, as the diagonal crack widened, with no brittle behavior. The result of this behavior can be attributed to the steel fibers being pulled from the concrete matrix.

In summary, the complete replacement of conventional reinforcing bars by deformed steel fibers at a volume of 1.5% is a feasible alternative to the current practice. Also, the SFRC specimen had better damage control than the RC specimen in terms of limiting cracking under service and ultimate loading. The SFRC specimen showed twice the ultimate capacity as used

in design, even with only bottom flexural reinforcement. It is expected that design deep beams with openings can be significantly simplified by using the proposed material solution.

Acoustic emission proved to be an effective tool to identify crack development and failure mechanism. In addition, acoustic emission identified to the increase in strength of the SFRC specimen resulted from the wider compressive strut than that of conventional RC specimen. The higher effective compressive strength of the strut (due to greater tensile strength of SFRC) could be another factor that led to the higher ultimate strength of the SFRC specimen.

The following table summarizes analysis and testing performed on deep beam with single opening:

Table 5.1 Summary of analysis and experimental testing

	RC Specimen	**RC with only bottom reinforcement**	**SFRC with only bottom reinforcement**
Design Load (kips)	31.4	-	14.3
Expected Load (kips)	70.25	14.3	-
Expected Load (kips)	70*	-	65

*Testing stopped due to instability

The RC specimen did take longer to construct since it had many reinforcing bars and there was much time invested in making sure that the reinforcing bars were properly placed, tied and had correct cover. On the other hand, constructing the SFRC specimen took very little time, since it had only two reinforcing bars. In an actual full sized beam, this issued would be aggravated because beams like these would be cast vertically and access to formwork would be limited.

5.2 Recommended Future Work

After completing the research, it was found the following issues should be investigated:

1. Similar deep beams should be tested using additional shear reinforcement to investigate stresses generated around web openings in beams.
2. Similar deep beams with different geometry and opening configuration should be investigated.
3. The effect of varying SFRC fiber dosages should be investigated on deep beams with web openings to evaluate its performance on structural applications.
4. The performance of different steel fibers should be investigated.
5. Further comparisons between conventional reinforced concrete and SFRC in structural applications
6. Develop a design aid that enables practitioners to design using SFRC for structural applications

APPENDIX A

CAST INPUT DATA - RC

The specimen's geometry was generated according to the software's instructions. The loading and boundary conditions were also established.

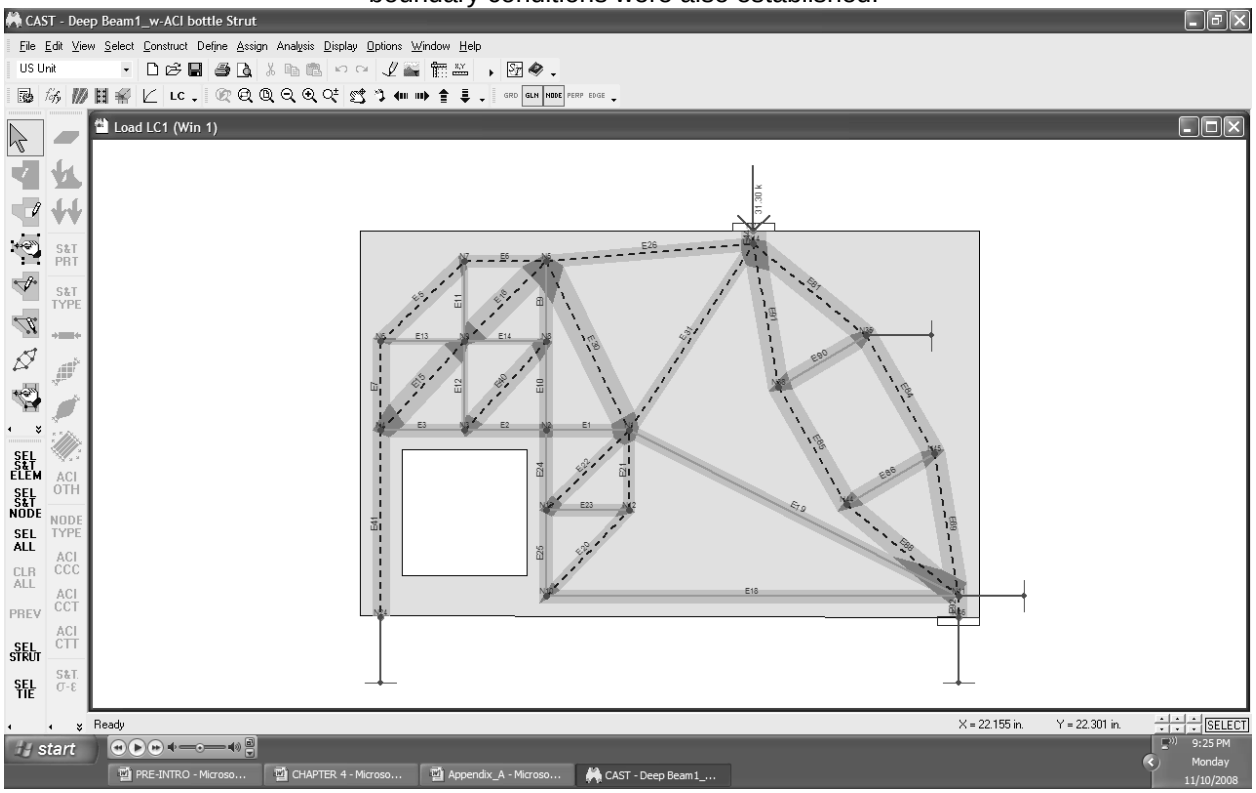

Figure A-1 General user-interface of CAST

The material properties as obtained from Chapter II were provided. Since there were the actual values, phi values were set to unity, as previously discussed.

Figure A-2 General properties defined

Concrete struts were defined according to ACI 318. The two types were bottle-shaped and prismatic shaped concrete struts.

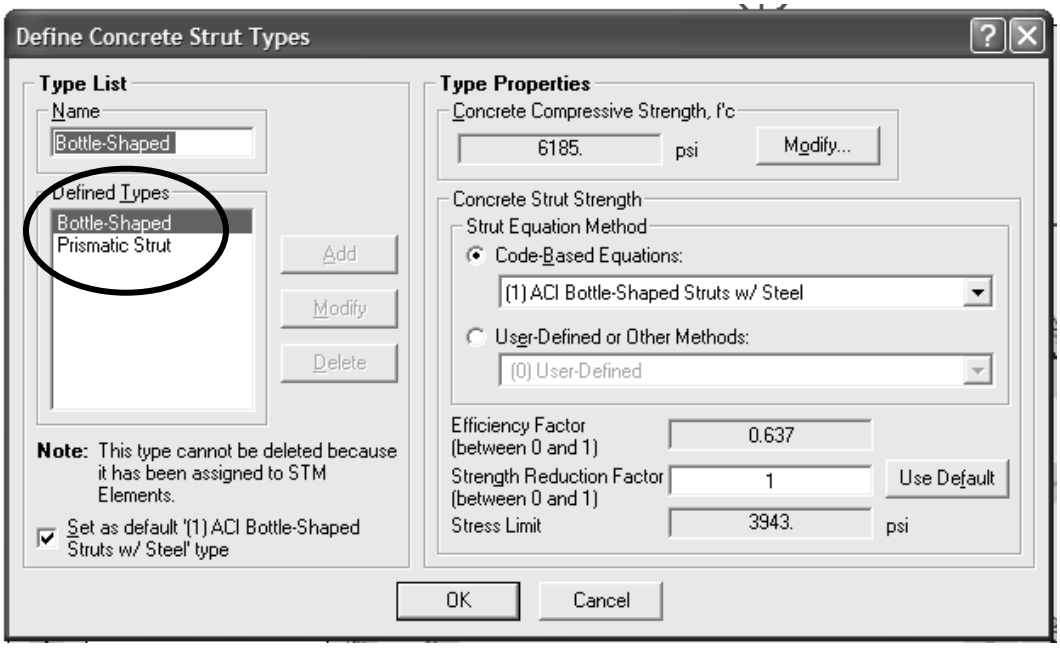

Figure A-3 Concrete Strut Types

Steel tensile ties were defined as either a single tie or a double tie. Since there was two No. 3 bars per layer, a single tie consisted of 0.22 in^2 and 0.44in^2, respectively.

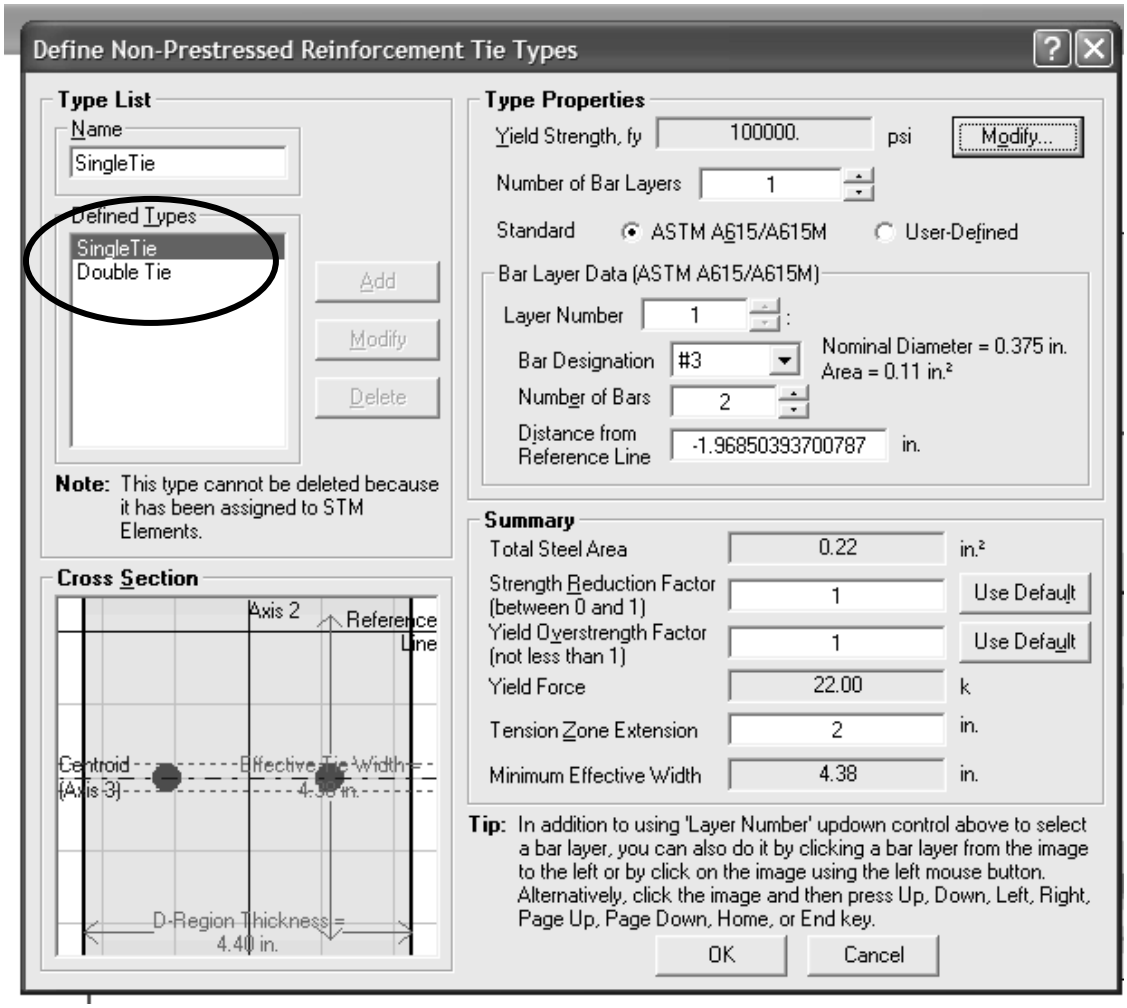

Figure A-4 Steel tensile ties

Another aspect of STM that must be considered is the nodal region. Nodes were either compression on all sides (C-C-C), tension on one side (C-C-T), or tension on more than one side (C-T-T). Accordingly, the strength-reduction ratios as recommended by ACI were used.

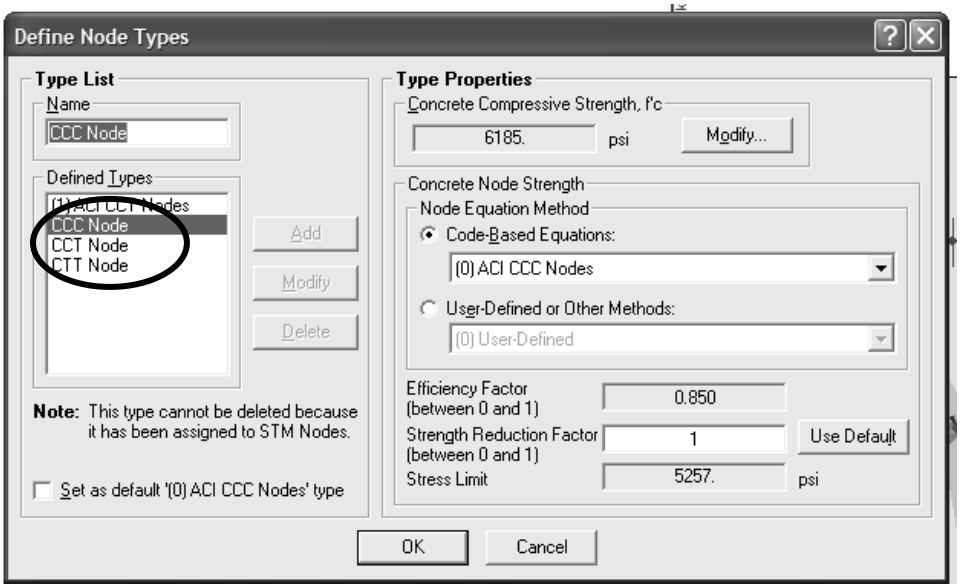

Figure A-5 Defining Node Types

The specimen was analyzed for adequacy for the given load. The software gives a color-coded graphical representation of the stresses in the concrete struts, as well as numerical analysis of the nodal zones. Any overstress component is coded in red and an over-strength (O/S) ratio greater than 1.

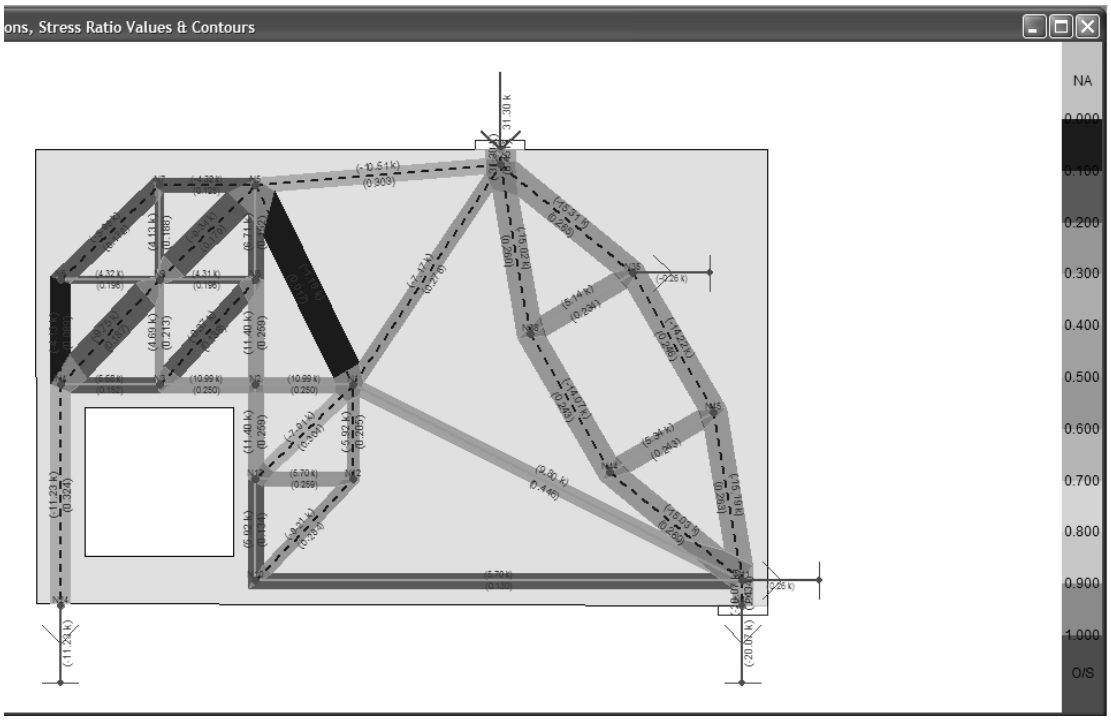

Figure A-6 Graphical interpretation of output data

APPENDIX B

CAST OUTPUT FILE FOR RC SPECIMEN

C A S T - Computer Aided Strut-and-Tie - Version 0.9.11 (Last Updated on 1/26/04)

File Name: Deep Beam1_w-ACI bottle Strut.txt

Date and Time Created: 9/27/2008 4:00:31 PM

Associated Input Data File Name: Deep Beam1_w-ACI bottle Strut.CST

P R O J E C T D E S C R I P T I O N:

PROJECT NAME: Deep Beam w/ Opening

DESIGNER: CAF

DATE: 7/28/2008

PROJECT NOTE: Original by Brena

D E S I G N C A L C U L A T I O N R E S U L T S:

LOAD CONDITION: LC1

ELEMENTS:				
ELEMNENT ID	Force	Stress	Stress Limit/Yield Force	
	(k)	(psi)	(psi)	(k)
E1	10.99	24968	-	44
E10	11.4	25905	-	44
E11	4.13	18777	-	22
E12	4.69	21325	-	22

E13	4.32	19636	-	22
E14	4.31	19569	-	22
E15	-9.75	738	3943	-
E16	-9.34	707	3943	-
E18	5.7	12952	-	44
E19	9.8	44557	-	22
E2	10.99	24968	-	44
E20	-8.21	1493	5257	-
E21	-5.92	1076	5257	-
E22	-7.91	1198	3943	-
E23	5.7	25905	-	22
E24	11.4	25905	-	44
E25	5.92	13444	-	44
E26	-10.51	1593	5257	-
E3	6.68	15183	-	44
E30	-1.16	88	5257	-
E31	-7.17	1086	3943	-
E40	-6.37	724	5257	-
E41	-11.23	1276	3943	-
E44	-31.3	2371	5257	-
E5	-5.98	679	3943	-
E6	-4.32	655	5257	-
E7	-4.13	469	5257	-
E81	-15.31	1391	5257	-
E84	-14.22	1293	5257	-
E85	-14.07	1279	5257	-
E86	5.34	24265	-	22
E88	-15.03	1366	5257	-
E89	-15.19	1381	5257	-
E9	6.71	15242	-	44
E90	5.14	23383	-	22
E91	-15.02	1365	5257	-
E92	-20.07	2281	5257	-

ELEMENT ID	STRESS RATIO	f'c RATIO	Beta RATIO
E1	0.25	NA	NA
E10	0.259	NA	NA
E11	0.188	NA	NA

E12	0.213	NA	NA
E13	0.196	NA	NA
E14	0.196	NA	NA
E15	0.187	0.119	0.14
E16	0.179	0.114	0.135
E18	0.13	NA	NA
E19	0.446	NA	NA
E2	0.25	NA	NA
E20	0.284	0.241	0.284
E21	0.205	0.174	0.205
E22	0.304	0.194	0.228
E23	0.259	NA	NA
E24	0.259	NA	NA
E25	0.134	NA	NA
E26	0.303	0.258	0.303
E3	0.152	NA	NA
E30	0.017	0.014	0.017
E31	0.276	0.176	0.207
E40	0.138	0.117	0.138
E41	0.324	0.206	0.243
E44	0.451	0.383	0.451
E5	0.172	0.11	0.129
E6	0.125	0.106	0.125
E7	0.089	0.076	0.089
E81	0.265	0.225	0.265
E84	0.246	0.209	0.246
E85	0.243	0.207	0.243
E86	0.243	NA	NA
E88	0.26	0.221	0.26
E89	0.263	0.223	0.263
E9	0.152	NA	NA
E90	0.234	NA	NA
E91	0.26	0.221	0.26
E92	0.434	0.369	0.434

NODES:				
NODE ID	NODE FACE	FORCE	STRESS	STRESS LIMIT
		(k)	(psi)	(psi)

N1	E1	10.99	1665	3154
	E19	9.8	1536	3154
	E21	-5.92	1076	3154
	E22	-7.91	1198	3154
	E30	-1.16	88	3154
	E31	-7.17	1086	3154
N10	E18	5.7	863	3154
	E20	-8.21	1493	3154
	E25	5.92	896	3154
N11	E18	5.7	863	4206
	E19	9.8	1536	4206
	E88	-15.03	1366	4206
	E89	-15.19	1381	4206
	E92	-20.07	2281	4206
N12	E20	-8.21	1493	4206
	E21	-5.92	1076	4206
	E23	5.7	863	4206
N13	E22	-7.91	1198	3154
	E23	5.7	863	3154
	E24	11.4	1727	3154
	E25	5.92	896	3154
N14	E26	-10.51	1593	5257
	E31	-7.17	1086	5257
	E44	-31.3	2371	5257
	E81	-15.31	1391	5257
	E91	-15.02	1365	5257
N2	E1	10.99	1665	3154
	E2	10.99	1665	3154
	E10	11.4	1727	3154
	E24	11.4	1727	3154
N24	E41	-11.23	1276	5257
N27	E44	-31.3	2371	5257
N3	E2	10.99	1665	3154
	E3	6.68	1012	3154
	E12	4.69	1422	3154
	E40	-6.37	724	3154
N35	E81	-15.31	1391	3154
	E84	-14.22	1293	3154
	E90	5.14	585	3154

N38	E85	-14.07	1279	3154
	E90	5.14	585	3154
	E91	-15.02	1365	3154
N4	E3	6.68	1012	4206
	E7	-4.13	469	4206
	E15	-9.75	738	4206
	E41	-11.23	1276	4206
N44	E85	-14.07	1279	3154
	E86	5.34	607	3154
	E88	-15.03	1366	3154
N45	E84	-14.22	1293	3154
	E86	5.34	607	3154
	E89	-15.19	1381	3154
N46	E92	-20.07	2281	NA
N5	E6	-4.32	655	4206
	E9	6.71	1016	4206
	E16	-9.34	707	4206
	E26	-10.51	1593	4206
	E30	-1.16	88	4206
N6	E5	-5.98	679	4206
	E7	-4.13	469	4206
	E13	4.32	1309	4206
N7	E5	-5.98	679	4206
	E6	-4.32	655	4206
	E11	4.13	1252	4206
N8	E9	6.71	1016	3154
	E10	11.4	1727	3154
	E14	4.31	1305	3154
	E40	-6.37	724	3154
N9	E11	4.13	1252	3154
	E12	4.69	1422	3154
	E13	4.32	1309	3154
	E14	4.31	1305	3154
	E15	-9.75	738	3154
	E16	-9.34	707	3154

NODE ID	NODE FACE	STRESS RATIO	f'c RATIO	Beta RATIO
N1	E11	0.397	0.202	0.238
	E12	0.451	0.23	0.27

	E13	0.415	0.212	0.249
	E14	0.414	0.211	0.248
	E15	0.234	0.119	0.14
	E16	0.224	0.114	0.135
N10	E11	0.397	0.202	0.238
	E12	0.451	0.23	0.27
	E13	0.415	0.212	0.249
	E14	0.414	0.211	0.248
	E15	0.234	0.119	0.14
	E16	0.224	0.114	0.135
N11	E11	0.397	0.202	0.238
	E12	0.451	0.23	0.27
	E13	0.415	0.212	0.249
	E14	0.414	0.211	0.248
	E15	0.234	0.119	0.14
	E16	0.224	0.114	0.135
N12	E11	0.397	0.202	0.238
	E12	0.451	0.23	0.27
	E13	0.415	0.212	0.249
	E14	0.414	0.211	0.248
	E15	0.234	0.119	0.14
	E16	0.224	0.114	0.135
N13	E11	0.397	0.202	0.238
	E12	0.451	0.23	0.27
	E13	0.415	0.212	0.249
	E14	0.414	0.211	0.248
	E15	0.234	0.119	0.14
	E16	0.224	0.114	0.135
N14	E11	0.397	0.202	0.238
	E12	0.451	0.23	0.27
	E13	0.415	0.212	0.249
	E14	0.414	0.211	0.248
	E15	0.234	0.119	0.14
	E16	0.224	0.114	0.135
N2	E11	0.397	0.202	0.238
	E12	0.451	0.23	0.27
	E13	0.415	0.212	0.249
	E14	0.414	0.211	0.248
	E15	0.234	0.119	0.14

	E16	0.224	0.114	0.135
N24	E11	0.397	0.202	0.238
	E12	0.451	0.23	0.27
	E13	0.415	0.212	0.249
	E14	0.414	0.211	0.248
	E15	0.234	0.119	0.14
	E16	0.224	0.114	0.135
N27	E11	0.397	0.202	0.238
	E12	0.451	0.23	0.27
	E13	0.415	0.212	0.249
	E14	0.414	0.211	0.248
	E15	0.234	0.119	0.14
	E16	0.224	0.114	0.135
N3	E11	0.397	0.202	0.238
	E12	0.451	0.23	0.27
	E13	0.415	0.212	0.249
	E14	0.414	0.211	0.248
	E15	0.234	0.119	0.14
	E16	0.224	0.114	0.135
N35	E11	0.397	0.202	0.238
	E12	0.451	0.23	0.27
	E13	0.415	0.212	0.249
	E14	0.414	0.211	0.248
	E15	0.234	0.119	0.14
	E16	0.224	0.114	0.135
N38	E11	0.397	0.202	0.238
	E12	0.451	0.23	0.27
	E13	0.415	0.212	0.249
	E14	0.414	0.211	0.248
	E15	0.234	0.119	0.14
	E16	0.224	0.114	0.135
N4	E11	0.397	0.202	0.238
	E12	0.451	0.23	0.27
	E13	0.415	0.212	0.249
	E14	0.414	0.211	0.248
	E15	0.234	0.119	0.14
	E16	0.224	0.114	0.135
N44	E11	0.397	0.202	0.238
	E12	0.451	0.23	0.27

	E13	0.415	0.212	0.249
	E14	0.414	0.211	0.248
	E15	0.234	0.119	0.14
	E16	0.224	0.114	0.135
N45	E11	0.397	0.202	0.238
	E12	0.451	0.23	0.27
	E13	0.415	0.212	0.249
	E14	0.414	0.211	0.248
	E15	0.234	0.119	0.14
	E16	0.224	0.114	0.135
N46	E11	0.397	0.202	0.238
	E12	0.451	0.23	0.27
	E13	0.415	0.212	0.249
	E14	0.414	0.211	0.248
	E15	0.234	0.119	0.14
	E16	0.224	0.114	0.135
N5	E11	0.397	0.202	0.238
	E12	0.451	0.23	0.27
	E13	0.415	0.212	0.249
	E14	0.414	0.211	0.248
	E15	0.234	0.119	0.14
	E16	0.224	0.114	0.135
N6	E11	0.397	0.202	0.238
	E12	0.451	0.23	0.27
	E13	0.415	0.212	0.249
	E14	0.414	0.211	0.248
	E15	0.234	0.119	0.14
	E16	0.224	0.114	0.135
N7	E11	0.397	0.202	0.238
	E12	0.451	0.23	0.27
	E13	0.415	0.212	0.249
	E14	0.414	0.211	0.248
	E15	0.234	0.119	0.14
	E16	0.224	0.114	0.135
N8	E11	0.397	0.202	0.238
	E12	0.451	0.23	0.27
	E13	0.415	0.212	0.249
	E14	0.414	0.211	0.248
	E15	0.234	0.119	0.14

	E16	0.224	0.114	0.135
N9	E11	0.397	0.202	0.238
	E12	0.451	0.23	0.27
	E13	0.415	0.212	0.249
	E14	0.414	0.211	0.248
	E15	0.234	0.119	0.14
	E16	0.224	0.114	0.135

APPENDIX C

CAST OUTPUT FILE FOR RC SPECIMEN WITH SINGLE BOTTOM TIE

C. CAST OUTPUT FILE FOR RC SPECIMEN WITH SINGLE BOTTOM TIE

C A S T - Computer Aided Strut-and-Tie - Version 0.9.11 (Last Updated on 1/26/04)

File Name: Deep Beam_SFRC.txt

Date and Time Created: 9/27/2008 4:02:18 PM

Associated Input Data File Name: Deep Beam_SFRC.CST

P R O J E C T D E S C R I P T I O N:

PROJECT NAME: Deep Beam w/ Opening SFRC

DESIGNER: CAF

DATE: 7/28/2008

PROJECT NOTE: Original by Brena

D E S I G N C A L C U L A T I O N R E S U L T S:

LOAD CONDITION: LC1

ELEMENTS:				
ELEMENT ID	FORCE	STRESS	LIMIT/YIELD FORCE	
	(k)	(psi)	(psi)	(k)
E1	10.99	1248	-	5.19
E10	11.4	1295	-	5.19
E11	4.13	469	-	5.19
E12	4.69	533	-	5.19
E13	4.32	491	-	5.19
E14	4.31	489	-	5.19
E15	-9.75	738	3943	-
E16	-9.34	707	3943	-
E18	5.7	57	-	59.26
E19	9.8	1114	-	5.19
E2	10.99	1248	-	5.19
E20	-8.21	1493	5257	-
E21	-5.92	1076	5257	-
E22	-7.91	1198	3943	-
E23	5.7	648	-	5.19
E24	11.4	1295	-	5.19
E25	5.92	672	-	5.19
E26	-10.51	1593	5257	-
E3	6.68	759	-	5.19
E30	-1.16	88	5257	-
E31	-7.17	1086	3943	-
E40	-6.37	724	5257	-
E41	-11.23	1276	3943	-
E44	-31.3	2371	5257	-
E5	-5.98	679	3943	-
E6	-4.32	655	5257	-
E7	-4.13	469	5257	-
E81	-15.31	1391	5257	-
E84	-14.22	1616	5257	-
E85	-14.07	1599	5257	-
E86	5.34	607	-	5.19
E88	-15.03	1366	5257	-
E89	-15.19	1381	5257	-
E9	6.71	762	-	5.19
E90	5.14	585	-	5.19
E91	-15.02	1365	5257	-

E92	-20.07	1825	5257	-

ELEMENT ID	STRESS RATIO	f'c RATIO	Beta RATIO
E1	2.116	NA	NA
E10	2.195	NA	NA
E11	0.796	NA	NA
E12	0.904	NA	NA
E13	0.832	NA	NA
E14	0.829	NA	NA
E15	0.187	0.119	0.14
E16	0.179	0.114	0.135
E18	0.096	NA	NA
E19	1.888	NA	NA
E2	2.116	NA	NA
E20	0.284	0.241	0.284
E21	0.205	0.174	0.205
E22	0.304	0.194	0.228
E23	1.098	NA	NA
E24	2.195	NA	NA
E25	1.139	NA	NA
E26	0.303	0.258	0.303
E3	1.287	NA	NA
E30	0.017	0.014	0.017
E31	0.276	0.176	0.207
E40	0.138	0.117	0.138
E41	0.324	0.206	0.243
E44	0.451	0.383	0.451
E5	0.172	0.11	0.129
E6	0.125	0.106	0.125
E7	0.089	0.076	0.089
E81	0.265	0.225	0.265
E84	0.307	0.261	0.307
E85	0.304	0.258	0.304
E86	1.028	NA	NA
E88	0.26	0.221	0.26
E89	0.263	0.223	0.263

E9	1.292	NA	NA
E90	0.991	NA	NA
E91	0.26	0.221	0.26
E92	0.347	0.295	0.347

NODES:				
NODE ID	NODE FACE	FORCE	STRESS	STRESS LIMIT
		(k)	(psi)	(psi)
N1	E1	10.99	1665	3154
	E19	9.8	1536	3154
	E21	-5.92	1076	3154
	E22	-7.91	1198	3154
	E30	-1.16	88	3154
	E31	-7.17	1086	3154
N10	E18	5.7	863	3154
	E20	-8.21	1493	3154
	E25	5.92	896	3154
N11	E18	5.7	863	4206
	E19	9.8	1536	4206
	E88	-15.03	1366	4206
	E89	-15.19	1381	4206
	E92	-20.07	1825	4206
N12	E20	-8.21	1493	4206
	E21	-5.92	1076	4206
	E23	5.7	863	4206
N13	E22	-7.91	1198	3154
	E23	5.7	863	3154
	E24	11.4	1727	3154
	E25	5.92	896	3154
N14	E26	10.51	1593	5257
	E31	-7.17	1086	5257
	E44	-31.3	2371	5257
	E81	-15.31	1391	5257
	E91	-15.02	1365	5257

N2	E1	10.99	1665	3154
	E2	10.99	1665	3154
	E10	11.4	1727	3154
	E24	11.4	1727	3154
N24	E41	-11.23	1276	5257
N27	E44	-31.3	2371	5257
N3	E2	10.99	1665	3154
	E3	6.68	1012	3154
	E12	4.69	1422	3154
	E40	-6.37	724	3154
N35	E81	-15.31	1391	3154
	E84	-14.22	1616	3154
	E90	5.14	585	3154
N38	E85	-14.07	1599	3154
	E90	5.14	585	3154
	E91	-15.02	1365	3154
N4	E3	6.68	1012	4206
	E7	-4.13	469	4206
	E15	-9.75	738	4206
	E41	-11.23	1276	4206
N44	E85	-14.07	1599	3154
	E86	5.34	607	3154
	E88	-15.03	1366	3154
N45	E84	-14.22	1616	3154
	E86	5.34	607	3154
	E89	-15.19	1381	3154
N46	E92	-20.07	1825	NA
N5	E6	-4.32	655	4206
	E9	6.71	1016	4206
	E16	-9.34	707	4206
	E26	-10.51	1593	4206
	E30	-1.16	88	4206
N6	E5	-5.98	679	4206
	E7	-4.13	469	4206
	E13	4.32	1309	4206
N7	E5	-5.98	679	4206
	E6	-4.32	655	4206
	E11	4.13	1252	4206
N8	E9	6.71	1016	3154

	E10	11.4	1727	3154
	E14	4.31	1305	3154
	E40	-6.37	724	3154
N9	E11	4.13	1252	3154
	E12	4.69	1422	3154
	E13	4.32	1309	3154
	E14	4.31	1305	3154
	E15	-9.75	738	3154
	E16	-9.34	707	3154

NODE ID	NODE FACE	STRESS RATIO	f'c RATIO	Beta RATIO
N1	E11	0.397	0.202	0.238
	E12	0.451	0.23	0.27
	E13	0.415	0.212	0.249
	E14	0.414	0.211	0.248
	E15	0.234	0.119	0.14
	E16	0.224	0.114	0.135
N10	E11	0.397	0.22	0.238
	E12	0.451	0.23	0.27
	E13	0.415	0.212	0.249
	E14	0.414	0.211	0.248
	E15	0.234	0.119	0.14
	E16	0.224	0.114	0.135
N11	E11	0.397	0.22	0.238
	E12	0.451	0.23	0.27
	E13	0.415	0.212	0.249
	E14	0.414	0.211	0.248
	E15	0.234	0.119	0.14
	E16	0.224	0.114	0.135
N12	E11	0.397	0.22	0.238
	E12	0.451	0.23	0.27
	E13	0.415	0.212	0.249
	E14	0.414	0.211	0.248
	E15	0.234	0.119	0.14
	E16	0.224	0.114	0.135
N13	E11	0.397	0.22	0.238
	E12	0.451	0.23	0.27
	E13	0.415	0.212	0.249

	E14	0.414	0.211	0.248
	E15	0.234	0.119	0.14
	E16	0.224	0.114	0.135
N14	E11	0.397	0.22	0.238
	E12	0.451	0.23	0.27
	E13	0.415	0.212	0.249
	E14	0.414	0.211	0.248
	E15	0.234	0.119	0.14
	E16	0.224	0.114	0.135
N2	E11	0.397	0.22	0.238
	E12	0.451	0.23	0.27
	E13	0.415	0.212	0.249
	E14	0.414	0.211	0.248
	E15	0.234	0.119	0.14
	E16	0.224	0.114	0.135
N24	E11	0.397	0.22	0.238
	E12	0.451	0.23	0.27
	E13	0.415	0.212	0.249
	E14	0.414	0.211	0.248
	E15	0.234	0.119	0.14
	E16	0.224	0.114	0.135
N27	E11	0.397	0.22	0.238
	E12	0.451	0.23	0.27
	E13	0.415	0.212	0.249
	E14	0.414	0.211	0.248
	E15	0.234	0.119	0.14
	E16	0.224	0.114	0.135
N3	E11	0.397	0.202	0.238
	E12	0.451	0.23	0.27
	E13	0.415	0.212	0.249
	E14	0.414	0.211	0.248
	E15	0.234	0.119	0.14
	E16	0.224	0.114	0.135
N35	E11	0.397	0.22	0.238
	E12	0.451	0.23	0.27
	E13	0.415	0.212	0.249
	E14	0.414	0.211	0.248
	E15	0.234	0.119	0.14
	E16	0.224	0.114	0.135

N38	E11	0.397	0.22	0.238
	E12	0.451	0.23	0.27
	E13	0.415	0.212	0.249
	E14	0.414	0.211	0.248
	E15	0.234	0.119	0.14
	E16	0.224	0.114	0.135
N4	E11	0.397	0.22	0.238
	E12	0.451	0.23	0.27
	E13	0.415	0.212	0.249
	E14	0.414	0.211	0.248
	E15	0.234	0.119	0.14
	E16	0.224	0.114	0.135
N44	E11	0.397	0.22	0.238
	E12	0.451	0.23	0.27
	E13	0.415	0.212	0.249
	E14	0.414	0.211	0.248
	E15	0.234	0.119	0.14
	E16	0.224	0.114	0.135
N45	E11	0.397	0.22	0.238
	E12	0.451	0.23	0.27
	E13	0.415	0.212	0.249
	E14	0.414	0.211	0.248
	E15	0.234	0.119	0.14
	E16	0.224	0.114	0.135
N46	E11	0.397	0.22	0.238
	E12	0.451	0.23	0.27
	E13	0.415	0.212	0.249
	E14	0.414	0.211	0.248
	E15	0.234	0.119	0.14
	E16	0.224	0.114	0.135
N5	E11	0.397	0.202	0.238
	E12	0.451	0.23	0.27
	E13	0.415	0.212	0.249
	E14	0.414	0.211	0.248
	E15	0.234	0.119	0.14
	E16	0.224	0.114	0.135
N6	E11	0.397	0.202	0.238
	E12	0.451	0.23	0.27
	E13	0.415	0.212	0.249

	E14	0.414	0.211	0.248
	E15	0.234	0.119	0.14
	E16	0.224	0.114	0.135
N7	E11	0.397	0.22	0.238
	E12	0.451	0.23	0.27
	E13	0.415	0.212	0.249
	E14	0.414	0.211	0.248
	E15	0.234	0.119	0.14
	E16	0.224	0.114	0.135
N8	E11	0.397	0.202	0.238
	E12	0.451	0.23	0.27
	E13	0.415	0.212	0.249
	E14	0.414	0.211	0.248
	E15	0.234	0.119	0.14
	E16	0.224	0.114	0.135
N9	E11	0.397	0.202	0.238
	E12	0.451	0.23	0.27
	E13	0.415	0.212	0.249
	E14	0.414	0.211	0.248
	E15	0.234	0.119	0.14
	E16	0.224	0.114	0.135

REFERENCES

AASHTO, “AASHTO LRFD Bridge Design Specifications,” American Association of State Highway and Transportation Officials, first edition, Washington, DC, 1994, 1091 pp., including interim revisions for 1996 and 1997.

ACI Committee 318. (2008), “Building Code Requirements for Structural Concrete (ACI 318-08) and Commentary (318R-08),” American Concrete Institute, Farmington Hills, MI

ACI Committee 544. (1996), “Report on Fiber Reinforced Concrete (ACI 544.1 R-96),” American Concrete Institute, Farmington Hills, MI

ASTM A 370 – 07a, “Standard Test Methods and Definitions for Mechanical Testing of Steel Products,” ASTM International, West Conshohocken, PA, pp. 191-195.

ASTM A 615/A 615M – 07, “Standard Specification for Deformed and Plain Carbon-Steel Bars for Concrete Reinforcement,” ASTM International, West Conshohocken, PA, pp. 325-329.

ASTM C 1609/C 1609M - 06, “Standard Test Method for Flexural Performance of Fiber-Reinforced Concrete (Using Beam With Third-Point Loading),” ASTM International, West Conshohocken, PA, pp. 831-838.

ASTM C 39/C 39M – 05, “Standard Test Method for Compressive Strength Cylindrical Concrete Specimens,” ASTM International, West Conshohocken, PA, pp. 22-28

ASTM C 78 – 02, “Test Method for Flexural Strength of Concrete (Using Simple Beam with Third-Point Loading,” ASTM International, West Conshohocken, PA, pp. 40-42.

ASTM C 617 – 98 (2003), “Practice for Capping Cylindrical Concrete Specimens,” ASTM International, West Conshohocken, PA, pp. 324-328.

Al-Nahlawi, Khaled A., Wight, James K., 1992, “Beam Analysis Using Concrete Tensile Strength in Truss Models,” ACI *Structural Journal,* V. 89, No. 3, May-Jun., pp.284-289.

Ashour, A. F.; Chung, H. S.; and Yang, K. H., 2007, “Influence of Inclined Web Reinforcement on Reinforced Concrete Deep Beams with Openings,” ACI *Structural Journal,* V. 104, Sept-Oct., pp. 580-589.

Breña, S. F.; and Morrison, M. C., 2007, “Factors Affecting Strength of Elements Designed Using Strut-and-Tie Models,” ACI *Structual Journal*, V. 104, No. 3, May-June., pp. 267-277.

Bae, S.; Breen, J. E,; Ley, M. T.; Ridding, K. A.,; and Widianto., 2007, “Experimental Verification of Strut-and-Tie Model Design Method,” ACI *Structural Journal,* V. 104, No. 6, Nov-Dec., pp. 749-755.

Breen, J. E,; and Maxwell, B. S., 2000, “Experimental Evaluation of Strut-and-Tie Model Applied to Deep Beam with Opening,” ACI *Structural Journal*, V. 97, No. 1, Jan-Feb., pp. 142-149.

Casanova, P.; and Rossi, P., “High Strength Concrete Beams Submitted to Shear: Steel Fibers Versus Stirrups,” Ed. Banthia, N.; MacDonald, C.; and Tatnall, P., “Structural Applications of Fiber Reinforced Concrete,” American Concrete Institute, Farmington Hills, MI., 1999.

Chao, S.-H. (2008), "Achieving “Green” Concrete through the Use of High Performance Fiber Reinforced Concrete," *ASCE Texas Section Fall Meeting*, Addison, TX, October 3rd, 2008.

Chen, B. S.; Hagenbergerm, M. J.; and Breen, J. E., 2002, “Evaluation of Strut-and-Tie Modeling Applied to Dapped Beams with Opening,” ACI *Structural Journal*, V. 99, No. 4, July-Aug., pp. 445-450

Colombo, S., Main, I.G., Forde, M.C., 2003, ASCE *Journal of Materials in Civil Engineering,* V.15, No. 3, Jun., pp. 280-286.

CSA Committee A23.3, “Design of Concrete Structures (CAN3-A23.3-M84),” Canadian Standards Association, Rexdale, ON, Canada, 1984, pp. 281

Darwish, I. Y. S.; and Narayanan, R., 1988, "Fiber Concrete Deep Beams in Shear," ACI *Structural Journal*, V. 85, No.2, Mar-April, pp. 141-149.

Dupont, D.; and Vandewalle, L., "Shear Capacity of Concrete Beams Containing Longitudinal Reinforcement and Steel Fibers." Ed. Banthia, N.; Criswell, M.; Tatnall, P.; and Folliard, K., Innovations in Fiber-Reinforced Concrete for Value, American Concrete Institute, Farmington Hills, MI., 2003.

Hibbeler, R.C., 2005, "Mechanics of Materials," 6th Edition, Prentice Hall p.123.

Kuchma, D.; and Park, J. W., 2007, "Strut-and-Tie Model Analysis for Strength Prediction of Deep Beams," ACI *Structural Journal,* V. 104, No. 6, Nov-Dec, pp. 657-666.

Kuchma, Daniel; Yindeesuk, Sukit; Nagle, Thomas; Hart, Jason; Lee, Heui H., 2008,"Experimental Validation of Strut-and-Tie Method for complex Regions," ACI *Structural Journal,* V. 105, No. 5, Sep-Oct., pp. 578-589.

Mehta, P. Kumar, Monteiro, Paulo J.M., 2006, "Concrete – Microstructure, Properties, and Materials," 3rd Edition, McGraw-Hill, New York, p. 502.

Mörsch, E., *Concrete-Steel Construction,* E.P. Goodrich, translation, McGraw-Hill, New York, 1909, pp. 368

Narayanan, R., and Darwish, I. Y. S., 1988, "Fiber Concrete Deep Beams in Shear," ACI *Structural Journal*, 85, No. 2, March-April., 141-149.

Ritter, W., "Die Bauweise Hennebique," *Schweizerische Bauzeitung*, V. 33, No. 7, Feb. 1899, pp. 59-61.

Schlaich, J.; Schäfer, K.; and Jennewein, M., 1987, "Toward a Consistent Design of Structural Concrete," PCI *Journal*, Special Report, V. 32, No. 3, pp. 74-150.

Tan, K. H.; and Zhang, N., 2007, "Size effect in RC deep beams: Experimental investigation and STM verification," Engineering Structures, V. 29, pp. 3241- 3254.

United States Green Building Council, News and Events: In the News: *Recession or Not, Green Building to Keep Growing*, LyndaDePillis, New York Observer, November 13, 2008. http://www.usgbc.org/News/USGBCInTheNewsDetails.aspx?ID=3876

BIOGRAPHICAL INFORMATION

Carlos Flores was born in Zacapuato, Gro., Mexico on May 7, 1983, the son of Virgilio and Carolina Flores. After completing his work at Adamson High School, Dallas, Texas, in 2001, he entered Mountain View College in Dallas, Texas. He received his Associates Degree in Arts in 2003. He soon entered The University of Texas at Arlington. He received the degree of Bachelor of Science in Architecture in May 2006. In August of 2007 he entered the Graduate School at the University of Texas at Arlington. During the following year he was employed by Wiss, Janney, Elstner, Associates and Raymond L. Goodson, Jr., Consulting Engineers. He is currently employed by Nelson Consulting Engineers focusing on investigation, rehabilitation and retrofit of new and existing structures. Carlos lives in Dallas, Texas. His short-term plans are to marry Esbeide Pereznegron, earn design experience and become a registered design professional. He will consider pursuing a doctoral degree as his long-term career goal. Carlos enjoys spending time with his family, various construction-related activities and spending his time in church. He regularly volunteers with non-for-profit organizations such as The Hispanic Scholarship Fund, Habitat for Humanity, ACE high school mentor program, among others, giving back to his community.